The University of Alberta
Printing Department
Edmonton, Alberta

THE UNIVERSITY OF ALBERTA

RELEASE FORM

NAME OF AUTHOR Joachim F. W. Gurke

TITLE OF THESIS FM DISTORTION IN INJECTION-LOCKED OSCILLATORS USED AS MICROWAVE AMPLIFIERS

DEGREE FOR WHICH THESIS WAS PRESENTED M. Sc.

YEAR THIS DEGREE GRANTED 1975

Permission is hereby granted to THE UNIVERSITY OF ALBERTA LIBRARY to reproduce single copies of this thesis and to lend or sell such copies for private, scholarly or scientific research purposes only.

The author reserves other publication rights, and neither the thesis nor extensive extracts from it may be printed or otherwise reproduced without the author's written permission.

THE UNIVERSITY OF ALBERTA

FM DISTORTION IN INJECTION-LOCKED OSCILLATORS USED AS MICROWAVE AMPLIFIERS

BY

© JOACHIM F. W. GURKE

A THESIS

SUBMITTED TO THE FACULTY OF GRADUATE STUDIES AND RESEARCH

IN PARTIAL FULFILMENT OF THE REQUIREMENTS FOR THE DEGREE

OF MASTER OF SCIENCE IN ELECTRICAL ENGINEERING

DEPARTMENT OF ELECTRICAL ENGINEERING

EDMONTON, ALBERTA

SPRING, 1975

THE UNIVERSITY OF ALBERTA

FACULTY OF GRADUATE STUDIES AND RESEARCH

The undersigned certify that they have read, and recommend to the Faculty of Graduate Studies and Research, for acceptance, a thesis entitled FM Distortion in Injection-Locked Oscillators Used as Microwave Amplifiers submitted by Joachim F. W. Gurke in partial fulfilment of the requirements for the degree of Master of Science in Electrical Engineering.

ABSTRACT

The dynamic behavior of injection-locked oscillators (ILO's) operating as FM amplifiers has been investigated. IMPATT diodes operating at X-band were used as the locked oscillators. The ILO has been modelled mathematically by the use of the generalized Adler's phase-locking equation, and ideal FM modulators and demodulators at the input and output respectively, thus simulating a baseband amplifier. This ILO amplifier has been characterized in conventional amplifier terminology by the use of FM input signals whose deviation and modulation rate approach the locking bandwidth. Theoretical results for the amplitude variation, the phase delay distortion and the nonlinear distortion of the fundamental output signal versus the modulating frequency have been obtained. The nonlinear distortion curve has been verified experimentally for a 34 dB gain case. The theoretical and experimental analysis of the distortion in FM ILO amplifiers indicates that for the output demodulated fundamental signal a) the distortion characteristics are sensitive to changes in the input modulating signal parameters but are not sensitive to changes in the locking signal amplitude, b) the amplitude is frequency dependent, c) the phase delay distortion is highly dependent upon all the input modulation parameters, and d) the nonlinear distortion

is dependent upon the modulating signal frequency. These distortion characteristics will aid in the design of microwave IMPATT diode oscillator-amplifiers for use as the output stages of microwave FM transmitters.

ACKNOWLEDGEMENTS

The author wishes to express his appreciation for the assistance of many people during the course of this research:

To Dr. P.A. Goud for his advice and encouragement during the supervision of this work.

To members of the Microwave Electronics Laboratory at the University of Alberta, who were closely involved in this research, for their assistance, understanding and encouragement.

To the author's parents for their encouragement and financial support during this work.

The author is also indebted to the following organizations:

To the National Research Council of Canada for their continued support of this research and for the provision of a research scholarship.

To the Department of Communications of Canada, Communications Research Centre, (Contract D16R-36001-1-0513) for the financial support of this research.

To the University of Alberta for financial assistance.

TABLE OF CONTENTS

		Page
I	INTRODUCTION.....	1
II	THEORETICAL ANALYSIS OF AN INJECTION-LOCKED OSCILLATOR (ILO).....	4
	2.1 Introduction.....	4
	2.2 The Generalized Adler's Phase-Locking Equation.....	4
	2.2-1 Basic concepts and Approximations.....	6
	2.2-2 Equivalent Circuit Represention.....	7
	2.2-3 Phasor Analysis.....	11
	2.2-4 Derivation of the Generalized Adler's Phase-Locking Equation.....	12
	2.2-5 Adler's Equation.....	16
	2.3 Steady-State ILO Characteristics.....	17
	2.4 Transient Response of an ILO.....	19
III	LOCKING TO A FREOUENCY MODULATED LOCKING SIGNAL.....	25
	3.1 Introduction	25
	3.2 Modelling.....	25
	3.3 Ouasi-Stationary Equation Analysis.....	26
	3.4 Linearized Equation Analysis.....	33
	3.5 Analysis Based Upon Adler's Equation.....	35
	3.6 Analysis Based Upon the Generalized Adler's Phase-Locking Equation.....	39
	3.7 Conclusion.....	41

Page

IV CHARACTERIZATION OF AN FM ILO AMPLIFIER 43

4.1 Introduction 43

4.2 ILO Amplifier Model 43

V FM DISTORTION IN A TUNED ILO AMPLIFIER 51

5.1 Introduction 51

5.2 Mathematical Modelling 51

5.3 Results of the Tuned Calculations 56

5.4 Conclusion 57

VI FM DISTORTION IN A DETUNED ILO AMPLIFIER 64

6.1 Introduction 64

6.2 Mathematical Modelling 65

6.3 Results of the Detuned Calculations 68

6.4 Conclusion 74

VII APPLICATION OF THE DISTORTION ANALYSIS IN THE DESIGN OF A SINGLE-STAGE FM ILO AMPLIFIER 75

7.1 Introduction 75

7.2 Design Contours 75

7.3 An Example of the Design Contour Applications 76

7.4 Conclusion and Summary 80

Page

VIII DISTORTION MEASUREMENTS OF A MICROWAVE FM ILO AMPLIFIER..... 82

8.1 Introduction..... 82

8.2 Theory, Experimental Set-Up and Measurement Techniques. 82

8.3 Experimental Results and Their Interpretation..... 96

IX SUMMARY AND CONCLUSIONS..... 104

REFERENCES..... 108

APPENDIX A SIGNAL DISTORTION IN TRANSMISSION SYSTEMS..... 114

APPENDIX B DETAILED ANALYSIS OF THE TUNED AND DETUNED DISTORTION IN ILO AMPLIFIERS..... 119

LIST OF TABLES

		Page
TABLE 2.3-1	A COMPARISON OF THE VARIOUS LIMITS PREDICTED BY THE GENERALIZED ADLER'S PHASE-LOCKING EQUATION (EQ. 2.2-20) WITH THOSE PREDICTED BY ADLER'S EQUATION(EQ. 2.2-22) WHEN THE QUASI-STATIONARY APPROXIMATION IS VALID	20
TABLE 5.3-1	COMPARISON OF NONLINEAR DISTORTION FOR THE VARIOUS PARAMETERS OF A TUNED ILO AMPLIFIER(DISTORTION EXPRESSED IN PERCENTAGES)	60
TABLE 5.3-2	COMPARISON OF PHASE DELAY DISTORTION(EXPRESSED IN DEGREES) FOR VARIOUS PARAMETERS OF A TUNED ILO AMPLIFIER	61
TABLE 5.3-3	RELATIVE AMPLITUDE VARIATION(EXPRESSED IN DB) FOR VARIOUS TUNED ILO AMPLIFIER PARAMETERS	62
TABLE 6.3-1	NONLINEAR DISTORTION(EXPRESSED IN PERCENTAGES) IN AN ILO AMPLIFIER MODEL WITH A GAIN EQUAL TO 15DB, A MAXIMUM LOCKING BANDWIDTH OF 17.86 MHZ, A PEAK FREQUENCY DEVIATION OF 0.75 Δ_o, AND FOR THE FOLLOWING NORMALIZED DETUNING FACTORS: 0.0, 0.1, AND 0.24	69
TABLE 6.3-2	PHASE DELAY DISTORTION(EXPRESSED IN DEGREES) IN AN ILO AMPLIFIER MODEL WITH A GAIN EQUAL TO 15DB, A MAXIMUM LOCKING BANDWIDTH OF 17.86 MHZ, A PEAK FREQUENCY DEVIATION OF 0.75 Δ_o, AND FOR THE FOLLOWING NORMALIZED DETUNING FACTORS: 0.0, 0.1, AND 0.24	70
TABLE 6.3-3	RELATIVE AMPLITUDE VARIATION(EXPRESSED IN DB) IN AN ILO AMPLIFIER MODEL WITH A GAIN EQUAL TO 15DB, A MAXIMUM LOCKING BANDWIDTH OF 17.86 MHZ, A PEAK FREQUENCY DEVIATION OF 0.75 Δ_o, AND FOR THE FOLLOWING NORMALIZED DETUNING FACTORS: 0.0, 0.1, AND 0.24	71
TABLE 8.3-1	EXPERIMENTAL DISTORTION MEASUREMENTS FOR A 34DB GAIN DETUNED SINGLE-STAGE ILO AMPLIFIER	99

LIST OF FIGURES

		Page
FIG. 2.2-1	EMBODIMENT OF THE INJECTION LOCKING CIRCUIT AT MICROWAVE FREQUENCIES.....	5
FIG. 2.2-2	EQUIVALENT CIRCUIT OF A "FREE-RUNNING" MICROWAVE OSCILLATOR WHERE $Z(\omega)$ IS THE CIRCUIT IMPEDANCE SEEN FROM THE DEVICE (-Z (A)=THE DEVICE IMPEDANCE).....	5
FIG. 2.2-3	INJECTION-LOCKED OSCILLATOR (ILO) EQUIVALENT CIRCUIT CONCEPT (WHERE Z =DIODE IMPEDANCE AND Z_c=CAVITY IMPEDANCE).....	9
FIG. 2.2-4	EQUIVALENT PARALLEL IMPEDANCE REPRESENTION OF AN ILO.....	10
FIG. 2.2-5	EQUIVALENT PARALLEL CIRCUIT FOR THE ILO.....	10
FIG. 2.2-6	THE PHASOR REPRESENTION OF THE SIGNALS IN THE ILO MODEL.....	13
FIG. 2.4-1	PLOT OF THE TRANSIENT PHASE RESPONSE EQ. 2.4-3 VERSUS THE NORMALIZED TIME FOR SEVERAL VALUES OF θ_o.....	24
FIG. 3.3-1	LOCATION OF RADIAN FREQUENCIES IN THE FREQUENCY DOMAIN FOR A SWEPT ILO AMPLIFIER WHEN $\Delta\omega_o<(\omega_s-\omega_o)<\Delta_o$	28
FIG. 3.3-2	A PLOT OF THE PHASE SHIFT EQ. 3.3-4 VERSUS THE NORMALIZED LOCKING BANDWIDTH (FOR$\Delta\omega_o$=0.0).....	30
FIG. 3.3-3	A PLOT OF THE ENVELOPE DELAY DISTORTION EQ. 3.3-7 VERSUS THE NORMALIZED LOCKING BANDWIDTH (FOR $\Delta\omega_o$=0.0, f_{max}=1.0 MHz).....	32
FIG. 3.4-1	PHASE VERSUS NORMALIZED FREQUENCY DEVIATION FOR THE LINEARIZED APPROXIMATE SOLUTION, EQ.3.4-4.....	36
FIG. 3.5-1	PHASE VERSUS NORMALIZED FREQUENCY DEVIATION FOR ADLER'S EQUATION.....	38
FIG. 3.6-1	PHASE VERSUS NORMALIZED FREQUENCY DEVIATION FOR SEVERAL POWER RATIOS FOR THE GENERALIZED ADLER'S PHASE-LOCKING EQUATION.....	40

		Page
FIG. 4.2-1	SCHEMATIC DIAGRAM OF THE ILO AMPLIFIER WITH AN IDEAL FM MODULATOR AND FM DEMODULATOR.....	44
FIG. 4.2-2	LINEARIZED TRANSFER CHARACTERISTICS FOR THE ILO AMPLIFIER MODEL OF FIG. 4.2-1.....	49
FIG. 5.3-1	FREQUENCY DEPENDENT DISTORTION CHARACTERISTICS FOR A TUNED SINGLE-STAGE ILO AMPLIFIER MODEL WITH A 34 DB GAIN.....	58
FIG. 5.3-2	FREQUENCY DEPENDENT DISTORTION CHARACTERISTICS FOR A TUNED SINGLE-STAGE ILO AMPLIFIER MODEL WITH A 15 DB GAIN.....	59
FIG. 6.3-1	FREQUENCY DEPENDENT DISTORTION CHARACTERISTICS FOR A DETUNED SINGLE-STAGE ILO AMPLIFIER MODEL WITH A 34 DB GAIN.....	72
FIG. 6.3-2	FREQUENCY DEPENDENT DISTORTION CHARACTERISTICS FOR A DETUNED SINGLE-STAGE ILO AMPLIFIER MODEL WITH A 15 DB GAIN.....	73
FIG. 7.2-1	CONSTANT NONLINEAR DISTORTION CONTOURS VERSUS THE NORMALIZED PEAK FREQUENCY DEVIATION AND MODULATING FREQUENCY FOR A POWER GAIN OF 15 DB AND FOR NORMALIZED DETUNING FACTORS EQUAL TO 0.0 AND 0.1.....	77
FIG. 7.2-2	CONSTANT PHASE DELAY DISTORTION CONTOURS VERSUS THE NORMALIZED PEAK FREQUENCY DEVIATION AND MODULATION FREQUENCY FOR A POWER GAIN OF 15 DB AND FOR NORMALIZED DETUNING FACTORS EQUAL TO 0.0 AND 0.1.....	78
FIG. 8.2-1	SCHEMATIC FORM OF THE EXPERIMENTAL SET-UP FOR THE MEASUREMENT OF THE NONLINEAR DISTORTION IN AN ILO AMPLIFIER.....	85
FIG. 8.2-2	A PHOTOGRAPH OF THE FM ILO NONLINEAR DISTORTION EXPERIMENTAL SET-UP.....	86
FIG. 8.2-3	A PLOT OF THE VOLTAGE AMPLITUDE DEFLECTION OF THE FREQUENCY DISCRIMINATOR VERSUS THE FREQUENCY DEVIATION (SWEPT FROM 9.040 TO 9.060 GHZ) FOR AN INPUT POWER LEVEL OF 0.2 MILLIWATTS.....	92
FIG. 8.2-4	FREQUENCY SPECTRUM FOR AN FM SIGNAL WITH CARRIER ZERO.....	95
FIG. 8.3-1	AN EXAMPLE OF THE DEMODULATED INPUT AND OUTPUT SIGNALS MEASURED FOR THE 34 DB CASE.....	100

Page

FIG. 8.3-2 A PLOT OF THE EXPERIMENTAL VERSUS THE THEORETICAL DISTORTION CHARACTERISTICS FOR THE 34 DB GAIN CASE OF THE DETUNED AMPLIFIER..... 101

FIG. A-1 ELEMENTARY BLOCK DIAGRAM OF A COMMUNICATION SYSTEM..... 115

FIG. A-2 FREQUENCY PLOT OF a)THE MAGNITUDE AND b)THE PHASE VARIATION FOR THE DISTORTIONLESS CASE OF EQ. A-3..... 117

CHAPTER I

INTRODUCTION

Under certain conditions, it is possible to synchronize the frequency and phase of a self-excited oscillator to a reference or locking signal[1-22]. This may be achieved by injecting the reference signal directly into the oscillator to be controlled[3,4]. In the stable locked condition the oscillator and reference signal frequencies will be identical and the oscillator will be referred to as being injection-phase locked[6,14]. The locking signal amplitude is smaller than the self-excited oscillator amplitude, therefore the injection-locked oscillator (ILO) can be modelled as a limiter-amplifier[12,17,23]. In the stable locked condition, the reference and oscillator frequencies will coincide exactly, however, this locked condition will exhibit a definite phase relationship. The locking process and mechanism when examined in terms of this phase relationship depend upon

1. the initial frequency difference between the locked and reference signal frequencies
2. the relative amplitudes of the locked oscillator and reference signals (this ratio is called the gain of the ILO)
3. the circuit parameters.

The injection-phase locked phenomenon can be further characterized by analogies to an oscillator operating into a mismatched load[4,15,21,24].

The aims of this work include the examination of the dynamic phase-locking properties of microwave IMPATT diode oscillators when the reference signal is angle-modulated. The ILO has been characterized within certain limits for the steady-state and transient conditions[1,4]. Several simplifications are applied to the mathematical model such that the analytic expressions can be used to characterize the ILO under low frequency modulated conditions. However, when the modulating frequency increases, the techniques discussed so far will not be valid. Therefore, the aim of this work is to characterize the ILO for modulating signals approaching the locking limits. This will be accomplished by modelling the ILO with the aid of the generalized Adler's phase-locking equation. The amplifier model will treat the reference (locking) and locked signals of the ILO as input and output signals of a baseband amplifier, respectively. The resulting mathematical treatment will be presented in the form of conventional distortion curves for each set of ILO amplifier parameters. The distortion curves are combined into design contours such that a circuit designer will use them in selecting ILO limiting parameters. Finally,

the theoretical description of the ILO characteristics are verified experimentally.

CHAPTER II

THEORETICAL ANALYSIS OF AN INJECTION-LOCKED OSCILLATOR (ILO)

2.1 Introduction

This chapter will derive the important relationships and equations applicable to the modelling of the injection-locking phenomenon that follows.

2.2 The Generalized Adler's Phase-Locking Equation

Several authors have derived phase-locking equations that may be used to model an injection-locked oscillator (ILO) at microwave frequencies [1-4,17]. It is propitious to discuss the derivations of these phase-locking equations in some detail so that the inherent assumptions will be understood in the context of this work. The results of these derivations will then be used as a basis for the description of the nonlinear distortion added by an ILO amplifier to modulated locking signals.

Let the simplified microwave circuit of Fig. 2.2-1 represent the typical schematic for the ILO considered in this study [4]. The microwave "locking signal" and the "output signal" are separated by a four-port microwave circulator. Therefore, for practical purposes, the input and output signals may be considered to be isolated. In the analysis to follow, it will be shown that the locking signal has a tendency to "pull" the

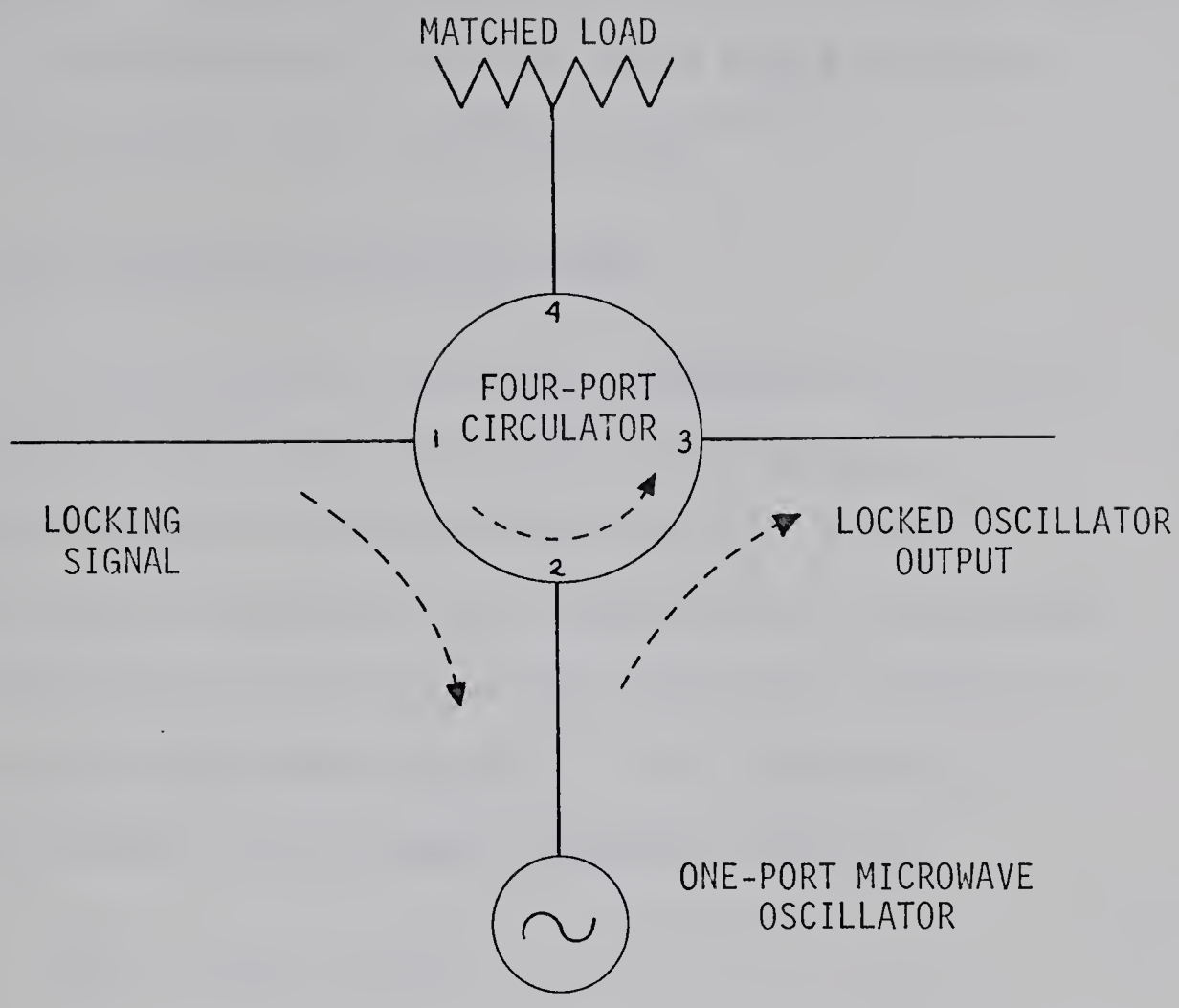

FIG. 2.2-1 EMBODIMENT OF THE INJECTION-LOCKING CIRCUIT AT MICROWAVE FREQUENCIES.

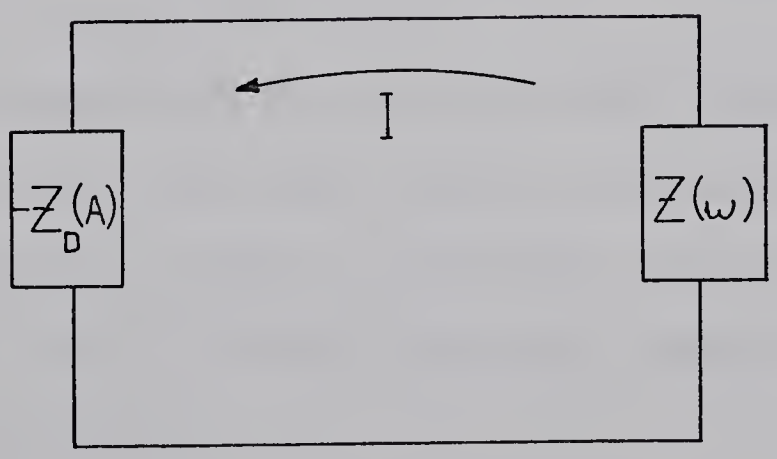

FIG.2.2-2 EQUIVALENT CIRCUIT OF A "FREE-RUNNING" MICROWAVE OSCILLATOR WHERE $Z(\omega)$ IS THE CIRCUIT IMPEDANCE SEEN FROM THE DEVICE($-Z_D(A)$ IS THE DEVICE IMPEDANCE).

frequency of the one-port microwave oscillator in a manner analogous to the frequency pulling which occurs when a microwave oscillator operates into a mismatched load[1-4,15].

2.2-1 Basic Concepts and Approximations

To facilitate an analytical mathematical treatment of the reflection-type amplifier, several simplifying physical assumptions need to be made at this juncture[1]. Firstly, it is assumed that the bandwidth of the resonant circuit surrounding the active device is much larger than the locking bandwidth or than any other modulating frequency. For a single-tuned resonant circuit the half-power bandwidth is given by

$$B.W. = \omega_o/Q_L = \omega_1 - \omega_2 \qquad (2.2\text{-}1)$$

where B.W. = Bandwidth (radians/sec)

ω_o = natural resonant radian frequency

ω_1, ω_2 = half-power point resonant radian frequency

Q_L = loaded quality factor

Secondly, it is assumed that the amplitude control mechanism of the oscillator acts much faster than the time period of the frequencies of interest; namely, a) modulating frequencies, b) beat frequencies, and c) "pulled" frequencies. Mathematically expressed, this means that

$$T' << 1/\Delta\omega_{max} \text{ or } 1/\omega_m \text{ or } 1/\Delta\omega_o \qquad (2.2\text{-}2)$$

where T' = time constant of the amplitude limiting mechanism

$\Delta\omega_{max}$ = maximum frequency deviation

$\Delta\omega_o$ = initial frequency difference

ω_m = modulating radian frequency

As a first approximation, the results achieved by ignoring the amplitude control mechanism are remarkably good[24]. As will be discussed later, the above assumption may not always be justified for the microwave oscillators used in this analysis. Thirdly, it is assumed that the input locking signal power is significantly smaller than the free-running oscillator power. As will be seen, this basic assumption leads to a simplified analysis that yields many of the basic ILO characteristics. However, most practical microwave ILO amplifiers will find application in an intermediate region, where the input and output levels differ by 10 to 20 dB. Consequently, the following analysis will contain an important improvement over Adler's simpler theory[1]. The next section will derive the locking equations applicable to this intermediate power range[3].

2.2-2 Equivalent Circuit Representation

The simplest equivalent circuit for a microwave oscillator is given for the "free-running" condition. Assuming for the moment that the device impedance is frequency independent, let the equation for the free-running

oscillator of Fig. 2.2-2 be given by

$$[\, \mathcal{Z}\ (\omega) - \mathcal{Z}_D(A)\ ]\cdot I = 0 \qquad (2.2\text{-}3)$$

where $\mathcal{Z}_D(A)$ is the device impedance, which is taken to be a function primarily of the current amplitude A, and where $\mathcal{Z}(\omega)$ is the circuit impedance as seen looking out from the device terminals[17].

To construct an equivalent circuit to provide a description of the injection-locking circuit of Fig. 2.2-1, let the input signal be represented by a current generator (it could analogously have been a voltage generator). Next, let the one-port microwave oscillator be represented by an equivalent parallel circuit impedance,the tuned cavity by an equivalent parallel circuit impedance. Thus it is seen that the equivalent circuit of Fig. 2.2-3 easily becomes Fig. 2.2-4 [17, 25-30]. For purposes of this study, the diode may be represented by its equivalent negative impedance $-G$ [20,21]. With reference to Fig. 2.2-5, the following symbols will be defined:

$\mathcal{Z}_D = -G_D$

G_D = Equivalent negative conductance of the free-running oscillator

$\mathcal{Z}_c$ = equivalent cavity impedance

$\mathcal{Z}_c'$ = equivalent cavity impedance plus the equivalent impedance plus the load

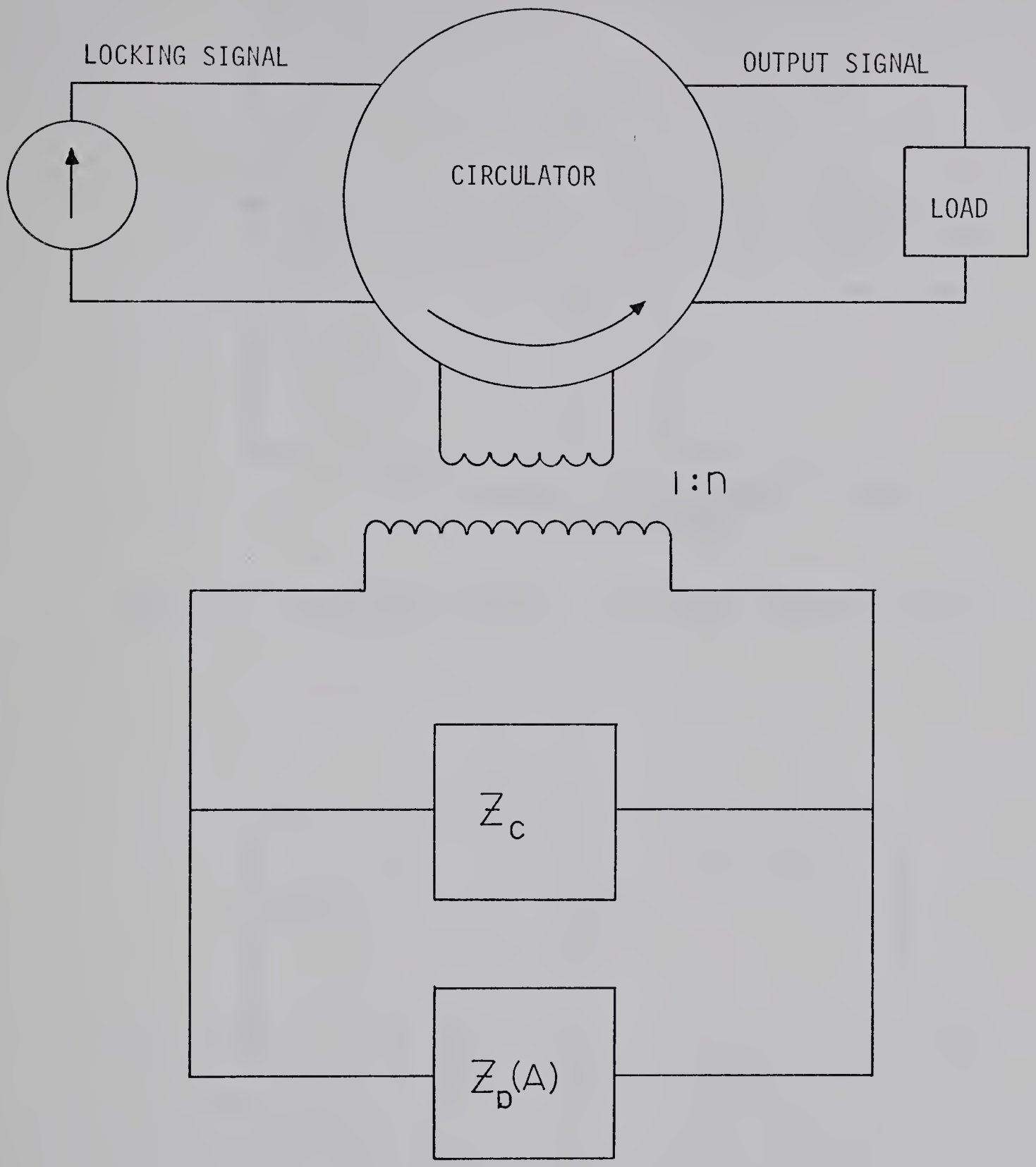

FIG. 2.2-3 INJECTION LOCKED OSCILLATOR(ILO) EQUIVALENT CIRCUIT CONCEPT(WHERE $Z_D(A)$= DIODE IMPEDANCE AND Z_C = CAVITY IMPEDANCE).

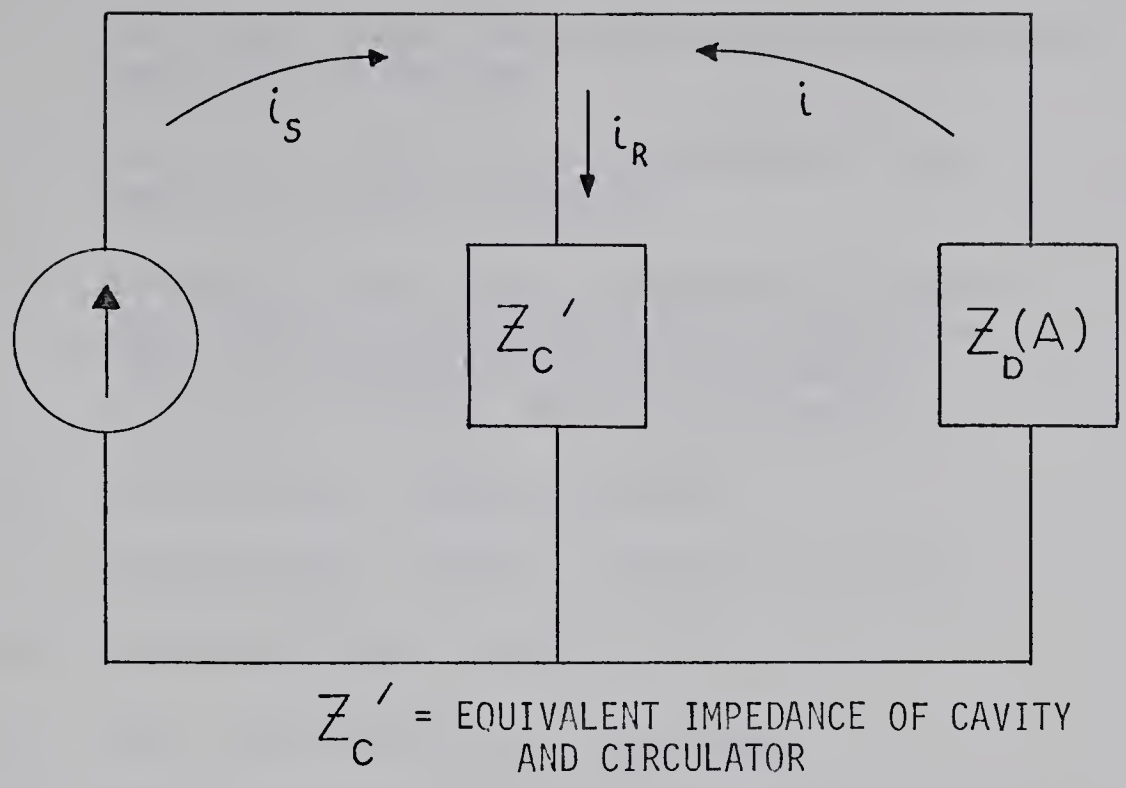

FIG. 2.2-4 EQUIVALENT PARALLEL IMPEDANCE REPRESENTATION OF AN ILO.

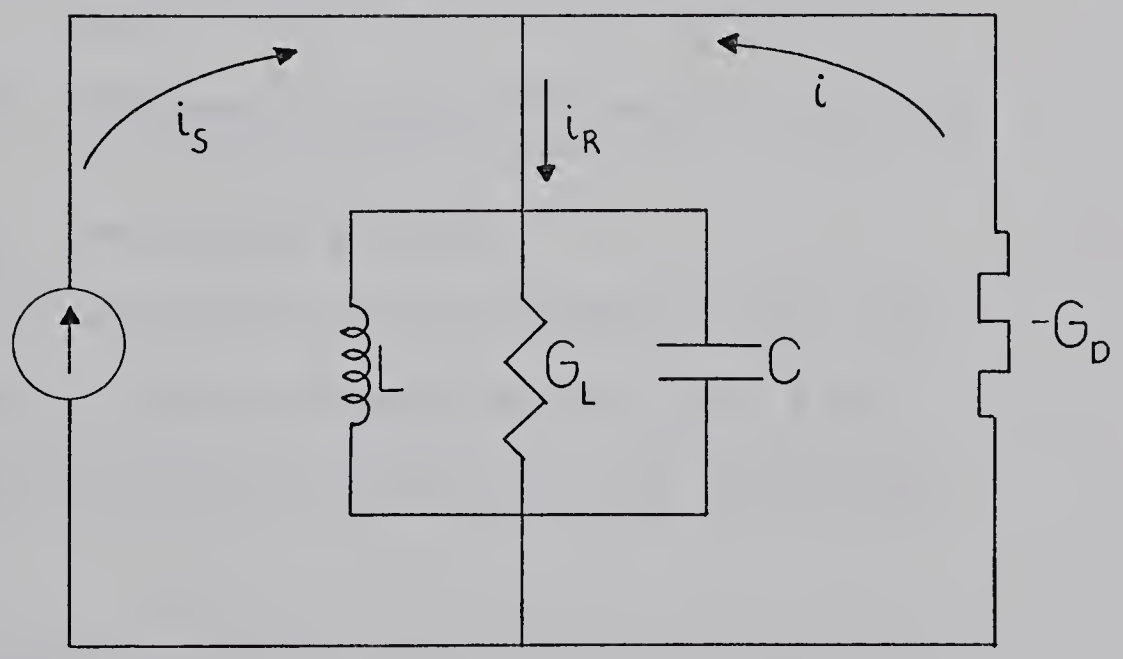

FIG. 2.2-5 EQUIVALENT PARALLEL CIRCUIT FOR THE ILO.

L = equivalent lumped shunt inductance of the tuned cavity near resonance

C = equivalent lumped shunt capacitance of the tuned cavity near resonance

G_L = equivalent lumped shunt conductance of the load (initially assumed to be a match) plus that of the tuned cavity near resonance plus the circulator equivalent impedance

i_s = instantaneous injected current

i = instantaneous "locked" oscillator current

i_R = resultant output current

$I_s = |i_s|$ = injected current amplitude

$I = |i|$ = oscillator current amplitude

$I_R = |i_R|$ = output current amplitude

ω_s = unmodulated injected signal radian frequency

ω_o = "free-running" oscillator radian frequency

$\alpha(t)$ = instantaneous phase shift of the locking signal

$\phi(t)$ = instantaneous phase shift added by the tuned circuit and other mis-matchs

Q_L = loaded quality factor

Even though the circulator has been replaced in Fig. 2.2-4 and Fig. 2.2-5, it must be remembered that i_s and i are isolated signals which add vectorially in the tuned output circuit.

2.2-3 Phasor Analysis

Let the injecting signal of Fig. 2.2-5 be represented by

$$i_s = I_s \sin(\omega_s t + \alpha(t)) \qquad (2.2\text{-}4)$$

where $\alpha(t)$ is a time-dependent phase shift. When the locked condition exists the locked oscillator current will be

$$i(t) = I \sin(\omega_s t + \alpha(t) - \theta(t)). \qquad (2.2\text{-}5)$$

Here $\theta(t)$ has been introduced to represent the instantaneous phase shift of the locked oscillator signal with reference to the injected signal. Thus the total instantaneous current flowing through the resonant circuit will be the vector sum of $i(t)$ and $i_s(t)$, which will be given by

$$i_R = I_R \sin(\omega_s t + \alpha(t) - \theta(t) + \phi(t)) \qquad (2.2\text{-}6)$$

where

$$I_R = \sqrt{I_s^2 + I^2 + 2II_s\cos\theta(t)} \qquad (2.2\text{-}7)$$

and

$$\phi(t) = \tan^{-1} \frac{I_s \cdot \sin(t)}{I + I_s \cos\theta(t)} \qquad (2.2\text{-}8)$$

The various signals are represented in the phasor diagram Fig. 2.2-6.

2.2-4 Derivation of the Generalized Adler's Phase-Locking Equation

Since the term $\phi(t)$ in Eq. 2.2-6 is the phase shift introduced by the addition of the tuned circuit, it follows

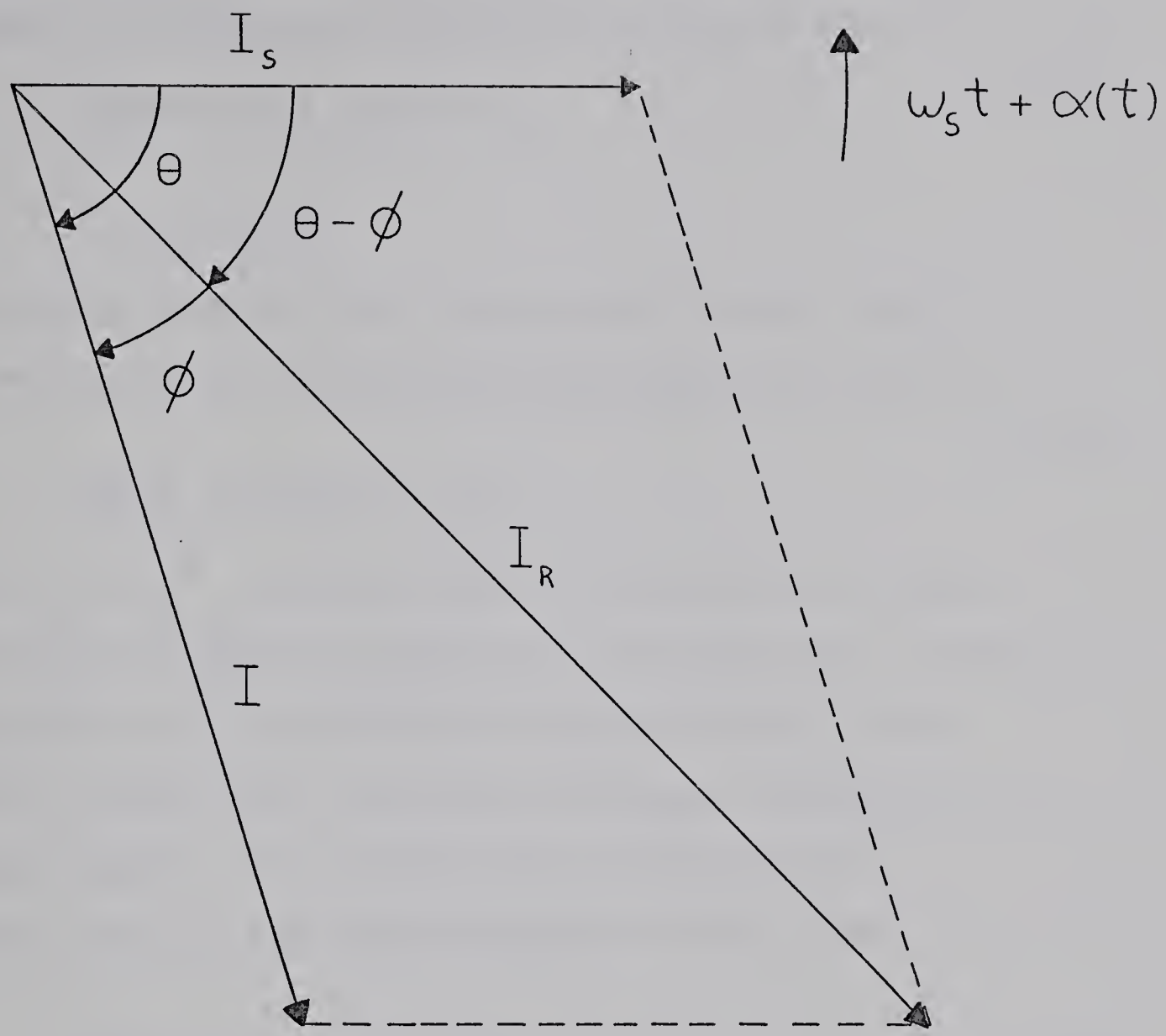

FIG. 2.2-6 THE PHASOR REPRESENTATION OF THE SIGNALS IN THE ILO MODEL.

that Eq. 2.2-8 may be simplified in terms of the other circuit parameters. For a single-tuned parallel circuit with lumped parameters, the phase shift across the circuit will vary as

$$\Phi(\omega)=\tan^{-1}[Q_L(\omega_o^2-\omega^2)/\omega_o^2] \qquad (2.2\text{-}9)$$

where $\omega_o = 1/\sqrt{LC}$

In the locked condition, the frequency ω will be very close to ω_o, so that Eq. 2.2-9 may be approximated quite accurately by

$$\Phi(\omega)\cong -\tan^{-1}[2Q_L(\omega-\omega_o)/\omega_o] \qquad (2.2\text{-}10)$$

when $\omega-\omega_o \ll \omega_o$ [28]. The phase shift introduced by the resonant circuit will be opposite to the phase shift of the total current, consequently the voltage across the resonant circuit will be exactly π radians out of phase with the voltage introduced by the injected signal. This principle will also apply to the currents; this Eq. 2.2-10 may be equated with Eq. 2.2-8:

$$\frac{I_S \sin\theta(t)}{I + I_S\cos\theta(t)} = \frac{2Q_L(\omega-\omega_o)}{\omega_o} \qquad (2.2\text{-}11)$$

Solving Eq. 2.2-11 for ω yields,

$$\omega = \omega_o + \frac{\Delta_o \sin\theta(t)}{1+R\cos\theta(t)} \qquad (2.2\text{-}12)$$

where $\Delta_o = \omega_o R/2Q_L$ (2.2-13)

and $R = I_S/I$ (2.2-14)

Thus the output phase angle from Eq. 2.2-6 and Fig. 2.2-6 is

$$\theta_R(t) = \omega_s t + \alpha(t) - \theta(t) + \phi(t) \tag{2.2-15}$$

and the output frequency is given by the derivative of Eq. 2.2-15:

$$\omega_R = \frac{d\,\theta_R(t)}{dt} = \omega_s + \frac{d\alpha(t)}{dt} + \frac{d\,\phi(t)}{dt} - \frac{d\theta(t)}{dt} \tag{2.2-16}$$

Now, combining Eq. 2.2-16 and Eq. 2.2-12 yields

$$\frac{d\theta(t)}{dt} - \frac{d\phi(t)}{dt} + \frac{\Delta_o \sin\theta(t)}{1+R\cos\theta(t)} = \Delta\omega_o + \frac{d\alpha(t)}{dt} \tag{2.2-17}$$

where $\Delta\omega_o = \omega_s - \omega_o$ (2.2-18)

= the initial radian frequency difference.

Then differentiating Eq. 2.2-8 yields

$$\frac{d\phi(t)}{dt} = \frac{R(\,R + \cos\theta(t))}{1 + R^2 + 2R\cos\theta(t)} \cdot \frac{d\,\theta(t)}{dt} \tag{2.2-19}$$

which will be used to eliminate the $\frac{d\phi}{dt}$ terms of Eq. 2.2-17; i.e.

$$\frac{d\theta(t)}{dt} = \left(\frac{1 + R^2 + 2R\cos\theta(t)}{1 + R\cos\theta(t)}\right) \left(\Delta\omega_o + \frac{d\alpha(t)}{dt} - \frac{\Delta_o \sin\theta(t)}{1 + R\cos\theta(t)}\right) \tag{2.2-20}$$

The solution to Eq. 2.2-20 yields the instantaneous change of phase between the input locking signal and the output signal from the locked negative conductance oscillator. Eq. 2.2-20 will hereafter be referred to as "the Generalized Adler's Phase-Locking Equation" because of its importance in the following work. To solve for $\phi(t)$, Eq. 2.2-20 may be substituted into Eq. 2.2-8. Further, the output frequency will be found by substituting Eq. 2.2-17 into Eq. 2.2-16 to yield

$$\omega_R(t) = \omega_o + \frac{\Delta_o \sin\theta(t)}{1 + R\cos\theta(t)} \qquad (2.2\text{-}21)$$

2.2-5 Adler's Equation

In special cases, Eq. 2.2-20 must be simplified by assuming a) a low level of injected locking power i.e. $R \ll 1$ and b) that there is no significant modulation on the injected signal (i.e. $\frac{d\alpha(t)}{dt} \cong 0$). Then Eq. 2.2-20 reduces to Adler's phase-locking equation which (when expressed in terms of the notation used in this thesis) becomes

$$\frac{d\theta(t)}{dt} = \Delta\omega_o - \Delta_o \sin\theta(t) \qquad (2.2\text{-}22)$$

where

$$\Delta_o = E_L \cdot \omega_o / 2 \cdot E_o \cdot Q_L \qquad (2.2\text{-}23)$$

(where E_L and E_o are the voltage amplitudes defined by Adler which are equivalent to the expressions used here). The

Generalized Adler's phase-locking equation that has been derived in this section provides the basis for extensive later work; in particular, it will be used to solve for the distortion behavior of ILO's.

2.3 Steady-State ILO Characteristics

This section will examine the locking equations derived in Section 2.2 by applying the quasi-stationary approximation to all time-dependent terms. The elimination of the transient solution will enable the locking equation limits to be examined for the steady-state case. For Adler's locking equation Eq. 2.2-22, the steady-state phase shift may be expressed as a function of normalized initial frequency difference; i.e.

$$\Theta = \sin^{-1} \Delta\omega_o / \Delta_o \qquad (2.3\text{-}1)$$

when $\frac{d\theta(t)}{dt} = 0$. When the quasi-stationary approximation is applied to the generalized Adler's phase-locking equation Eq. 2.2-20, the steady-state phase shift may be expressed as

$$\Theta = \sin^{-1}\left(\frac{u}{1 + u^2R^2}\left[1 \pm R\sqrt{1 - u^2(1 - R^2)}\right]\right) \qquad (2.3\text{-}2)$$

where $u = \Delta\omega_o/\Delta_o$ and $R = I_s/I$ (from Eq. 2.2-14), the plus sign applies for $u>0$ and, alternately, the minus sign applies for $u<0$. It is evident that Eq. 2.3-2 reduces to Eq. 2.3-1 for $R<<1$. Now let these two "steady-state" results be

examined for their limit variation when certain parameters are changed.

Firstly, let the maximum initial frequency difference occur when $\sin\theta$ has its maximum value (i.e. $\sin\theta = 1$) in Eq. 2.2-21; i.e.,

$$|\Delta\omega_o|_{max} = \Delta_o \tag{2.3-3}$$

Utilizing a similar normalizing procedure, the generalized Adler's phase-locking equation Eq. 2.2-20 yields its maximum allowable initial frequency difference; namely,

$$|\Delta\omega_o|_{max} = \Delta_o / (1 - R^2)^{1/2} \tag{2.3-4}$$

Secondly, the maximum allowable phase shift $|\theta|_{max}$ that an ILO will permit and still maintain the locked condition is $\frac{\pi}{2}$ for Eq. 2.2-21. For the generalized Adler's phase-locking equation $|\theta|_{max}$ is

$$|\theta|_{max} = \frac{\pi}{2} + \cos^{-1}(1 - R^2)^{\frac{1}{2}} \tag{2.3-5}$$

It is interesting to note that the generalized Adler's phase-locking equation predicts a) a maximum allowable phase shift in excess of $\frac{\pi}{2}$ and b) a maximum locking bandwidth in excess of Δ_o. In both cases the limits are directly proportional to the injected signal amplitude I_s and inversely proportional to the "free-running" oscillator amplitude I. When the ratio R is expressed in terms of power it becomes

$$R = (P_S/P)^{1/2} \tag{2.3-6}$$

where P_S refers to the injected power and P refers to the "free-running" oscillator power. When R is expressed in a different form, the ratio of injected to output power will give the gain of the ILO as an amplifier, where gain is defined as

$$G = -10 \log_{10} P_S/P \quad dB \tag{2.3-7}$$

or

$$G = -20 \log_{10} R \quad dB \tag{2.3-8}$$

Several authors have documented extensive investigations of this "steady-state" analysis [1,8-12,27]. For the purposes of this work the results predicted by the "steady-state" analysis will be exploited in a simplified theory to justify the experimental set-up. Therefore, in Table 2.3-1 the maximum locking bandwidth and the maximum phase shift limits predicted by the generalized Adler's phase-locking equation are compared with the predictions from Adler's equation for similar values of gain. An examination of Table 2.3-1 shows that only for gains in excess of 20dB will both equations predict essentially identical results.

2.4 Transient Response of an ILO

In this section Mackey's[4] approach to describing the transient behavior of ILO's is reviewed and an attempt

TABLE 2.3-1 A COMPARISON OF THE VARIOUS LIMITS PREDICTED BY THE GENERALIZED ADLER'S PHASE-LOCKING EQUATION (EQ 2.2-20) WITH THOSE PREDICTED BY ADLER'S EQUATION (EQ. 2.2-22) WHEN THE QUASI-STATIONARY APPROXIMATION IS VALID.

R	GAIN= -20logR	FREQUENCY DIFFERENCE*	PHASE DIFFERENCE**
1.00×10^{-4}	80 dB	5.00×10^{-9}	5.73×10^{-3}
1.00×10^{-3}	60 dB	5.00×10^{-7}	5.73×10^{-2}
1.00×10^{-2}	40 dB	5.00×10^{-5}	5.73×10^{-1}
2.00×10^{-2}	34 dB	2.00×10^{-4}	1.15
5.00×10^{-2}	26 dB	1.25×10^{-3}	2.87
7.00×10^{-2}	23.1dB	2.46×10^{-3}	4.01
1.00×10^{-1}	20 dB	5.04×10^{-3}	5.74
1.50×10^{-1}	16.5dB	1.14×10^{-2}	8.63
2.00×10^{-1}	14 dB	2.05×10^{-2}	1.15×10^{1}
3.16×10^{-1}	10 dB	1.11×10^{-1}	1.84×10^{1}
5.62×10^{-1}	5 dB	8.27×10^{-1}	3.42×10^{1}

* Normalized initial frequency difference predicated by Eq. 2.2-20 minus the result of Eq. 2.2-22; namely, $\frac{1}{\sqrt{1-R^2}} - 1$

** Maximun initial phase difference predicated by Eq. 2.2-20 minus the result from Eq. 2.2-22. This result is expressed in degrees, i.e. $\cos^{-1}\sqrt{1-R^2}$

is made to apply those concepts to the present study of ILO's. The previous section discussed the ILO characteristics when the quasi-stationary approximation was valid. However, when the ILO is subjected to a step change in the locking frequency or to some other form of modulating signal with a short rise time, the ILO is not expected to track this change instantaneously. The transient phase response of an ILO to such a frequency step will be discussed next in order to find an upper limit on the modulation rate for such an ILO.

When the locking signal changes at rates in excess of $\Delta_o/2\pi$ Hz the quasi-stationary approximation will no longer be valid. Consequently, the solution to the phase equations, Eqs. 2.2-20 and 2.2-22 must take into account the time-dependent terms. When Adler's equation is solved in the time domain (as a first approximation of the expected results), the integration must be performed as

$$\int_{\theta_o}^{\theta} \frac{d\theta(t)}{\sin\theta - u} = -\Delta_o \int_o^t dt \qquad (2.4\text{-}1)$$

where $\theta(0) = \theta_o$, $u = \Delta\omega_o/\Delta_o$ and $u < 1$. When $\theta(t)$ is integrated it becomes

$$\theta(t) = 2\tan^{-1}\left\{\frac{1}{u}\left[1 - (1-u^2)^{\frac{1}{2}} \tanh^{-1}\left(C_1 + \frac{\Delta_o(1-u^2)^{\frac{1}{2}}t}{2}\right)\right]\right\} \qquad (2.4\text{-}2)$$

where

$$C_1 = \tanh^{-1} \left[1-u\tan(\theta_o/2) \right] / (1-u^2)^{1/2}$$

For the special case of u=0, Eq. 2.3-1 leads directly to

$$\theta(t) = 2 \tan^{-1} (e^{-\Delta_o t} \tan \theta_o/2) \qquad (2.4\text{-}3)$$

If $\theta(t)$ is limited to less than 60 degrees, then the approximation $\tan \theta \cong \theta$ is valid to better than 10 percent of $\theta(t)$. Consequently, Eq. 2.4-3 may be simplified to

$$\theta(t) = \theta_o e^{-\Delta_o t} \qquad (2.4\text{-}4)$$

This approximate solution gives an elementary estimate of the decay time of the phase shift $\theta(t)$. This time is

$$t' = 1/\Delta_o \text{ sec.} \qquad (2.4\text{-}5)$$

for $\theta_o < \pi/3$ and $\theta(\infty) = u = 0$. The decay time t' suggests that the upper limit on the modulating frequency appears to be $\Delta_o/2\pi$ Hz. The simplified solutions discussed thus far do not apply if a) $\theta_o > \pi/2$ b) $u \neq 0$, or c) the generalized Adler's phase-locking equation needs to be solved as the phase equation (i.e. increased complexity for the lower gain cases). Thus, these more general solutions will all have decay times significantly in excess of those estimated in Eq. 2.4-5. These more complex solutions are discussed in great detail in the literature[3,4] . For the purposes of this study the result that may be used from the transient

response work is that normally the decay time is contained in periods of time less than $t' \leq 5/\Delta_o$ sec.

A more practical approach to the quantizing of a numerical value for the limit of the modulating frequency in an ILO is the subject of the next several chapters. To close this section a single graph of the time response of Eq. 2.4-3 for several values of θ_o is included to illustrate the general concepts of the decay time for a step change in frequency (see Fig. 2.4-1). Any degradation of parameters from those assumed will result in a much longer settling time and a lower limit to the modulating frequency. Lastly this graph also indicates that this approach is not practical in estimating accurately the numerical value of the distortion that an ILO adds to a modulating signal.

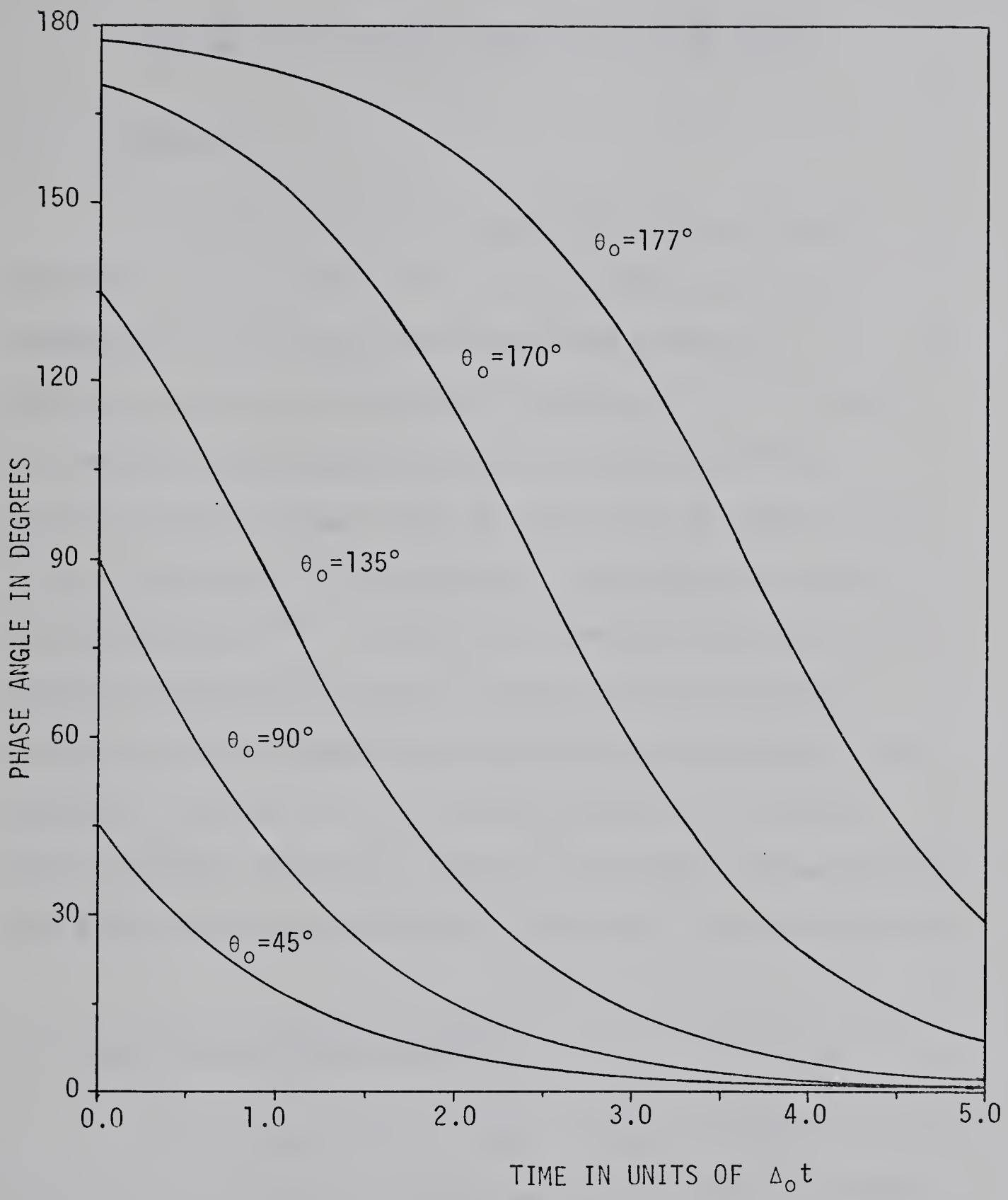

FIG. 2.4-1 PLOT OF THE TRANSIENT PHASE RESPONSE EQ. 2.4-3 VERSUS THE NORMALIZED TIME FOR SEVERAL VALUES OF θ_o.

CHAPTER III

LOCKING TO A FREQUENCY MODULATED LOCKING SIGNAL

3.1 Introduction

In this chapter, the phase shift versus frequency deviation characteristics of ILO's are used as an aid in interpreting ILO behavior under modulated conditions [1-12]. The modulating signal $\alpha(t)$ (defined in section 3.2) will be used to sweep the ILO through its entire locking range ($\pm\Delta_0$), starting with low sweep rates and progressing to higher rates. Several procedures will be employed to describe the deviation characteristics [8-21]. Initially, elementary analysis will be employed to describe the phase variation and more complex solutions will be sought as a more accurate description of the phenomena involved. Lastly, an examination will be made of the assumptions upon which several of the phase-locking equations are based, when the limits of their applicability are approached.

3.2 Modelling and Signal Analysis

For the work that follows, let the ILO model as shown in Fig. 2.2-1 be used. The injected current (following Section 2.2) is given by

$$i_s = I_s \sin(\omega_s t + \alpha(t)) \qquad (3.2\text{-}1)$$

where i_s = the injected signal current at microwave frequencies

I_s = the magnitude of the injected signal

ω_s = unmodulated injected signal radian frequency

and the modulating signal is given by

$$\alpha(t) = \int (A_m \sin \omega_m t)\, dt \qquad (3.2\text{-}2)$$

where A_m = the peak frequency deviation (PFD)

ω_m = the modulating radian frequency

β = the modulation index

$\beta = A_m/\omega_m$

Consequently, the output signal current will be, from Eq. 2.2-6

$$i_R = I_R \sin(\omega_o t + \alpha(t) - \theta(t) + \phi(t)) \qquad (3.2\text{-}3)$$

where $$I_R = I\left[1 + R^2 + 2R\cos\theta\right]^{1/2} \qquad (3.2\text{-}4)$$

and $$\phi(t) = \tan^{-1}(R\sin\theta/1 + R\cos\theta) \qquad (3.2\text{-}5)$$

where $\theta(t)$ will be found by the solution of

$$\frac{d\theta(t)}{dt} = \left[\frac{1+R^2+2R\cos\theta(t)}{1+R\cos\theta(t)}\right].\left[\Delta\omega_o + \frac{d\alpha(t)}{dt} - \frac{\Delta_o \sin\theta(t)}{1+R\cos\theta(t)}\right] \qquad (3.2\text{-}6)$$

3.3 Quasi-Stationary Equation Analysis

Initially let the ILO be swept at low rates so that

only an approximate solution will be required to provide the necessary accuracy for the description of the ILO characteristics (recall the applicability of the quasi-stationary approximation). To put these simplifications on a more mathematical basis, let the gain of the ILO be greater than 20 dB (i.e. $R << 1$, then $\phi << \theta$, and $I_R \cong I$). Then the output current may be approximated by

$$i_R = I_R \sin(\omega_s t + \alpha(t) - \theta(t)) \qquad (3.3\text{-}1)$$

where $\theta(t)$ is found by solving Eq. 3.2-6; namely,

$$\frac{d\theta(t)}{dt} = \Delta\omega_o + \frac{d\alpha}{dt} - \Delta_o \sin\theta \qquad (3.3\text{-}2)$$

Let the modulating signal Eq. 3.2-2 sweep the ILO through its entire locking range (i.e. $A_m = \Delta_o$) at very low rates (i.e. $\omega_m << \Delta_o$). Then $\frac{d\theta}{dt}$ will approach zero and the quasi-stationary approximation will be valid. It is possible to approximate the effect of $\frac{d\alpha}{dt}$ at any instant of time as an instantaneous radian frequency ω, i.e.

$$\omega = \omega_s + \left| A_m \sin \omega_m t \right| \qquad (3.3\text{-}3)$$

where ω_s is defined as in Fig. 3.2-1. The phase shift θ will be given by solving Eq. 3.3-2 for $\frac{d\theta}{dt} = 0$, and the result is a simple analytic solution

$$\theta = \sin^{-1}\left[\frac{\omega - \omega_s + \Delta\omega_o}{\Delta_o}\right] \qquad (3.3\text{-}4)$$

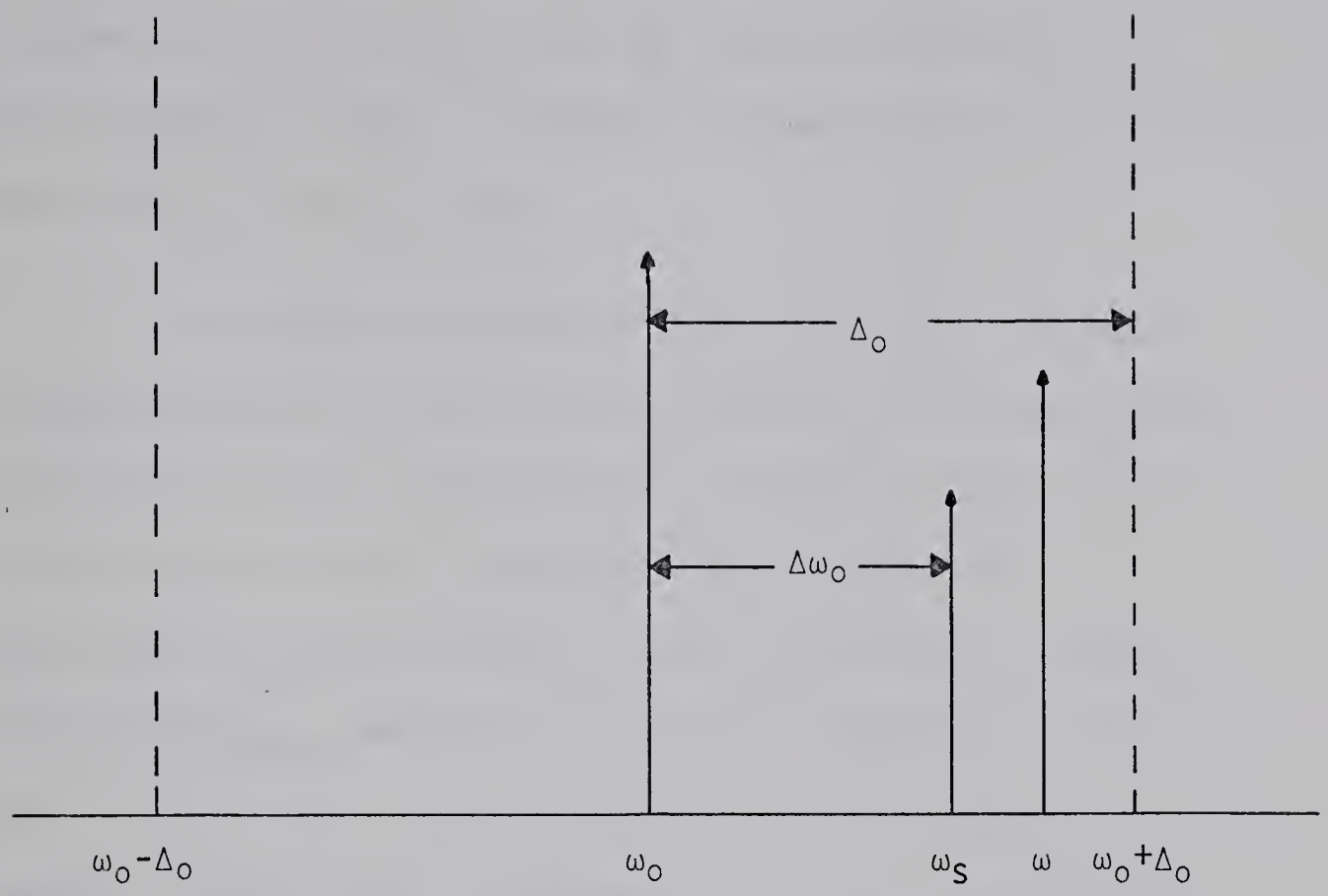

ω_o = "FREE-RUNNING" LOCKED OSCILLATOR RADIAN FREQUENCY

ω_s = "FREE-RUNNING" UNMODULATED LOCKING SIGNAL RADIAN FREQUENCY

$\Delta\omega_o$ = $\omega_s-\omega_o$ = INITIAL FREQUENCY DIFFERENCE

ω = INSTANTANEOUS RADIAN FREQUENCY OF THE ILO WITH A MODULATING SIGNAL APPLIED

$\Delta_o = \frac{\omega_o R}{2Q_L}$ = HALF-LOCKING BANDWIDTH

G = -20 LOG R = GAIN EXPRESSED IN DB

FIG 3.3-1 LOCATION OF RADIAN FREQUENCIES IN THE FREQUENCY DOMAIN FOR A SWEPT ILO AMPLIFIER WHEN $\Delta\omega_o < (\omega - \omega_o) < \Delta_o$

To aid in the proper visualization of the various radian frequencies $\omega, \omega_s, \omega_o, \Delta\omega_o$ and the frequency limit Δ_o, at a given instant of time, an example is shown in Fig. 3.3-1 for the case of $\Delta\omega_o < (\omega - \omega_o) < \Delta_o$.

When the instantaneous injected signal ω is swept through the entire locking range of the ILO, the phase versus frequency deviation characteristics is shown in Fig. 3.2-2 for the case of Adler's Equation. These phase shift characteristics may be used to predict the useable symmetric bandwidth $|A_m|_{max}$ and/or the permissible modulating frequency that the modulating signal may have given a certain $\Delta\omega_o$. For example, if the initial frequency difference is set at 0.15 then only 0.85 of the normalized deviation remains for a symmetric sweep. Additionally, if the modulating frequency is such that its effects may not be ignored then by standard FM analysis the addition of the symmetric deviation and the modulating frequency should total less than 0.85 (as a first approximation).

This basic analysis may also be used to predict some of the distortion that may be involved in the transmission by an ILO amplifier. Appendix A defines the transmission distortion concepts that are relevant to this study. For the purposes of this thesis, let the distortionless transmission for an ILO be summarized as

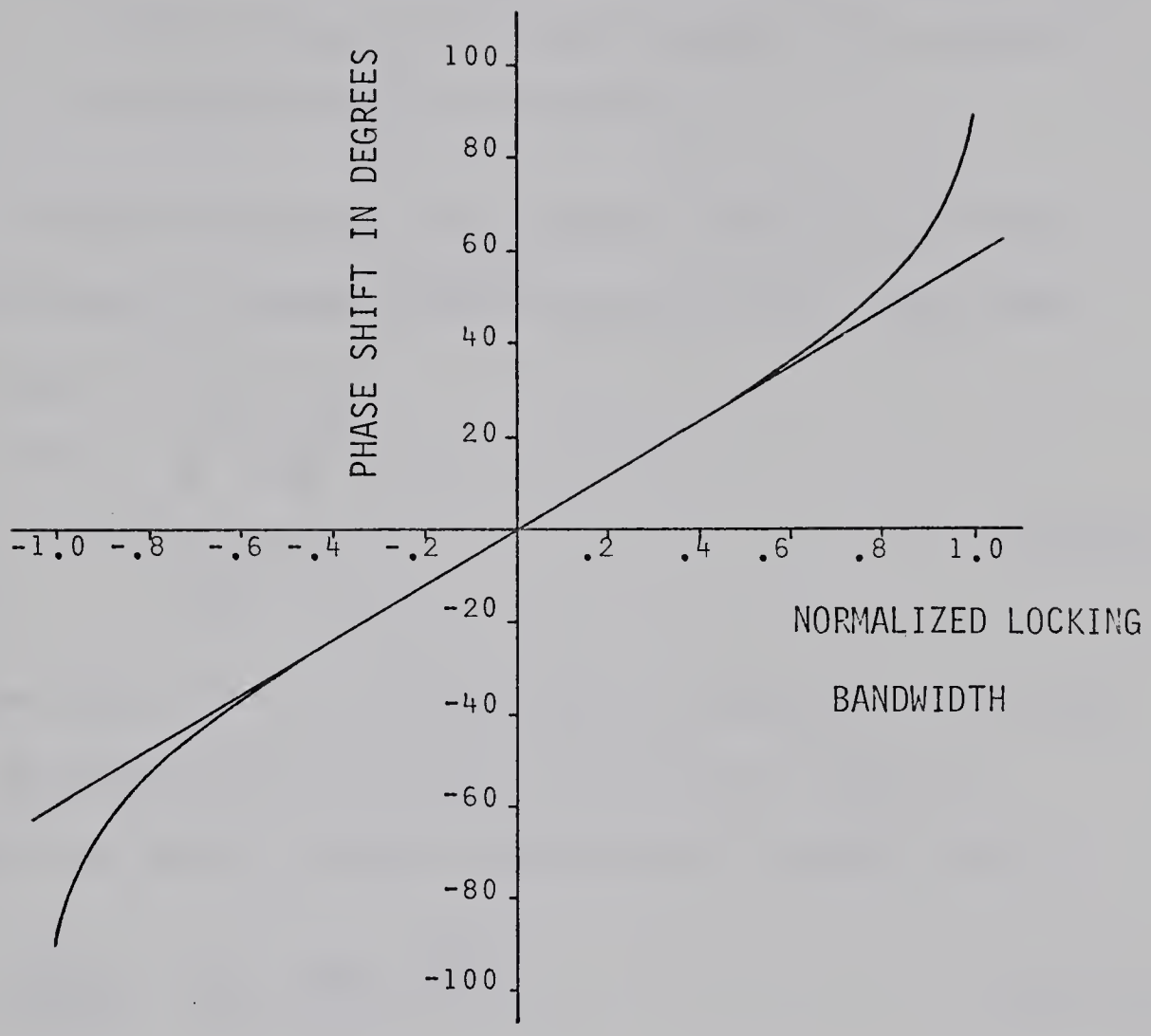

FIG. 3.3-2 A PLOT OF THE PHASE SHIFT EQ. 3.3-4 VERSUS THE NORMALIZED LOCKING BANDWIDTH(FOR $\Delta\omega_o$=0.0).

a) a gain versus frequency characteristic that is constant and,

b) a phase shift versus frequency deviation that varies linearily with the frequency (or a constant envelope delay characteristic).

The envelope delay characteristic (EDD) of an ILO may be approximated by expanding the phase shift of Eq. 3.3-4 about ω_o in a power series; i.e.,

$$\theta \cong z + \frac{z^3}{6} + \frac{3z^5}{40} + \ldots.$$

where $$z = \frac{\omega - \omega_s + \Delta\omega_o}{\Delta_o} \qquad (3.3\text{-}5)$$

The higher order terms of z produce the nonlinearity in the phase shift. By approximating θ with Eq. 3.3-4 and Eq. 3.3-5, it is possible to obtain a simple expression for the EDD; namely,

$$\frac{d\theta}{d(\omega-\omega_o)} = \frac{1}{\Delta_o} \cdot \frac{1}{\sqrt{1-z^2}} \ \frac{\text{sec}}{\text{rad}} \qquad (3.3\text{-}6)$$

When expressed in more conventional units of EDD (i.e. nanoseconds per megahertz), the variable part of Eq. 3.3-6 becomes

$$\text{EDD } \left(\frac{\text{ns}}{\text{MHz}}\right) = \frac{159.2}{f_{max}}\left[\frac{1}{\sqrt{1-z^2}} - 1\right] \qquad (3.3\text{-}7)$$

where $f_{max} = \frac{\Delta_o}{2\pi}$ (expressed in megahertz). The EDD characteristic is shown in Fig. 3.3-3 for the simplification

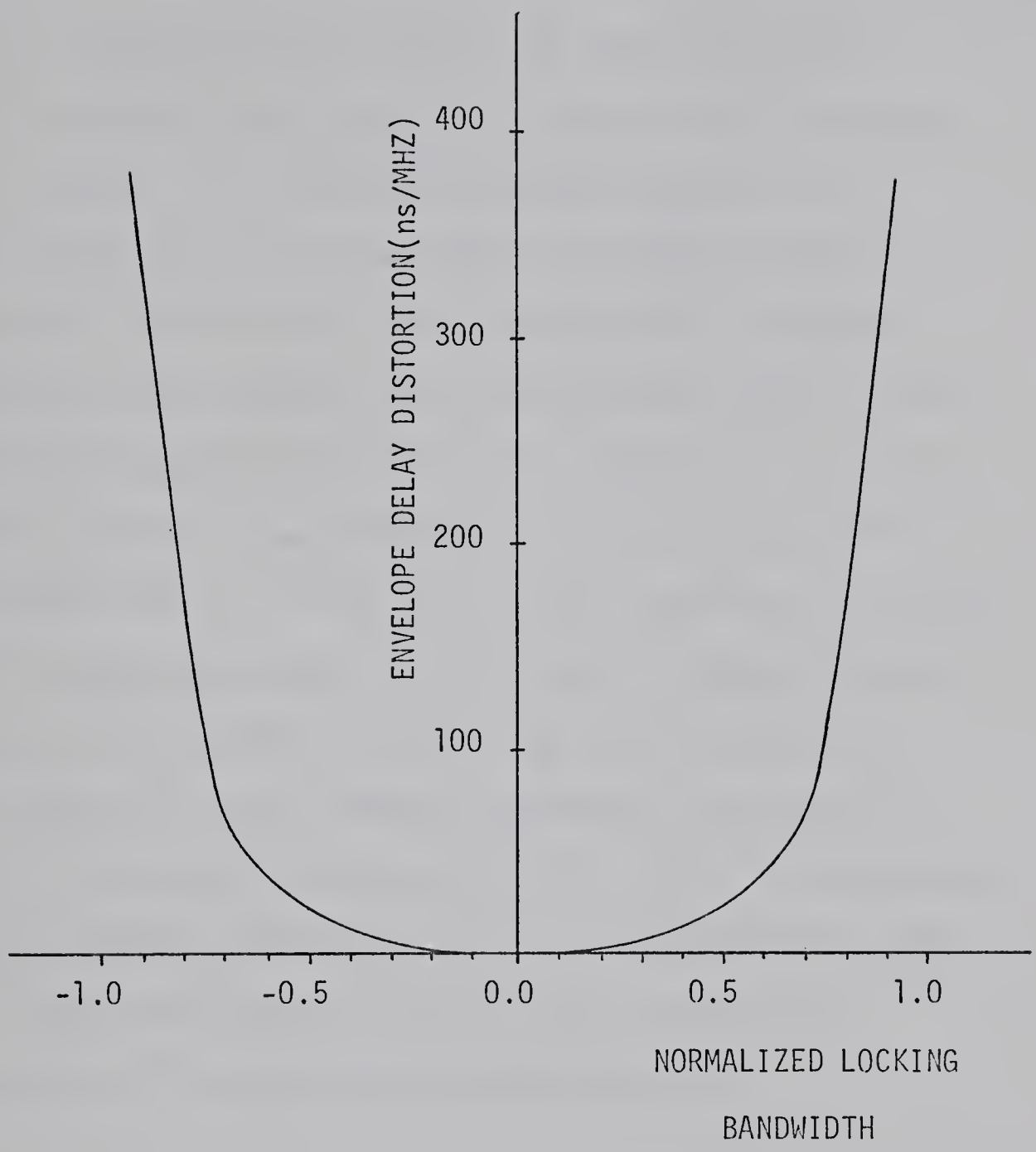

FIG. 3.3-3 A PLOT OF THE ENVELOPE DELAY DISTORTION EQ. 3.3-7 VERSUS THE NORMALIZED LOCKING BANDWIDTH(FOR $\Delta\omega_o$=0.0 AND f_{max}= 1.0MHZ).

as per Eq. 3.3-7.

In the work thus far, it has been assumed that $\Delta\omega_b = 0$ to simplify the results(here referred to as the tuned case). However, it is unlikely that the injected carrier signal frequency and the free-running oscillator frequency will remain identical for a long period of time. Numerous factors have been observed that cause the oscillators to drift (including temperature dependences)[14]. Therefore, it would be more realistic to work through the theoretical model for the detuned case (i.e. $\Delta\omega_b \neq 0$). The only additional distortion that the simple approaches to the distortion characterization predict is a non-symmetrical phase and EDD characteristic. This suggests that less symmetric bandwidth is available to satisfy a particular distortion criterion. When the modulating frequency increases and approaches Δ_o, the approximation $\frac{d\theta}{dt} = 0$ is no longer valid and more sophisticated mathematical techniques will be required to describe the ILO.

3.4 Linearized Equation Analysis

When the quasi-stationary approximation is not valid the dynamic characteristics of the ILO amplifier must be studied by the use of time-dependent solutions to the phase equations.

It will be recalled that Adler's equation is valid for the case when $R<<1$, $\phi<<\theta$ and $I_R \cong I$. When the modulating signal is a sinusoid of the form of Eq. 3.2-2 then Eq. 2.2-22 becomes

$$\frac{d\theta}{dt} = \Delta\omega_o + A_m \sin\omega_m t - \Delta_o \sin\theta \qquad (3.4\text{-}1)$$

Eq. 3.4-1 is nonlinear and may not be solved analytically for the sinusiodal forcing function in a reasonable fashion. However, in that region defined by the maximum frequency deviation $\left|\omega_o + A_m\right|$ and when this is kept less than $0.7\Delta_o$ it is possible to approximate $\sin\theta$ by θ to better than 10 percent. Then the analytic solution to

$$\frac{d\theta}{dt} + \Delta_o\theta = \Delta\omega_o + A_m \sin\omega_m t \qquad (3.4\text{-}2)$$

for $\theta(0) = \theta_o$ is

$$\theta(t) = \left[\theta_o - \frac{\Delta\omega_o}{\Delta_o} + \frac{A_m\omega_m}{\Delta_o{}^2+\omega_m{}^2}\right] e^{-\Delta_o t} + \frac{\Delta\omega_o}{\Delta_o}$$

$$+ \frac{A_m/\Delta_o}{\sqrt{1+\left(\frac{\omega m}{\Delta_o}\right)^2}} \sin\left(\omega_m t - \tan^{-1}\frac{\omega m}{\Delta_o}\right) \qquad (3.4\text{-}3)$$

After the transient solution to $\theta(t)$ becomes negligible in amplitude, the steady-state solution becomes

$$\theta_{ss}(t) = \frac{\Delta\omega_o}{\Delta_o} + \frac{A_m/\Delta_o}{\sqrt{1+\frac{\omega_m}{\Delta_o}^2}} \sin\left(\omega_m t - \tan^{-1}\frac{\omega_m}{\Delta_o}\right) \qquad (3.4\text{-}4)$$

In Fig. 3.4-1 the steady-state solution, Eq. 3.4-4, is displayed as a function of instantaneous normalized frequency deviation (i.e. $\frac{\Delta\omega_o + A_m \sin \omega_m t}{\Delta_o}$) for the following set of parameters:

$$\omega_o/2\pi = 10 \text{ GHz}$$

$$\Delta\omega_o = 0$$

$$A_m = 0.5\,\Delta_o$$

$$\Delta_o/2\pi = 10 \text{ MHz}$$

$$R = 0.1$$

$$\omega_m/2\pi = 200 \text{ kHz}, 2 \text{ MHz}, 10 \text{ MHz}$$

As the modulating frequency increases the phase angle versus frequency deviation characteristics show an ellipse with an increasing minor axis. This phenomenon for the linearized approximation may be entirely explained by the arctangent term of the phase in Eq. 3.4-4.

3.5 Analysis Based Upon Adler's Equation

When the frequency deviation is no longer limited to the range discussed in Section 3.4, then, as $|\Delta\omega_o + A_m|$ approaches Δ_o the approximation $\sin\theta \cong \theta$ will no longer be valid. Therefore, Adler's nonlinear phase equation must now be solved for the accurate representation of the frequency

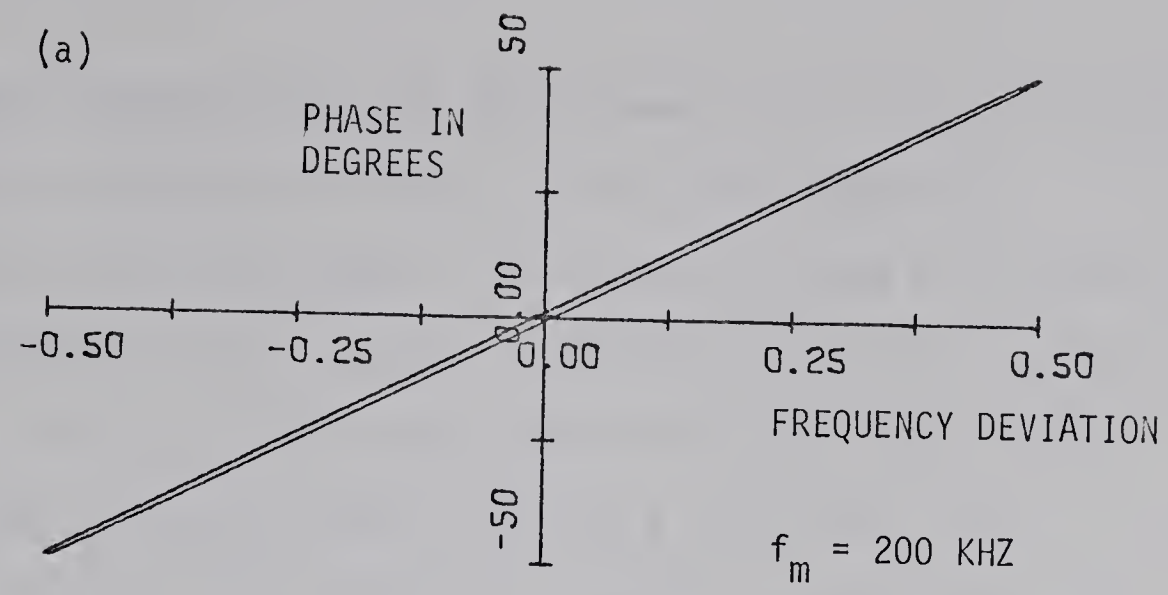

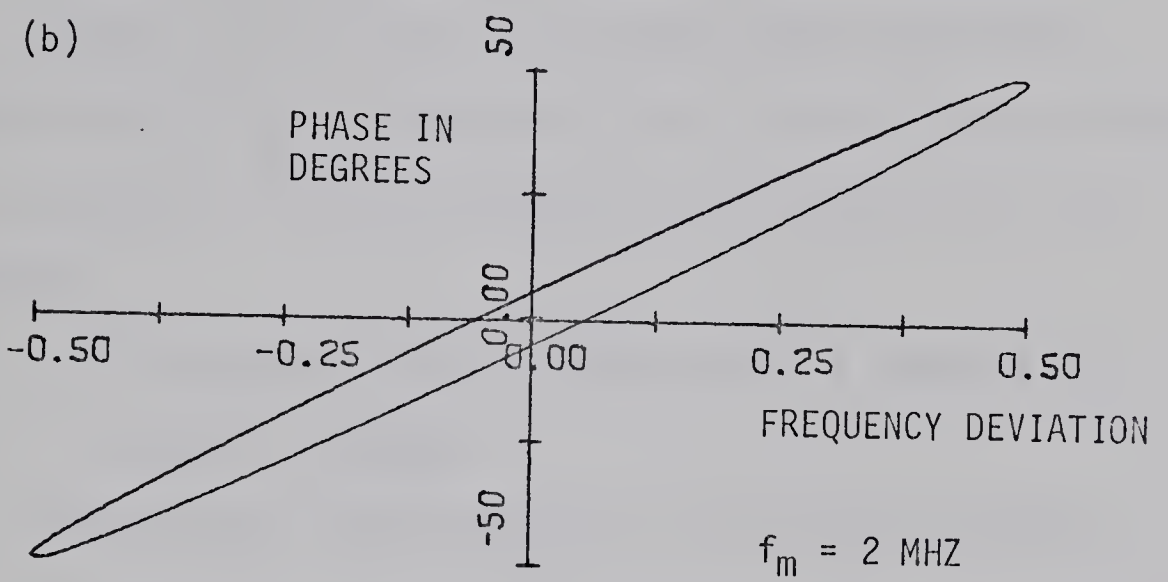

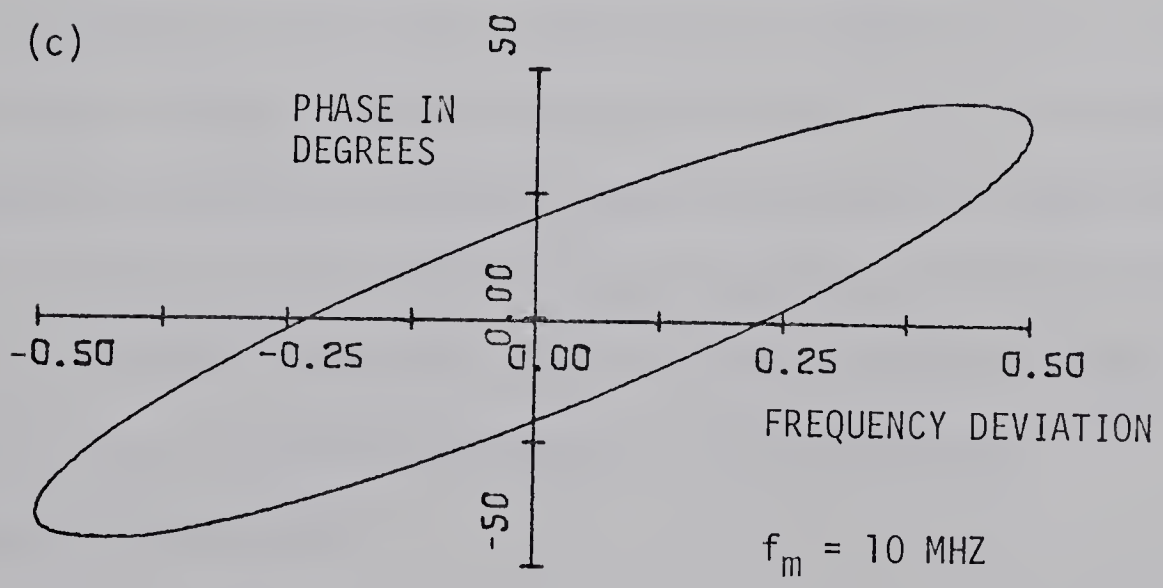

FIG. 3.4-1 PHASE VERSUS NORMALIZED FREQUENCY DEVIATION FOR THE LINEARIZED APPROZIMATE SOLUTION, EQ. 3.4-4.

deviation characteristics at the extremes of the range. Standard numerical techniques were used to solve Adler's nonlinear equation in the time domain. The results of these calculations are displayed in Fig. 3.5-1 in a graphical form similar to that of Fig. 3.4-1. Eq. 3.4-1 was solved for the following set of parameters: $\omega_o/2\pi$ = 10 GHz, Q_L = 50, R = 0.1, $\Delta\omega_o$ = 0, Gain = 20 dB, $\Delta_o/2\pi$ = 10 MHz, $A_m = 0.99\Delta_o$, and for the following modulating frequencies: $\omega_m/2\pi$ = 200 kHz, 2 MHz, 10 MHz. Several observations may be made about these plots. Since each modulating frequency cycle will trace out one circuit around the graph it may be seen that at the higher modulating frequencies:

a) it may take several cycles before a steady state cycle is achieved

b) the major and minor axes of the ellipse (steady-state) are displaced from those values they would have with the linearized approximation.

As a consequence, it has proven laborious to attempt to use the phase versus frequency deviation characteristics in this form to describe the distortion characteristics in analytic or numerical form. As will be shown in this study, the basis provided by the examination of the phase plots may be applied in another manner to arrive at an "engineering solution" to the distortion characterization problem.

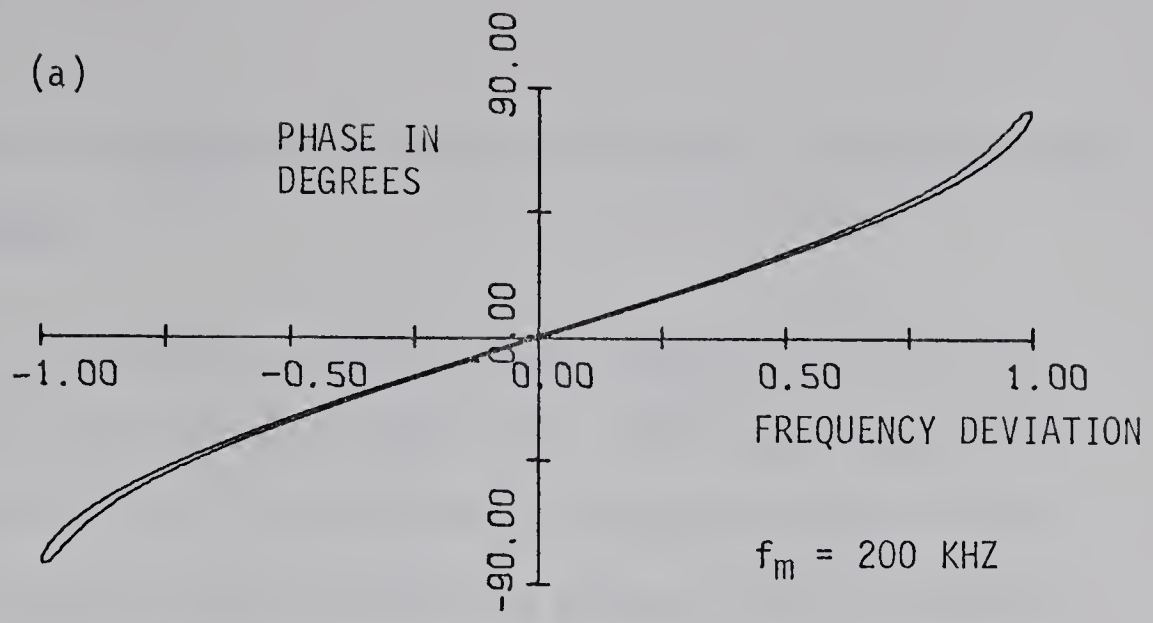

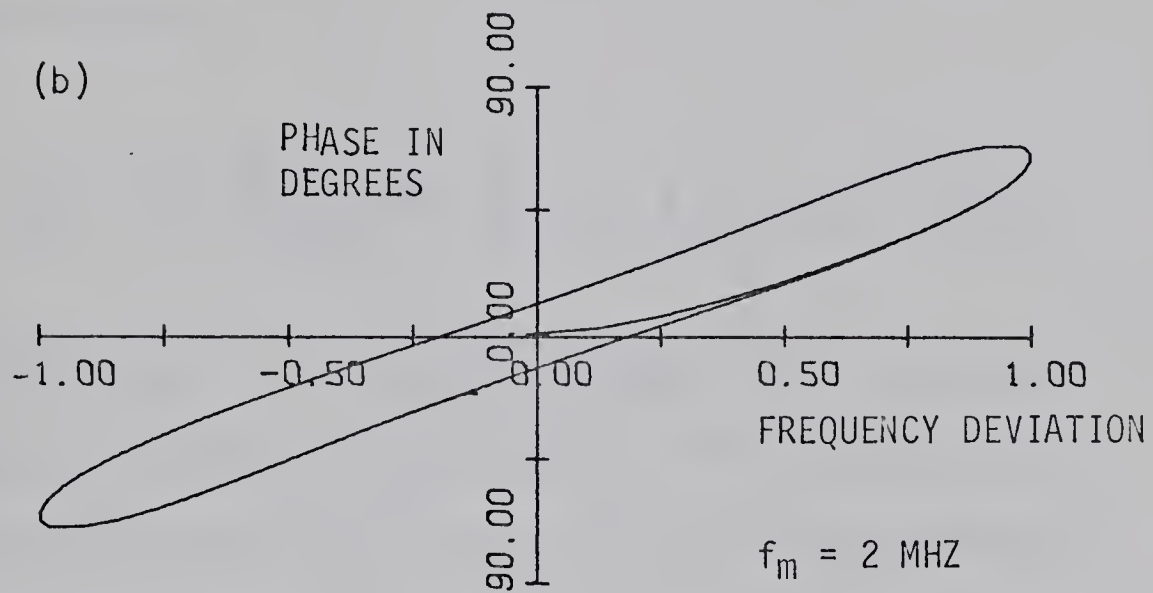

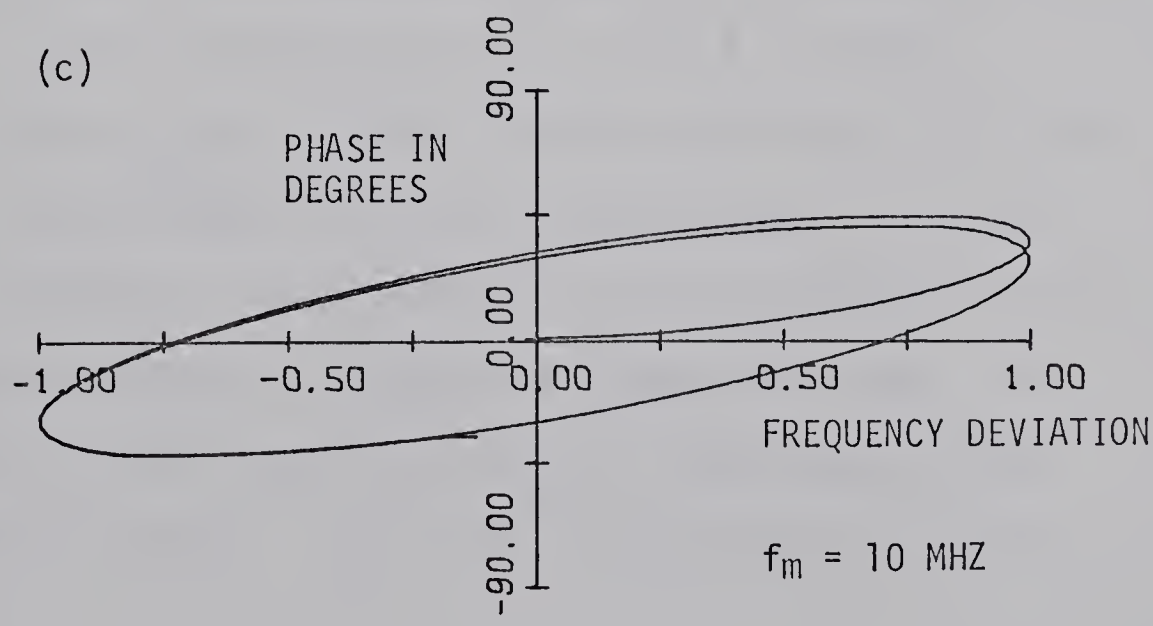

FIG. 3.5-1 PHASE VERSUS NORMALIZED FREQUENCY DEVIATION FOR ADLER'S EQUATION.

3.6 Analysis Based Upon the Generalized Adler's Phase-Locking Equation

The previous sections have examined the linear and nonlinear phase dependent equations. Additionally, when the approximation $R \ll 1$ is no longer valid, then the generalized Adler's equation must be solved in place of Adler's equation. For reference purposes it is repeated here with a sinusoidal modulation term as

$$\frac{d\theta}{dt} = \left[\frac{1+R^2+2R\cos\theta}{1+R\cos\theta}\right] \times \left[\Delta\omega_o + A_m \sin\omega_m t - \frac{\Delta_o \sin\theta}{1+R\cos\theta}\right] \tag{3.6-1}$$

The solution to Eq. 3.6-1 is nonlinear and similar numerical techniques to Section 3.5 were required. The important added dimension to the solutions is the variation of the hysteresis in the phase display due to the gain. Eq. 3.6-1 is solved and displayed (as in the previous sections) for the following parameters: $\omega_o/2\pi = 10$ GHz, $\Delta\omega_o = 0$, $Q_L = 50$, $A_m = 0.99\Delta_o$, $\Delta_o/2\pi = 10$ MHz, $\omega_m/2\pi = 10$ MHz, and the gains are 10, 20, and 30 dB. As can be seen from Fig. 3.6-1 decreases in the gain of the ILO produce a deterioration in the time required for the phase characteristic to achieve its steady-state value. As before, the initial condition of $\theta_o(0) = 0$ has been used for illustrative purposes. It is also observed that a greater

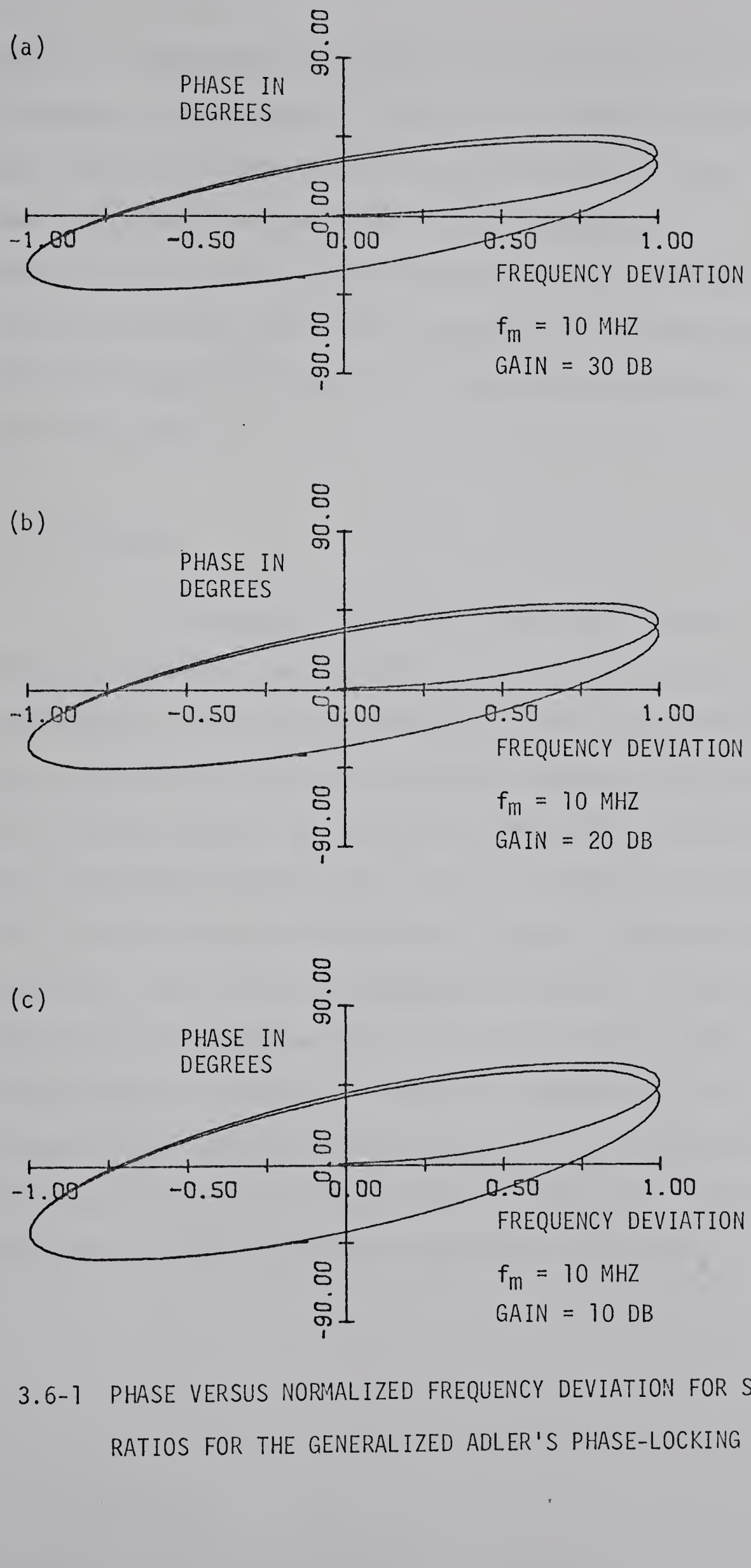

FIG. 3.6-1 PHASE VERSUS NORMALIZED FREQUENCY DEVIATION FOR SEVERAL POWER RATIOS FOR THE GENERALIZED ADLER'S PHASE-LOCKING EQUATION.

amount of steady-state phase shift occurs when the power ratio is lowered. Unfortunately, this method of display does not lend itself to a convenient and accurate solution to the numerical distortion quantities required for the ILO characterization. As will be shown in succeeding chapters, a slightly different form of the same equations combined with a different display will result in a reasonable distortion characterization.

3.7 Conclusion

In this chapter the dynamic phase shift versus frequency deviation characteristics of the ILO's have been displayed for a variety of parameters. These plots indicate that the nonlinear distortion effect of the generalized Adler's phase-locking equation is observed in the differences that occur from the ellipses of Fig. 3.4-1. The amount of discrepancy will be influenced by the modulating frequency, the peak frequency deviation, and the circuit parameters of the ILO. These phase shift deviation characteristics are a valuable aid in the visualization of the manner in which the phase decays to its steady-state value given certain changes in the variable parameters. The possibility of using these plots on a basis for a detailed description of the distortion in ILO's was investigated.

After considerable effort it was found that the results from the phase approach (as detailed in the previous sections) did not yield the distortion quantities in the desired analytic form. However, when a few changes are introduced into the manner in which the ILO is modelled (as will be performed in the following chapters) it will be feasible to arrive at numerical quantities for the distortion effects. It is expected that future work by other investigators will duplicate these numerical results.

CHAPTER IV

CHARACTERIZATION OF AN FM ILO AMPLIFIER

4.1 Introduction

This chapter discusses in detail the frequency modulated ILO amplifier model that is required for the distortion analysis to follow. The dynamic behavior of the ILO has been characterized in the previous chapters. The resulting mathematical ILO model will then be treated with conventional amplifier terminology and techniques.

4.2 ILO Amplifier Model

The modelling of the ILO amplifier in this section will be based upon the concepts of injection-locking and transmission distortion systems discussed in Chapters II and III, Appendix A and in the literature [32-40]. The ILO model will be used to identify three main types of distortion; namely,

a) amplitude distortion

b) phase or envelope delay distortion

c) nonlinear distortion

Let the model of an injection-locked oscillator as shown in Fig. 4.2-1 represent a microwave FM ILO amplifier operating as a reflection type amplifier. When ideal FM modulators and FM demodulators are added to the input and output respectively

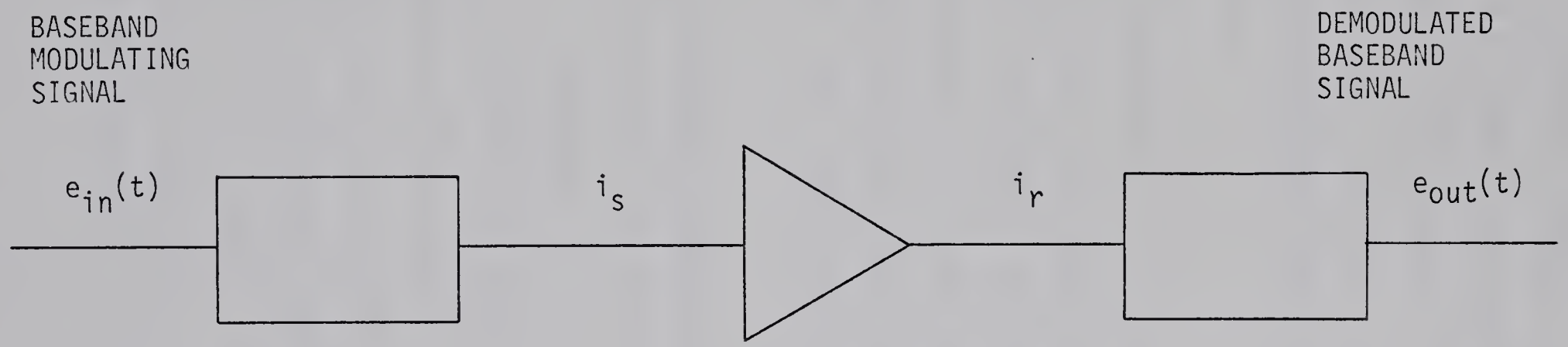

FIG. 4.2-1 SCHEMATIC DIAGRAM OF THE ILO AMPLIFIER WITH AN IDEAL FM MODULATOR AND FM DEMODULATOR.

of the ILO amplifier of Fig. 4.2-1 it is seen that this represents a baseband repeater. That this repeater has an intermediate microwave stage does not alter the analysis since it merely adds complexity and distortion at the intermediate stage. Therefore, the FM modulator, ILO amplifier model, and FM demodulator, will be an equivalent to a microwave repeater link.

A comparison of the baseband output signal $e_{out}(t)$ of Fig. 4.2-1 with the baseband input signal $e_{in}(t)$ will yield several conventional amplifier parameters. This justifies the entire approach, since the simplicity of this model enables the interrelationships of the various parameters to be understood more clearly. Now, these conventional amplifier parameters; namely,

a) the gain variation versus the bandwidth,

b) the phase and envelope delay variation versus the bandwidth,

and, c) the nonlinear distortion versus the bandwidth characteristics will be expanded upon in terms of the equations of Chapters II and III. Let the baseband modulating signal $e_{in}(t)$ in Fig. 4.2-1 be given by a single-tone sinusoid (e.g. Eq. 3.2-2); further, let the resulting FM injected signal be given by the incident microwave signal Eq. 2.2-4, the output FM modulated signal will be given by Eq. 2.2-6, and its frequency variation

by Eq. 2.2-21. The demodulated output signal will be given by

$$e_{out}(t) = K_o \left[-\Delta\omega_o + \frac{\Delta_o \sin\theta(t)}{1+R\cos\theta(t)} \right] \qquad (4.2\text{-}1)$$

where K_o is the gain of the frequency discriminator used in the FM demodulator.

As is normal practice in analyses of this nature, a simplified solution will be examined first, then the solution will be expanded to more complex cases. Therefore, let the generalized Adler's phase-locking equation Eq. 2.2-20 be approximated for the high gain case (i.e. $R \ll 1$, $I_R \cong I$ and $\phi \ll \theta$). Additionally, let the peak deviation frequency (PFD) be less than seventy percent of the maximum locking bandwidth; i.e. $|A_m + \Delta\omega_o| < .7\Delta_o$. This will permit the nonlinearity from Adler's equation, Eq. 2.2-22, to be approximated by θ, i.e. $\sin\theta \cong \theta$ to better than ten percent. Thus the steady-state analytic solution for $\theta(t)$ is

$$\theta(t) = \frac{\Delta\omega_o}{\Delta_o} + \frac{A_m/\Delta_o}{\sqrt{1+\left(\frac{\omega_m}{\Delta_o}\right)^2}} \sin\left(\omega_m t - \tan^{-1}\frac{\omega_m}{\Delta_o}\right) \qquad (4.2\text{-}2)$$

By applying similar approximations to Eq. 4.2-1 $e_{out}(t)$ becomes

$$e_{out}(t) \cong K_o(-\Delta\omega_o + \Delta_o\theta) \qquad (4.2\text{-}3)$$

Substituting Eq. 4.2-2 into Eq. 4.2-3 yields

$$e_{out}(t) \cong \frac{A_m K_o}{\sqrt{1+\left(\frac{\omega_m}{\Delta_o}\right)^2}} \sin\left(\omega_m t - \tan^{-1}\frac{\omega_m}{\Delta_o}\right) \qquad (4.2\text{-}4)$$

It is noteworthy that the simple analytic solution for $e_{out}(t)$ does not depend on $\Delta\omega_o$. However, as will be shown shortly, the $\Delta\omega_o$ term does play an important role in the even components of the nonlinear distortion.

By using the above linearized locking equation solution it is possible to represent the FM ILO amplifier and the ideal modulator and demodulator by a simple transfer function; namely,

$$G(\omega_m) = e_{out}(t)/e_{in}(t)$$

$$= \frac{K_o \quad e^{-j \tan^{-1} \omega_m/\Delta_o}}{\sqrt{1+\left(\frac{\omega_m}{\Delta_o}\right)^2}} \qquad (4.2\text{-}5)$$

It is noted that the frequency dependence of the magnitude of the transfer function is similar to the expression derived and plotted in the literature[8-13]. Additionally, Eq. 4.2-5 predicts that the phase shift of the ILO amplifier model will not be a linear function of ω_m, especially when ω_m approaches Δ_o. It is expected that there will be more phase distortion as ω_m approaches Δ_o (as shown in Chapter III).

To aid in the interpretation of Eq. 4.2-5, the

distortion-producing terms of the frequency-dependent magnitude and phase will be isolated and displayed in simple visual form. The purpose of this technique is simply to model the ILO in conventional amplifier parameters. The magnitude of a "distortionless transfer function" should ideally be frequency-independent. Consequently, the normalized frequency-dependent part of the magnitude of Eq. 4.2-5 will be plotted in dB as

$$\left|G(\omega_m)\right| = -20 \log_{10} \left[1 + \left(\frac{\omega_m}{\Delta_o} \right)^2 \right] \qquad (4.2\text{-}6)$$

Next, the phase delay characteristic of the transfer function must be compared to the distortionless linear variation; i.e. this difference will be expressed in degrees as

$$\Delta\theta = 180/\pi \cdot \left(\tan^{-1} \frac{\omega_m}{\Delta_o} - \frac{\omega_m}{\Delta_o} \right) \qquad (4.2\text{-}7)$$

Eq. 4.2-7 indicates that $\Delta\theta$ will produce a frequency-dependent phase shift (or EDD) in the demodulated output signal of the ILO amplifier when compared to the reference input signal. Fig. 4.2-2 is included to display the two equations Eq. 4.2-6 and Eq. 4.2-7 as a function of modulating frequency.

It is interesting to note that the maximum modulating frequency predicted from the transient response solutions (from Section 2.4) suggests that the 3 dB bandwidth of the linearized model is identical to the previous result; namely,

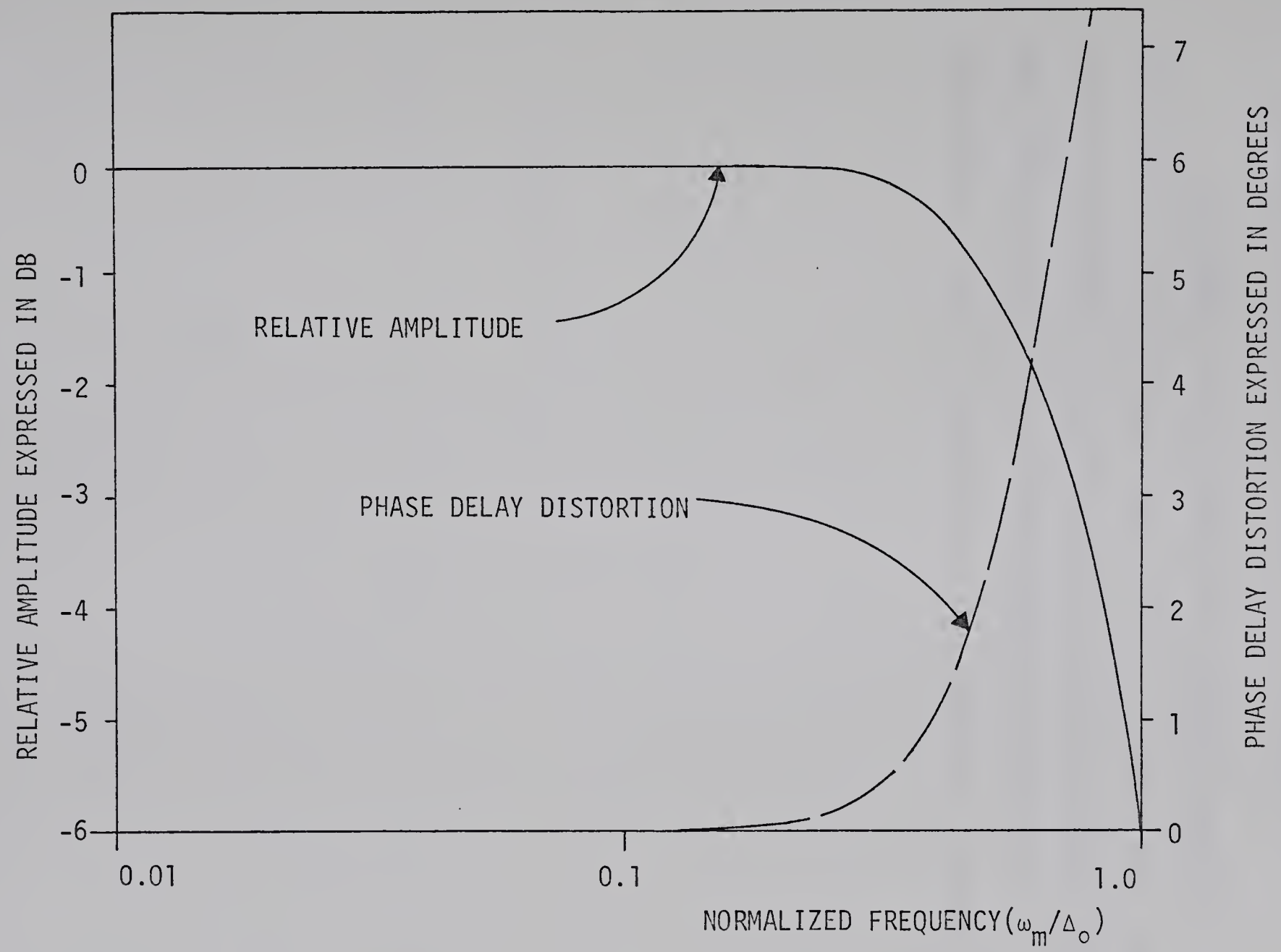

FIG 4.2-2 LINEARIZED TRANSFER CHARACTERISTICS FOR THE ILO AMPLIFIER MODEL OF FIG 4.2-1.

$$\left.\frac{\Delta_o}{2\pi}\right| \begin{array}{l} \text{Hz.} \\ @\ 3\text{dB} \end{array}$$

The model of the baseband ILO repeater developed here will have application in the following chapters when more accurate equations are used to describe the ILO characteristics. The resulting description of the distortion of the ILO in conventional amplifier terminology will justify this approach.

CHAPTER V

FM DISTORTION IN A TUNED ILO AMPLIFIER

5.1 Introduction

In this chapter the generalized Adler's phase-locking equation is used to describe the frequency dependence of the nonlinear and delay distortion of the FM modulation in an ILO amplifier when the initial frequency difference is zero (i.e. $\Delta\omega_0 = 0$). This will be called the tuned case. A method of approximate solution to the resulting nonlinear equations will also be discussed in detail. Finally, the results of this study will be presented in tabular and graphical form.

5.2 Mathematical Modelling

The analysis of the FM distortion produced by the ILO modelled in Chapter IV will be presented in the following work. Consequently, let baseband input and output signals, ideal FM modulators and FM demodulators and the ILO amplifier of Fig. 4.2-1 be used for the description of the distortion effects. The distortion will be found by comparing the output and input baseband signals. Let the input baseband modulating signal be modulated by a single-frequency sinusoid, i.e.

$$\Omega_{in} = \frac{d\alpha(t)}{dt} = A_m \sin\omega_m t \qquad (5.2\text{-}1)$$

where ω_m is the modulating frequency (simply referred to as the frequency), $A_m = k\Delta_o$ and $k \leq 1$. Using Fig. 2.2-5 and Fig. 4.2-1 the injected modulated microwave signal will be

$$i_s = I_s \sin(\omega_s t + \alpha(t)) \tag{5.2-2}$$

while the output microwave signal will be given by

$$i_R = I_R \sin(\omega_s t + \alpha(t) - \theta(t) + \phi(t)) \tag{5.2-3}$$

where the symbols are identical to those defined in Chapter II.

Then the output signal frequency delivered to the load of Fig. 2.2-5 (at microwave frequencies) will be given by

$$\omega_R = \omega_s + \frac{d\alpha}{dt} - \frac{d\theta}{dt} + \frac{d\phi}{dt} \tag{5.2-4}$$

and the demodulated output frequency will be given by

$$\begin{aligned} \omega_{out}(t) &= \omega_R - \omega_s \\ &= \omega_o - \omega_s + \frac{\Delta_o \sin\theta(t)}{1+R\cos\theta(t)} \\ &= -\Delta\omega_o + \frac{\Delta_o \sin\theta(t)}{1+R\cos\theta(t)} \end{aligned} \tag{5.2-5}$$

Eq. 5.2-5 was solved by the use of Eq. 4.2-1, Eq. 2.2-16 and Eq. 2.2-21. Finally, the solution for $\theta(t)$ is given by Adler's generalized (nonlinear) equation as

$$\frac{d\theta(t)}{dt} = \left[\frac{1+R^2+2R\cos\theta(t)}{1+R\cos\theta(t)}\right]\cdot\left[\Delta\omega_o + \frac{d\alpha(t)}{dt} - \frac{\Delta_o \sin\theta(t)}{1+R\cos\theta(t)}\right] \tag{5.2-6}$$

To evaluate Eq. 5.2-5, the solution to Eq. 5.2-6 must be solved

numerically and substituted into Eq. 5.2-5 to obtain the output baseband demodulated signal. It must be recalled that ideal FM modulators and demodulators have been assumed in this analysis (and for simplicity their gains have been set at unity).

For most cases of practical interest $|\theta| < \frac{\pi}{2}$, and as such the solution to Eq. 5.2-6 may be obtained by the technique of successive approximations that is outlined in Appendix B. The tuned case will be discussed in detail in this chapter while the detuned case (i.e. $\Delta\omega_0 \neq 0$) will be dealt with in the following chapter. When the tuned case assumptions (i.e. $\Delta\omega_0 = 0$) are applied to the previous equations Eq. 5.2-6 reduces to

$$\frac{d\theta(t)}{dt} = \left[\frac{1+R^2+2R\cos\theta(t)}{1+R\cos\theta(t)}\right].\left[\frac{d\alpha(t)}{dt} - \frac{\Delta_0 \sin\theta(t)}{1+R\cos\theta(t)}\right] \tag{5.2-7}$$

while Eq. 5.2-5 reduces to

$$\omega_{out}(t) = \frac{\Delta_0 \sin\theta(t)}{1+R\cos\theta(t)} \tag{5.2-8}$$

The demodulated input and output signals will be given by (using the symbols defined with Fig. 4.2-1):

$$e_{in}(t) = A_m \sin\omega_m t \tag{5.2-9}$$

and

$$e_{out}(t) = K_0\left(\frac{\Delta_0 \sin\theta(t)}{1+R\cos\theta(t)}\right) \tag{5.2-10}$$

(here K_o is set equal to unity). To solve for $\theta(t)$ in Eq. 5.2-6 a truncated series approximation technique, described in Appendix B was used. As a result, it is possible to reduce Eq. 5.2-6 to

$$\frac{d\,\theta(t)}{dt} = \sum_{n=0}^{7} P_n\,\theta^n \qquad (5.2\text{-}11)$$

where the coefficients P_o through P_7 are defined as in Eq. B-11. The validity of this technique depends on the fact that for $\theta < 1$ radian and for a given "weak" nonlinearity the first few terms of the series approximation to Eq. 5.2-6 are quite accurate. Additionally, when a recursive technique is applied to Eq. 5.2-11, an approximate solution for $\theta(t)$ is obtained (refer to Chapter IV and to Appendix B). When the solution is limited to the first ten harmonic terms it may be expressed as

$$\theta(t) = A_o + \sum_{k=1}^{10} \left[A_k \sin K\omega_m t + B_k \cos K\omega_m t\right] \qquad (5.2\text{-}12)$$

where A_o, A_k and B_k are frequency-dependent coefficients whose accurate calculation is performed as described in Appendix B.

Using a similar approach, the demodulated output signal will be approximated by

$$e_{out}(t) = K_o \Delta_o \sum_{n=1}^{4} R_n\,\theta^{2n-1} \qquad (5.2\text{-}13)$$

which results from substituting B-13 and Eq. 5.2-12 into Eq. 5.2-7 and the coefficients R_1 through R_4 are defined as in Eq. B-13. The demodulated output will then be approximated by

$$e_{out}(t) = C_o + \sum_{k=1}^{10} \left[\sqrt{S_k^2 + C_k^2} \sin(K\omega_m t - \tan^{-1} \frac{C_k}{S_k}) \right] \quad (5.2\text{-}14)$$

where C_o, S_k and C_k are calculated by the techniques outlined in Appendix B. The first few terms of the approximate output solution contain most of the power spectrum. A comparison of the output signal Eq. 5.2-14 and the input signal Eq. 5.2-1 for the tuned case shows that $C_o = 0$ and that the power spectrum is contained in the odd-numbered components (the third and fifth harmonics are the predominant terms). In the more general detuned case, Chapter VII will show that the output power will also appear in the even harmonic components and in general, $C_o \neq 0$. For certain circuit configurations and modulation parameters, the second and fourth harmonics could contain as much distorted power as the odd harmonics.

The complexity of the output waveform for the simple sinusoidal modulation precludes studies with more complex modulating waveforms using the techniques outlined in Appendix B. As a consequence, several display techniques will be used to aid in describing the distortion produced by the ILO amplifier. Firstly, let the demodulated output fundamental amplitude be compared to the input modulating amplitude and let this ratio be expressed in dB, as

$$\left| G\ (\omega_m) \right| = 20\log_{10} \frac{(S_1^{\,2} + C_1^{\,2})^{1/2}}{A_m} \qquad (5.2\text{-}15)$$

Several tables and graphs will display this relation in detail. Secondly, the phase delay distortion of the fundamental will be expressed as the actual phase minus the linear (i.e. distortionless) portion of the phase, i.e.

$$\Delta\Theta(\text{degree}) = \pi \left(\tan^{-1} \frac{C_1}{S_1} - \frac{\omega_m}{\Delta_o} \right) \qquad (5.2\text{-}16)$$

Thirdly, the percentage of the output signal that is contained in the harmonic components versus the magnitude of the fundamental is a useful measure of ILO amplifier performance. This will be expressed as a percentage nonlinear distortion (i.e. in a form analogous to Eq. B-30)

$$ND(\%) = 100x \left[\frac{\sum_{k=2}^{10} (S_k^{\,2} + C_k^{\,2})}{S_1^{\,2} + C_1^{\,2}} \right]^{1/2} \qquad (5.2\text{-}17)$$

5.3 Results of the Tuned Calculations

The formulas of Section 5.2 were programmed and solved numerically . The results of these calculations; namely,

a) the nonlinear distortion

b) the phase delay distortion, and

c) the relative fundamental amplitude variation

versus the normalized modulating frequency are given in Figs. 5.3-1 and 5.3-2 and Tables 5.3-1 through 5.3-3 for a number of variable parameters. Four cases have been chosen as representive, and the amplifier parameters used are summarized below (note that these are all tuned cases, $\Delta\omega_o=0$)

Case #1 Gain = 34dB

$\Delta_o/2\pi$ = 2.0 MHz

A_m/Δ_o = 0.1

Case #2 Gain = 34dB

$\Delta_o/2\pi$ = 2.0 MHz

A_m/Δ_o = 0.75

Case #3 Gain = 15dB

$\Delta_o/2\pi$ = 17.86 MHz

A_m/Δ_o = 0.1

Case #4 Gain = 15dB

$\Delta_o/2\pi$ = 17.86

A_m/Δ_o = 0.75

(A_m/Δ_o is the normalized peak frequency deviation)

5.4 Conclusion

Examination of the figures and tables of the previous section reveals the following ILO behavior in the tuned state:

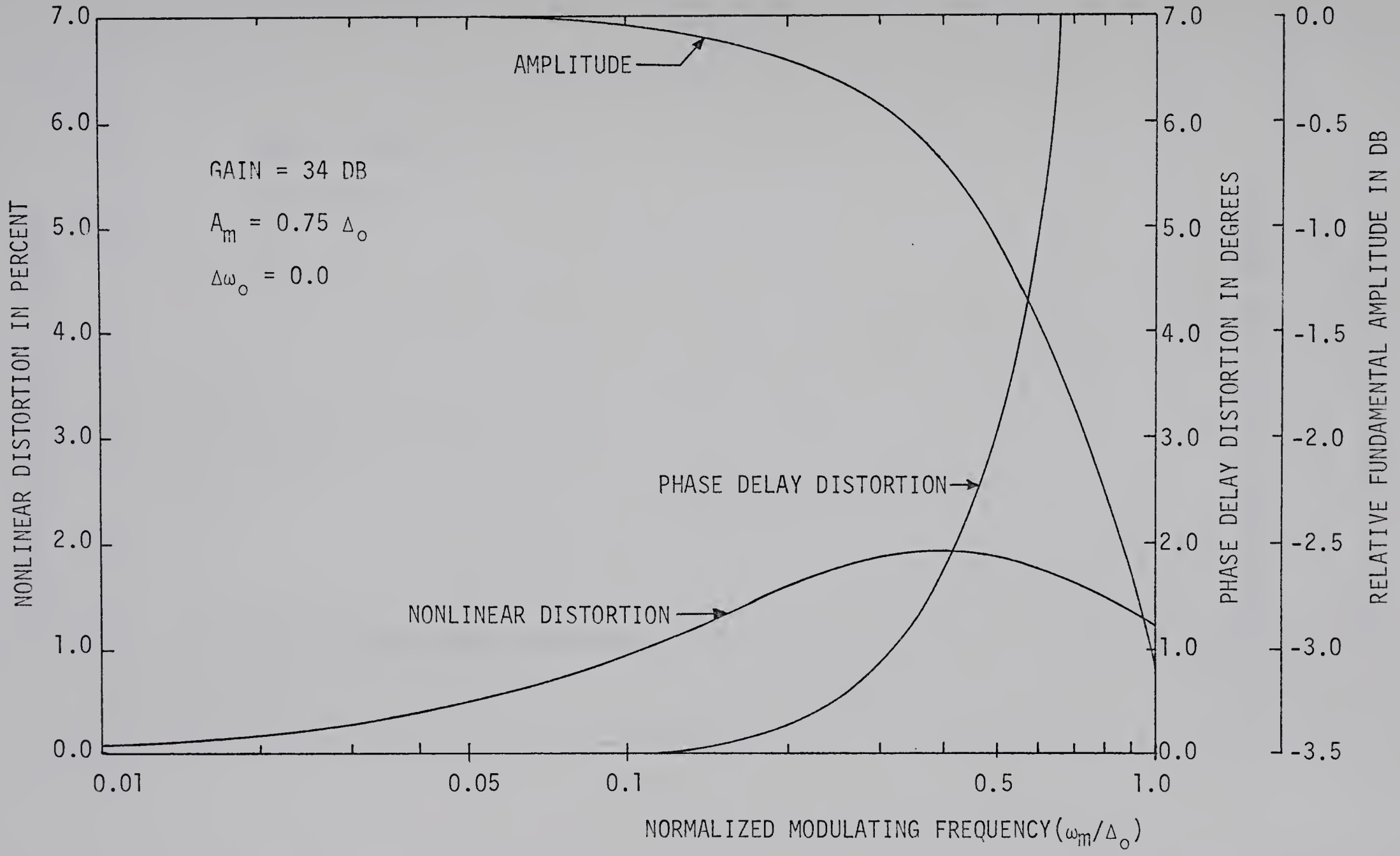

FIG. 5.3-1 FREQUENCY DEPENDENT DISTORTION CHARACTERISTICS FOR A TUNED SINGLE-STAGE ILO AMPLIFIER MODEL WITH A 34 DB GAIN.

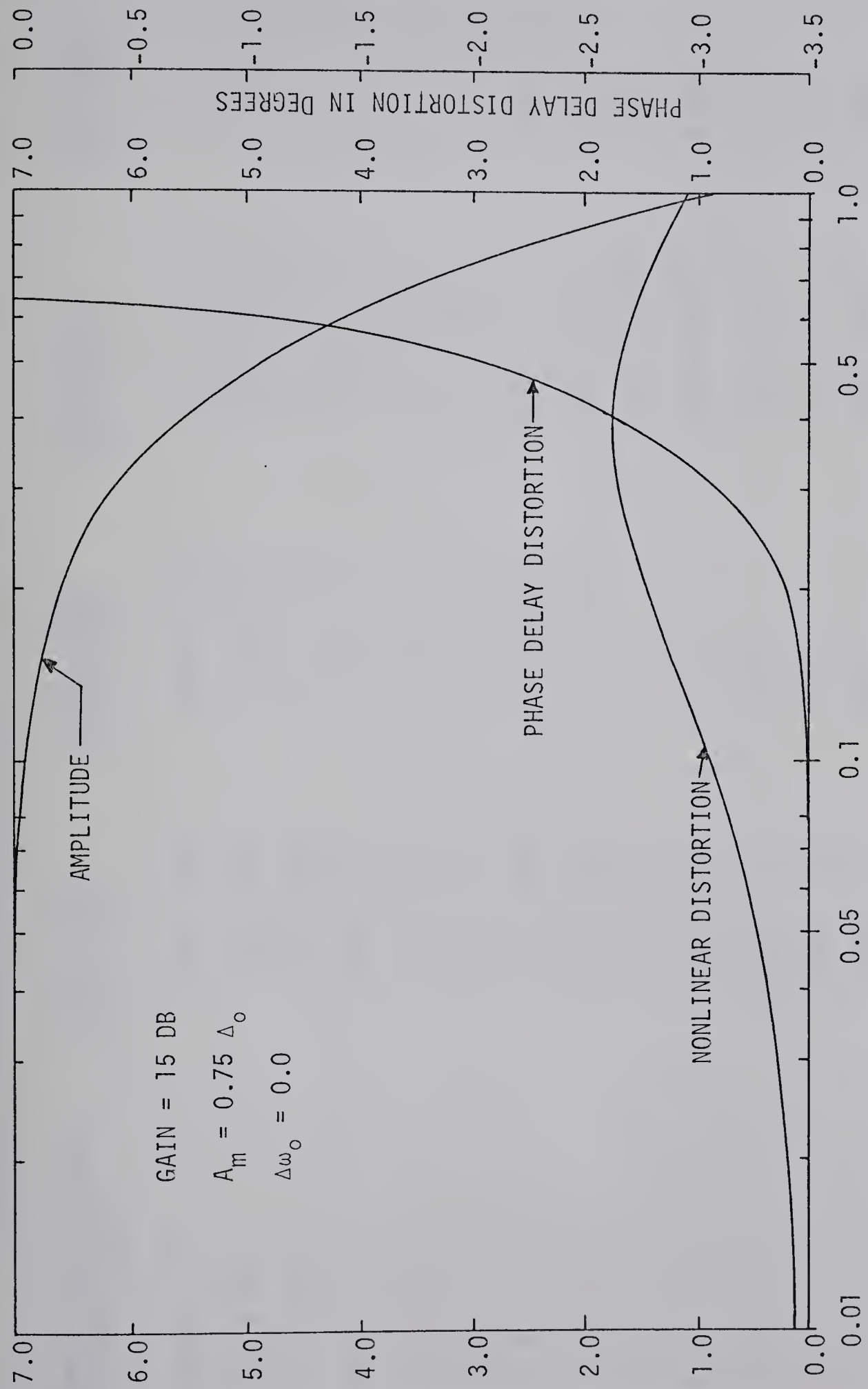

FIG. 5.3-2 FREQUENCY DEPENDENT DISTORTION CHARACTERISTICS FOR A TUNED SINGLE-STAGE ILO AMPLIFIER MODEL WITH A 15 DB GAIN.

TABLE 5.3-1 COMPARISON OF NONLINEAR DISTORTION FOR VARIOUS PARAMETERS OF A TUNED ILO AMPLIFIER
(DISTORTION EXPRESSED IN PERCENTAGES)

NORMALIZED MODULATING FREQUENCY (ω_m/Δ_o)	GAIN= 34dB $A_m= 0.1\Delta_o$	GAIN= 34dB $A_m= 0.75\Delta_o$	GAIN= 15dB $A_m= 0.1\Delta_o$	GAIN= 15dB $A_m= 0.75\Delta_o$
5.00×10^{-4}	6.28×10^{-5}	6.80×10^{-3}	5.70×10^{-5}	7.33×10^{-3}
1.00×10^{-3}	1.26×10^{-4}	1.14×10^{-2}	1.10×10^{-4}	1.10×10^{-2}
1.00×10^{-2}	1.25×10^{-3}	1.06×10^{-1}	1.14×10^{-3}	9.51×10^{-2}
1.58×10^{-2}	1.99×10^{-3}	1.68×10^{-1}	1.80×10^{-3}	1.50×10^{-1}
2.50×10^{-2}	3.14×10^{-3}	2.65×10^{-1}	2.85×10^{-3}	2.37×10^{-1}
4.00×10^{-2}	4.96×10^{-3}	4.17×10^{-1}	4.49×10^{-3}	3.73×10^{-1}
6.28×10^{-2}	7.75×10^{-3}	6.47×10^{-1}	7.02×10^{-3}	5.80×10^{-1}
1.00×10^{-1}	1.19×10^{-2}	9.71×10^{-1}	1.08×10^{-2}	8.76×10^{-1}
1.58×10^{-1}	1.75×10^{-2}	1.38	1.59×10^{-2}	1.25
2.51×10^{-1}	2.37×10^{-2}	1.76	2.14×10^{-2}	1.60
3.98×10^{-1}	2.76×10^{-2}	1.91	2.50×10^{-2}	1.74
6.30×10^{-1}	2.68×10^{-2}	1.68	2.34×10^{-2}	1.54
1.00	1.98×10^{-2}	1.18	1.79×10^{-2}	1.08

TABLE 5.3-2 COMPARISON OF PHASE DELAY DISTORTION (EXPRESSED IN DEGREES) FOR VARIOUS PARAMETERS OF A TUNED ILO AMPLIFIER.

NORMALIZED MODULATING FREQUENCY (ω_m/Δ_o)	GAIN= 34dB $A_m = 0.1\Delta_o$	GAIN= 34dB $A_m = 0.75\Delta_o$	GAIN= 15dB $A_m = 0.1\Delta_o$	GAIN= 15dB $A_m = 0.75\Delta_o$
1.00×10^{-3}	--	--	--	--
1.00×10^{-2}	1.90×10^{-5}	3.65×10^{-5}	2.00×10^{-5}	3.33×10^{-5}
1.58×10^{-2}	7.60×10^{-5}	1.44×10^{-4}	7.7×10^{-5}	1.33×10^{-4}
2.50×10^{-2}	3.02×10^{-4}	5.75×10^{-4}	3.05×10^{-4}	5.33×10^{-4}
4.0×10^{-2}	1.21×10^{-3}	2.29×10^{-3}	1.2×10^{-3}	2.13×10^{-4}
6.28×10^{-2}	4.82×10^{-3}	9.07×10^{-3}	4.82×10^{-3}	8.44×10^{-3}
1.0×10^{-1}	1.91×10^{-2}	3.71×10^{-2}	1.91×10^{-2}	3.32×10^{-2}
1.58×10^{-1}	7.55×10^{-2}	1.39×10^{-1}	7.5×10^{-2}	1.29×10^{-1}
2.51×10^{-1}	2.94×10^{-1}	5.11×10^{-1}	2.9×10^{-1}	4.84×10^{-1}
3.98×10^{-1}	1.11	1.79	1.11	1.71
6.3×10^{-1}	3.92	5.78	3.92	5.58
1.0	1.24×10^{1}	1.65×10^{1}	1.24×10^{1}	1.61×10^{1}

TABLE 5.3-3 RELATIVE AMPLITUDE VARIATION (EXPRESSED IN DB) FOR VARIOUS TUNED ILO AMPLIFIER PARAMETERS.

NORMALIZED MODULATING FREQUENCY (ω_m/Δ_o)	GAIN= 34dB $A_m = 0.1\Delta_o$	GAIN= 34dB $A_m = 0.75\Delta_o$	GAIN= 15dB $A_m = 0.1\Delta_o$	GAIN= 15dB $A_m = 0.75\Delta_o$
5.0×10^{-4}	---	---	---	---
1.0×10^{-3}	-3.1×10^{-6}	-6.2×10^{-6}	-3.1×10^{-6}	-6.7×10^{-6}
1.0×10^{-2}	-4.3×10^{-4}	-5.1×10^{-4}	-4.2×10^{-4}	-5.07×10^{-4}
1.58×10^{-2}	-1.09×10^{-3}	-1.32×10^{-3}	-1.1×10^{-3}	-1.29×10^{-3}
2.50×10^{-2}	-2.74×10^{-3}	-3.31×10^{-3}	-2.7×10^{-3}	-3.23×10^{-3}
4.0×10^{-2}	-6.89×10^{-3}	-8.3×10^{-3}	-6.9×10^{-3}	-8.13×10^{-3}
6.28×10^{-2}	-1.73×10^{-2}	-2.08×10^{-2}	-1.73×10^{-2}	-2.04×10^{-2}
1.0×10^{-1}	-4.33×10^{-2}	-5.25×10^{-2}	-4.33×10^{-2}	-5.09×10^{-2}
1.58×10^{-1}	-1.08×10^{-1}	-1.29×10^{-1}	-1.08×10^{-1}	-1.26×10^{-1}
2.51×10^{-1}	-2.66×10^{-1}	-3.12×10^{-1}	-2.7×10^{-1}	-3.0×10^{-1}
3.98×10^{-1}	-6.4×10^{-1}	-7.29×10^{-1}	-6.4×10^{-1}	-7.20×10^{-1}
6.3×10^{-1}	-1.46	-1.60	-1.46	-1.58
1.0	-3.01	-3.17	-3.01	-3.16

1) the nonlinear distortion increases with increasing normalized modulating frequency and increasing PFD but only slightly with increasing gain,
2) phase delay distortion increases with increasing normalized modulating frequency but changes only slightly with increasing PFD and increasing gain,
3) the relative amplitude variation shows a decrease with increasing normalized frequency but is affected only slightly by increase in gain or PFD.

CHAPTER VI

FM DISTORTION IN A DETUNED ILO AMPLIFIER

6.1 Introduction

In this chapter the solution to the generalized Adler's equation for the injection-locking phenomenon is discussed for the detuned case (i.e. $\Delta\omega_o \neq 0$). The results of calculations for both the tuned and detuned cases are compared in tabular form and by the use of appropriate graphs. These results will form the basis for the theoretical characterization of a single-stage ILO amplifier with respect to its distortion effects on the modulating signals involved.

The tuned condition for the signals involved in ILO's is not likely to be realized exactly in practice (it has been suggested that, if negative feedback is used, it may be possible to correct the amplifier free-running frequency). For example, the free-running frequency of the microwave oscillators used in this study is dependent on the ambient temperature and its variation, the temperature characteristics of the cavity, and numerous other factors that are discussed in more detail in the experimental chapter. In practice, these factors may cause the free-running oscillator frequency to drift over a significant portion of the locking bandwidth during an experimental run

(i.e. a short period of time). These variations may be expressed as part of the noise associated with these oscillators and the drift will then be the predominant factor over a period of time. It is vital that the dependence of the microwave oscillator frequency on the numerous factors mentioned above be minimized for the ILO to be practical for system applications. Consequently, a study of the distortion characteristics of the ILO's in the detuned case has a very practical application.

6.2 Mathematical Modelling

The previous chapter discussed the nonlinear and phase delay distortion and the amplitude variations of the modulated signals in a tuned ILO amplifier. The same technique that is described in Appendix B will be used to solve the appropriate nonlinear differential equations for the detuned case (i.e. $\Delta\omega_o \neq 0$).

As before, the input modulating signal to the ILO amplifier model of Fig. 4.2-1 will be a single-frequency sinusoid

$$e_{in}(t) = \frac{d\alpha}{dt} = A_m \sin\omega_m t \qquad (6.2\text{-}1)$$

where the symbols of Chapter V apply. The output baseband signal will then be (from Eq. 4.3-1)

$$e_{out}(t) = -\Delta\omega_o + \frac{\Delta_o \sin\theta}{1+R\cos\theta} \qquad (6.2\text{-}2)$$

where the demodulator gain has been set equal to unity and

$$\frac{\Delta\omega_o}{\Delta_o} \leq 1.$$

When the output baseband signal's coefficient terms are approximated by the first four terms of their appropriate power series expansion (following Appendix B), Eq. 6.2-2 will become Eq. B-13, i.e.

$$\omega_{out} = \omega_o + \Delta_o \sum_{n=1}^{4} R_n \theta^{2n-1} \qquad (6.2\text{-}3)$$

where the 'R' terms are defined as follows

$$R_1 = 1/(1+R)$$

$$R_2 = (2R-1)/6$$

$$R_3 = (1-13R+16R^2)/120$$

$$R_4 = (-1+60R-279R^2+272R^3)/5040$$

The solution to $\theta(t)$ will be given by the approximation to the generalized Adler's locking equation Eq. B-11, i.e.

$$\frac{d\theta}{dt} = \sum_{n=o}^{7} P_n \theta^n \qquad (6.2\text{-}4)$$

where the coefficients P_o through P_7 are defined as in Appendix B. The demodulated output will be found numerically by the recursive solution of Eq. 6.2-4 and Eq. 6.2-3 as described by the method of Appendix B.

When the output solution to Eq. 6.2-4 is limited to the first ten harmonic terms it may be expressed as

$$\theta(t) = A_o + \sum_{k=1}^{10} (A_k \sin k\omega_m t + B_k \cos k\omega_m t) \qquad (6.2\text{-}5)$$

where A_o, A_k, and B_k are frequency dependent coefficients whose accurate calculation is performed as described in Appendix B. The demodulated output baseband signal will be approximated and rewritten as

$$e_{out}(t) = C_o + \sum_{k=1}^{10} \left[(S_k^2 + C_k^2)^{1/2} \sin(k\omega_m t - \tan^{-1}\frac{C_k}{S_k}) \right] \qquad (6.2\text{-}6)$$

where C_o, S_k and C_k are calculated by the techniques outlined in Appendix B. The evaluation of Eq. 6.2-6 resulted from the recursive substitution of the linearized solution to Eq. 6.2-4, using the procedure described in Appendix B and with the aid of a computer program.

The results of these calculations will be tabulated in the form of normal amplifier distortion parameters. Firstly, let the demodulated output fundamental amplitude be compared to the the unmodulated input amplitude and that this ratio be expressed in in dB as

$$\left| G(\omega_m) \right| = 20\log \left[\frac{(S_1^2 + C_1^2)^{1/2}}{A_m} \right] \qquad (6.2\text{-}7)$$

Secondly, let the phase delay distortion of the fundamental be expressed as the actual phase minus the linear (i.e. distortionless) portion of the phase, i.e.

$$\Delta\theta = \tan^{-1}\frac{C_1}{S_1} - \frac{\omega_m}{\Delta_0} \text{ (radians)} \qquad (6.2\text{-}8)$$

Thirdly, let the percentage of the output signal that is contained in the harmonic components versus the magnitude of the fundamental be the measure of the percentage nonlinear distortion, i.e.

$$ND(\%) = 100 \times \left[\frac{\sum_{k=2}^{10}(S_k^2 + C_k^2)}{S_1^2 + C_1^2}\right]^{1/2} \qquad (6.2\text{-}9)$$

For the tuned case ($\omega_s = \omega_0$), only the odd harmonic amplitudes are nonzero in value while for the detuned case ($\Delta\omega_0 \neq 0$) all the harmonic amplitudes are expected to have nonzero contributions. In practice the second harmonic will often become comparable to the third and fifth harmonic amplitudes.

6.3 Results of the Detuned Calculations

As examples of the results of the calculations that are expected the Tables 6.3-1 through 6.3-3 and Figs. 6.3-1 and 6.3-2 are included as being representative of the ILO parameters. Several cases were selected to display a) the nonlinear distortion, b) the phase delay distortion, and c) the relative fundamental amplitude variation versus the normalized modulating frequency. The ILO parameters included a normalized peak frequency deviation of 0.75, normalized detuning factors of 0.0, 0.1, and 0.24,

TABLE 6.3-1 NONLINEAR DISTORTION (EXPRESSED IN PERCENTAGES) IN AN ILO AMPLIFIER MODEL WITH A GAIN EQUAL TO 15DB, A MAXIMUM LOCKING BANDWIDTH OF 17.86 MHZ, A PEAK FREQUENCY DEVIATION OF $0.75\Delta_o$, AND FOR THE FOLLOWING NORMALIZED DETUNING FACTORS: 0.0, 0.1, AND 0.24.

NORMALIZED MODULATING FREQUENCY	$\Delta\omega_o$=0.0	$\Delta\omega_o = 0.1\Delta_o$	$\Delta\omega_o = 0.24\Delta_o$
5.0×10^{-4}	7.33×10^{-3}	1.73×10^{-2}	5.13×10^{-2}
1.0×10^{-3}	1.10×10^{-2}	2.03×10^{-2}	5.70×10^{-2}
1.0×10^{-2}	9.51×10^{-2}	1.24×10^{-1}	2.90×10^{-1}
1.58×10^{-2}	1.50×10^{-1}	1.95×10^{-1}	4.55×10^{-1}
2.5×10^{-2}	2.375×10^{-1}	3.07×10^{-1}	7.13×10^{-1}
4.0×10^{-2}	3.73×10^{-1}	4.82×10^{-1}	1.11
6.3×10^{-2}	5.8×10^{-1}	7.47×10^{-1}	1.66
1.0×10^{-1}	8.76×10^{-1}	1.13	2.40
1.58×10^{-1}	1.25	1.60	3.24
2.51×10^{-1}	1.6	2.06	4.01
3.98×10^{-1}	1.74	2.17	4.38
6.3×10^{-1}	1.54	2.13	4.12
1.0	1.08	1.65	3.24

TABLE 6.3-2 PHASE DELAY DISTORTION (EXPRESSED IN DEGREES) IN AN ILO AMPLIFIER MODEL WITH A GAIN EQUAL TO 15 DB, A MAXIMUM LOCKING BANDWIDTH OF 17.86 MHZ A PEAK FREQUENCY DEVIATION OF $0.75\Delta_o$, AND FOR THE FOLLOWING NORMALIZED DETUNING FACTORS: 0.0, 0.1, AND 0.24.

NORMALIZED MODULATING FREQUENCY	$\Delta\omega_o = 0.0$	$\Delta\omega_o = 0.1\Delta_o$	$\Delta\omega_o = 0.24\Delta_o$
5.0×10^{-4}	-----	-----	-----
1.0×10^{-3}	-----	-----	-----
1.0×10^{-2}	3.33×10^{-5}	3.7×10^{-5}	6.3×10^{-5}
1.58×10^{-2}	1.33×10^{-4}	1.46×10^{-4}	2.55×10^{-4}
2.5×10^{-2}	5.33×10^{-4}	5.85×10^{-4}	1.0×10^{-3}
4.0×10^{-2}	2.13×10^{-3}	2.3×10^{-3}	4.21×10^{-3}
6.3×10^{-2}	8.44×10^{-3}	9.2×10^{-3}	2.24×10^{-2}
1.0×10^{-1}	3.32×10^{-2}	3.6×10^{-2}	8.19×10^{-2}
1.58×10^{-1}	1.29×10^{-1}	1.43×10^{-1}	2.7×10^{-1}
2.51×10^{-1}	4.84×10^{-1}	5.2×10^{-1}	8.64×10^{-1}
3.98×10^{-1}	1.71	1.95	2.62
6.3×10^{-1}	5.58	5.81	7.51
1.0	1.61×10^{1}	1.65×10^{1}	1.98×10^{1}

TABLE 6.3-3 RELATIVE AMPLITUDE VARIATION (EXPRESSED IN DB) IN AN ILO AMPLIFIER MODEL WITH A GAIN EQUAL TO 15DB, A MAXIMUM LOCKING BANDWIDTH OF 17.86 MHZ, A PEAK FREQUENCY DEVIATION OF $0.75\Delta_o$, AND FOR THE FOLLOWING NORMALIZED DETUNING FACTORS: 0.0, 0.1, AND 0.24.

NORMALIZED MODULATING FREQUENCY	$\Delta\omega_o = 0.0$	$\Delta\omega_o = 0.1\Delta_o$	$\Delta\omega_o = 0.24\Delta_o$
5.0×10^{-4}	-----	-----	-----
1.0×10^{-3}	-6.7×10^{-6}	-7.9×10^{-6}	-1.09×10^{-5}
1.0×10^{-2}	-5.07×10^{-4}	-5.3×10^{-4}	-5.6×10^{-4}
1.58×10^{-2}	-1.29×10^{-3}	-1.3×10^{-3}	-1.42×10^{-3}
2.5×10^{-2}	-3.23×10^{-3}	-3.3×10^{-3}	-3.6×10^{-3}
4.0×10^{-2}	-8.13×10^{-3}	-8.3×10^{-3}	-9.1×10^{-3}
6.3×10^{-2}	-2.04×10^{-2}	-2.1×10^{-2}	-2.5×10^{-2}
1.0×10^{-1}	-5.09×10^{-2}	-5.2×10^{-2}	-6.25×10^{-2}
1.58×10^{-1}	-1.26×10^{-1}	-1.3×10^{-1}	-1.5×10^{-1}
2.51×10^{-1}	-3.07×10^{-1}	-3.1×10^{-1}	-3.52×10^{-1}
3.98×10^{-1}	-7.2×10^{-1}	-7.5×10^{-1}	-8.0×10^{-1}
6.3×10^{-1}	-1.58	-1.6	-1.70
1.0	-3.16	-3.18	-3.31

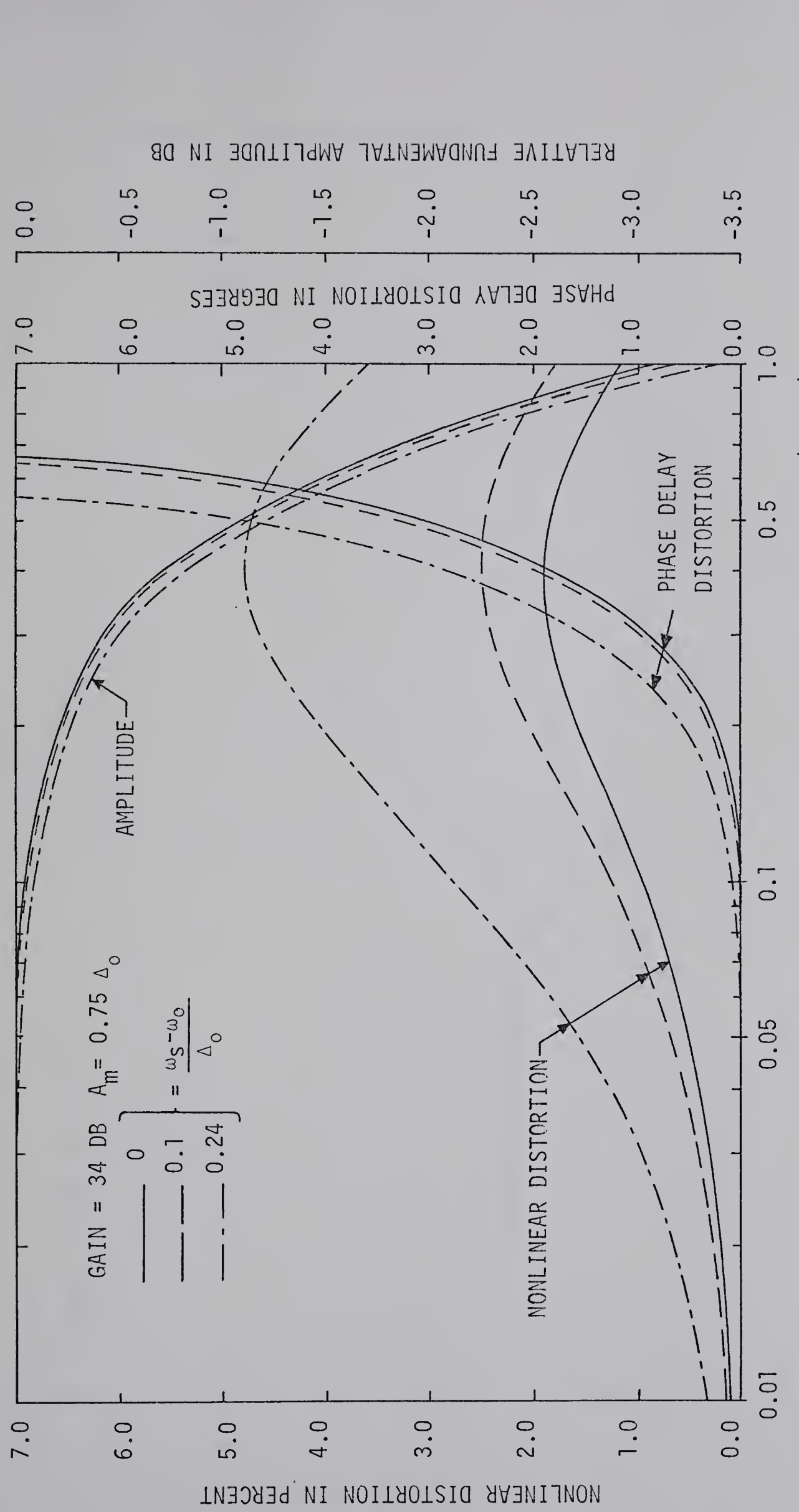

FIG. 6.3-1 FREQUENCY DEPENDENT DISTORTION CHARACTERISTICS FOR A DETUNED SINGLE-STAGE ILO AMPLIFIER MODEL WITH A 34 DB GAIN.

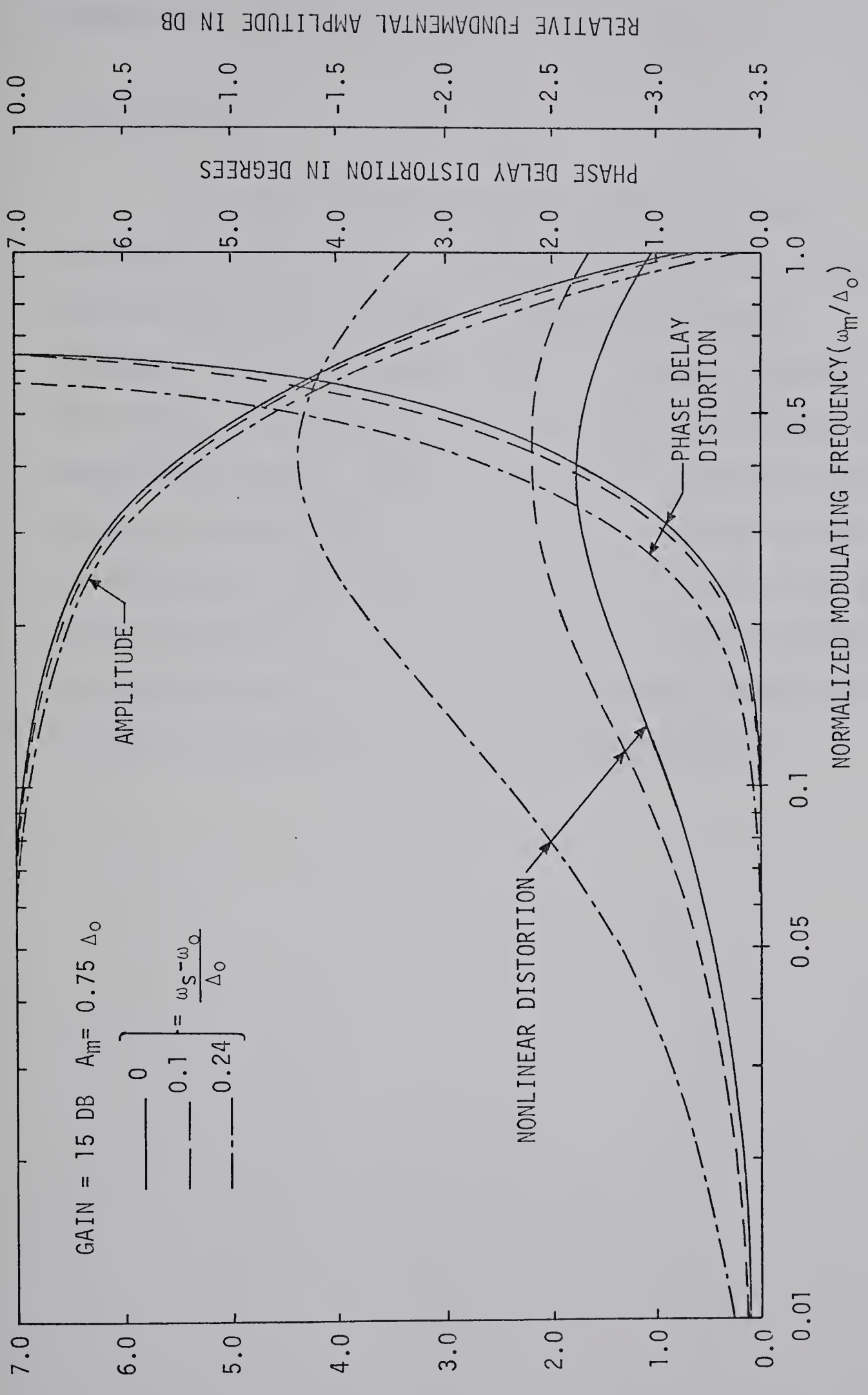

FIG. 6.3-2 FREQUENCY DEPENDENT DISTORTION CHARACTERISTICS FOR A DETUNED SINGLE-STAGE ILO AMPLIFIER MODEL WITH A 15 DB GAIN.

respectively, for each power gain of 34 dB and 15 dB.

6.4 Conclusion

Fig. 6.3-1 and 6.3-2 show that both the relative fundamental amplitude (i.e. frequency response) and the phase delay distortion as a function of normalized modulating frequency are not appreciably affected by frequency detuning, PFD changes, or power gain changes (provided these changes are comparatively small). However, the nonlinear distortion does increase with increases in the normalized modulating frequency, with increases in the normalized PFD and with increases in the normalized detuning. The nonlinear distortion is not strongly dependent on the power gain, so a few distortion curves suffice to give a good estimate of the anticipated distortion.

CHAPTER VII

APPLICATION OF THE DISTORTION ANALYSIS IN THE DESIGN OF A SINGLE-STAGE FM ILO AMPLIFIER

7.1 Introduction

The calculated results derived in the previous chapters will now be used as the basis for a new display of the distortion parameters. These "design contours" are useful when utilized in the design of a single-stage ILO amplifier.

7.2 Design Contours

It is advantageous to use the distortion characteristics of the nonlinear ILO amplifier model (i.e. Fig. 4.2-1) to predict the allowable limits for the parameters of an FM injected signal. That is, the ILO amplifier distortion added to a modulated signal will be below some specified system objective if the modulating signal amplitude and/or frequency remains below certain limits. It is apparent that for each set of ILO parameters, a new family of distortion curves (similar to those shown in Figs. 5.3-1, 5.3-2, 6.3-1, 6.3-2) will be required to accurately portray these features. For weakly dependent distortion characteristics (e.g. relative amplitude variation, etc.) only one of the family of curves will be required for a good practical estimate of the expected performance. However,

for those parameters upon which the distortion characteristics are strongly dependent, a more convenient form of display is required (rather than using a multiplicity of graphs). It is expedient to graphically display constant nonlinear distortion contours and the constant phase delay distortion contours versus the highly dependent variables. As a practical example the constant nonlinear distortion of the ILO amplifier is displayed in Fig. 7.2-1 for a constant gain of 15 dB (when the data points are compared with other power gains, there is little change). These contours are plotted as functions of the normalized PFD and normalized modulating frequency, with the amount of detuning as a parameter. A similar procedure was followed for the phase delay distortion contours for the 15 dB gain case(Fig. 7.2-2). Finally, an examination of Table 5.3-1 indicates that only small changes occur in these contours as a function of gain. It may be predicted that these curves for the 15 dB case have wide practical applicability in describing the ILO behavior.

7.3 An Example of Design Contour Applications

To demonstrate how the design contours of Fig. 7.2-1 and Fig. 7.2-2 may be used to define the limitations of the ILO behavior a design example follows to illustrate the use of these curves. Let it be assumed that the ILO amplifier may be characterized by a loaded Q of 50, a free running oscillator frequency

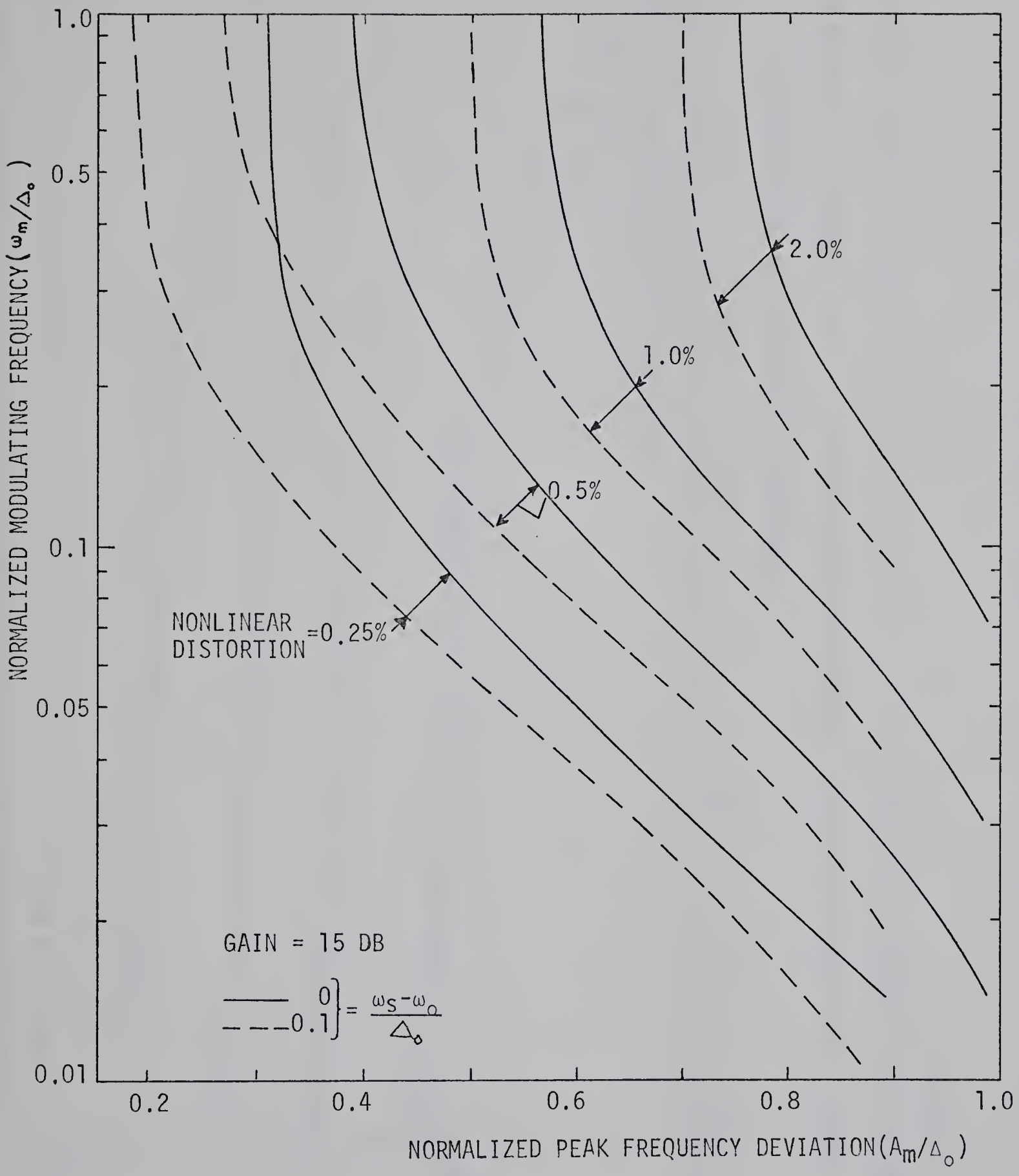

FIG. 7.2-1 CONSTANT NONLINEAR DISTORTION CONTOURS VERSUS THE NORMALIZED PEAK FREQUENCY DEVIATION AND MODULATING FREQUENCY FOR A POWER GAIN OF 15 DB AND FOR NORMALIZED DETUNING FACTORS EQUAL TO 0.0 AND 0.1.

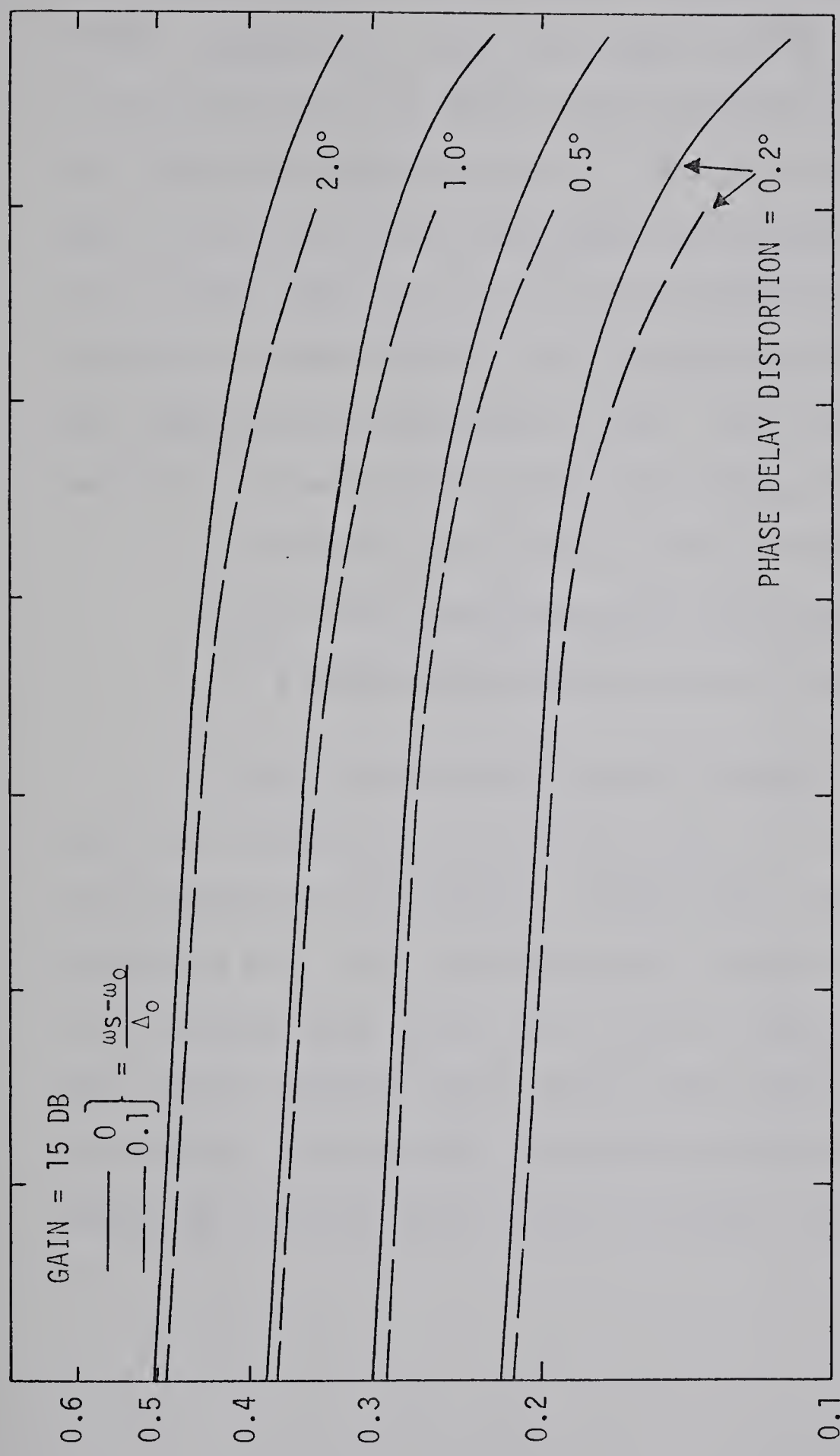

FIG. 7.2-2 CONSTANT PHASE DELAY DISTORTION CONTOURS VERSUS THE NORMALIZED PEAK FREQUENCY DEVIATION AND MODULATING FREQUENCY FOR A POWER GAIN OF 15 DB AND FOR NORMALIZED DETUNING FACTORS EQUAL TO 0.0 AND 0.1.

of 10 GHz and that the power gain of the ILO is adjusted to 15 dB. Consequently, $\Delta_0/2\pi$ will equal 17.8 MHz. Further, let it be assumed that the "free-running" frequency drifts slowly over the region bounded by $f_0 \pm 1.78$ MHz, i.e. $\Delta\omega_0/\Delta_0 \leq 0.1$. Now if the maximum normalized modulating frequency is 0.336 (i.e. 6 MHz), there will be some maximum PFD that will be permitted in order that the output modulation distortion will not exceed the specified system values. For illustrative purposes, let the following reasonable limits be chosen; namely,

a) 1.0% for the maximum nonlinear distortion

b) 1.0^{o} for the maximum phase delay distortion, and

c) a maximum permissible relative signal loss of 3 dB.

Then, by examining the design contours in Figs. 7.2-1 and 7.2-2 the normalized maximum allowable PFD is estimated to be 0.52 and 0.64 respectively. In this case, the nonlinear distortion will limit the PFD more than the other parameters. It is expected that, with proper baseband compensation networks, the frequency response could be made quite linear over the band of interest. Consequently, the relative signal loss limit will not be the limiting factor in most practical cases.

Summary of the Assumed Design Example Conditions

$Q_L = 50$

$f_o = 10$ GHz

$\Delta_o/2\pi = 17.8$ MHz

$\Delta\omega_o/\Delta_o \leq .1$

$f_m = 6$ MHz

$|G| = 15.0$ dB

loss ≤ 3.0 dB

nonlinear distortion $\leq 1.0\%$

phase delay distortion $\leq 1.0^o$

Resultant Limiting Parameter

$$PFD/\Delta_o \leq .52$$

To summarize then, the PFD should not exceed 9.25 MHz in this example for the distortion to stay within the limits. It is expected that Figs. 7.2-1 and 7.2-2 may form the basis of the design procedure for a single-stage ILO amplifier.

7.4 Conclusion and Summary

The previous three chapters form the basis for the

theoretical description of the distortion added to the modulating signal by a certain type of single-stage FM ILO amplifier model. The results reported in this work have been published [25,26]. In summary, the most important results of the application of this theory are the following conclusions about the ILO model; namely,

a) both the nonlinear and the phase-delay distortion will increase with increasing modulating frequency and increased peak frequency deviation of the modulating signal.

b) both types of distortion increase significantly when the sum of the PFD and $\Delta\omega_0$ approach Δ_0.

c) the nonlinear distortion appears to have a maximum when $\omega_m \approx \frac{\Delta_0}{2}$. The relative amplitude variation shows that harmonics beyond Δ_0 in frequency will be attenuated severely.

d) power gain variations appear to have little effect on the distortion characteristics.

e) if a small PFD or large phase delay are allowed, then it is possible to modulate the ILO at frequencies in excess of Δ_0 and still have some acceptable form of transmission.

f) in the work it has been assumed that the sum of the frequency detuning and the peak frequency deviation total less than Δ_0.

CHAPTER VIII

DISTORTION MEASUREMENTS OF A MICROWAVE FM ILO AMPLIFIER

8.1 Introduction

In the previous chapters, the FM ILO amplifier has been modelled theoretically by describing its effect on the modulating signals (both at RF and as well at baseband frequencies). In this chapter, the experiments that were used to verify a part of these theoretically predicted distortion characteristics will be presented, as well as the practical limitations of these measurements.

8.2 Theory, Experimental Set-Up, and Measurement Techniques

Many basic ILO measurements have been reported in the literature [3,8-14,27]. In this chapter, it will be assumed that the reader will refer to the literature and in particular to B.C. So's [3] doctoral dissertation for a) the theoretical basis of many of the basic measurements, b) the experimental set-up for several basic experiments and c) the results of these experiments. A short listing of the relevant experiments will be included (particularly those which apply to the experimental work of this chapter); namely,

1) measurements of the locking range

   a) output spectra

b) locking range variation with power ratio

c) oscillator quality factor derived from the locking bandwidth

2) measurement of the phase angle difference between the locked oscillator output and the locking signal, and the phase angle variation with initial frequency difference

3) intermodulation signals in injection phase-locked oscillators

Since most of the measurements were required for the calibration and alignment procedures of the following experimental work, the remainder of the chapter will build upon this base and detail the additional work that was done.

The purpose of the following experimental work was to verify the basic distortion theory derived in the previous chapters and reported upon in the literature [3,8-14,18]. The types of distortion that are to be measured include:

a) loss of the demodulated signal amplitude with increasing frequency,

b) the phase delay distortion of the demodulated output signal versus the input signal,

and, c) the nonlinear distortion of the demodulated output signal.

Several investigators have reported success in measuring the

relative power loss (most of them express it in slightly different mathematical forms) [8-14] . Thus it remains for the phase delay distortion and the nonlinear distortion to be verified. After extensive work using the available instrumentation, it was only found practical to measure the nonlinear distortion. Consequently, this chapter will now detail a method of measuring the output signal's nonlinear distortion in an attempt to verify the theoretically predicted distortion parameters. The nonlinear distortion added to an FM modulating signal and amplified by the ILO will be measured in a circuit configuration very similar to the model shown in Fig. 4.2-1. Basically, the nonlinear distortion added by the FM ILO amplifier to the modulating signal is obtained by comparing the harmonic content present on the demodulated output signal with that of the demodulated input signal. By using demodulators with similar characteristics it is possible to measure the main effect of the nonlinear distortion — namely, the harmonic content of the demodulated signal.

The experimental circuit used to verify these nonlinear characteristics is shown in Fig. 8.2-1 and Fig. 8.2-2. A microwave oscillator operating in the X-band frequency range was used as the ILO (this oscillator is similar to the one So used in his study). A baseband single-tone sinusoid is used to modulate the voltage across a varactor diode in the

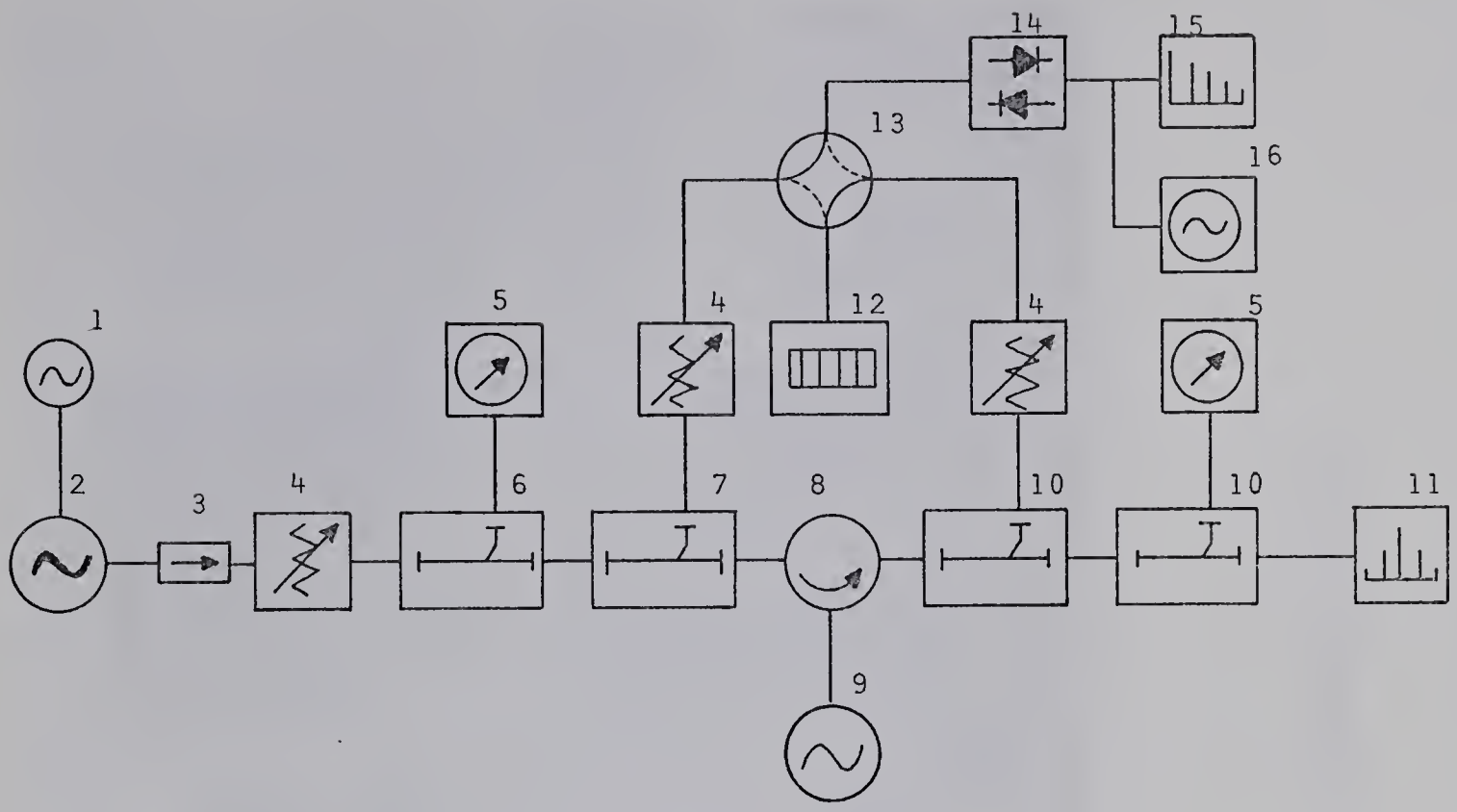

1. LOW FREQUENCY MODULATING OSCILLATOR
2. VARACTOR-TUNED GUNN DIODE FM OSCILLATOR
3. ISOLATOR
4. PRECISION ATTENUATOR
5. POWER METER
6. 10 DB DIRECTIONAL COUPLER
7. 30 DB DIRECTIONAL COUPLER
8. FOUR-PORT CIRCULATOR
9. IMPATT DIODE OSCILLATOR
10. 20 DB DIRECTIONAL COUPLER
11. RF SPECTRUM ANALYZER
12. DIGITAL FREQUENCY COUNTER
13. WAVEGUIDE SWITCH
14. FREQUENCY DISCRIMINATOR
15. LOW FREQUENCY SPECTRUM ANALYZER
16. OSCILLOSCOPE

FIG. 8.2-1 SCHEMATIC FORM OF THE EXPERIMENTAL SET-UP FOR THE MEASUREMENT OF THE NONLINEAR DISTORTION IN AN ILO AMPLIFIER.

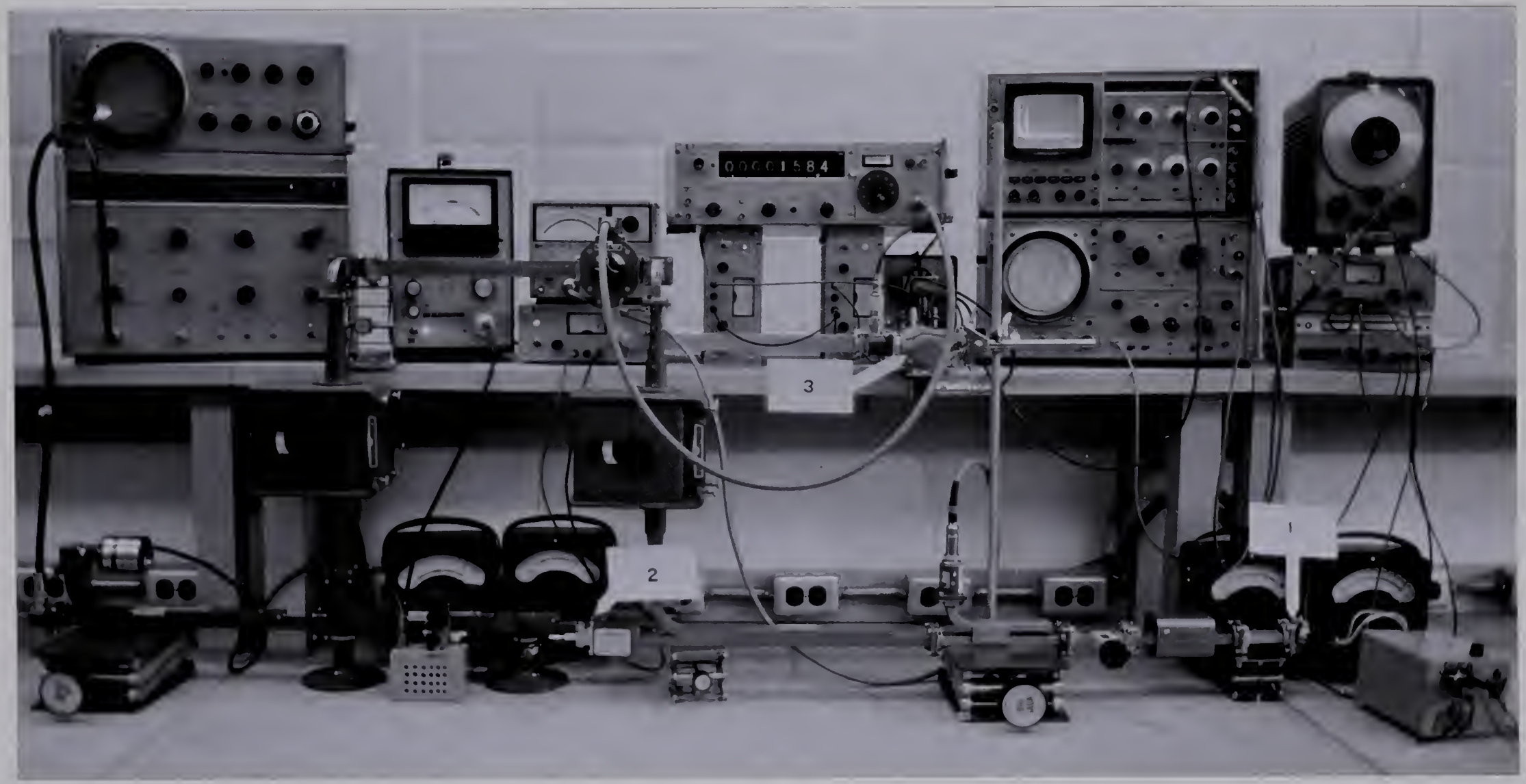

FIG. 8.2-2 A PHOTOGRAPH OF THE FM ILO NONLINEAR DISTORTION EXPERIMENTAL SET-UP

varactor tuned Gunn diode oscillator (2). The numbers in the brackets here refer to specific equipment and to locations in Fig. 8.2-1. The Gunn diode oscillator was used to produce the incident microwave locking signal. This FM locking signal was then injected into the cavity of an IMPATT diode oscillator (9) through a 40 dB isolator (3), a precision attenuator (4) set such that the desired locking power gain was achieved, a 10 dB precision coupler (6) for power monitoring purposes, a precision 3 dB coupler (7), and into port 1 of a high gain four-port circulator (8). The locking signal power level was monitored with a power meter (5) connected to the auxiliary arm of the 10 dB directional coupler (6). The locking signal power level was adjusted for different gain ratios by adjusting the precision attenuator (4). This monitoring circuit was used to obtain an estimate of the correct power level, the final adjustments were made by observing and measuring the bandwidth relations to provide the most correct answer. The power reaching the IMPATT diode was reduced by about 3 dB, since the locking signal power is reduced by the 3 dB precision attenuator (7) and ports 1-2 of the high gain four-port circulator (8). Paths 1-2 of the circulator have a return loss of about 40 dB or better. The isolator (3) and the adjustable attenuator (4) assure that the locking signal is adequately isolated from the rest of the system. The locked

oscillator output signal is dissipated in the matched 50 ohm termination of the RF spectrum analyzer (11), after having passed through the circulator path 2-3, and the two 20 dB couplers (10). Any reflected power from the output circulator circuit must pass through the circulator path 3-4 and is dissipated in a matched load connected to port 4. This circulator path 1-4 provides isolation in the order of 52 dB while the insertion losses of paths 1-2 and 2-3 are about 0.2 dB. The IMPATT diode output power is monitored by a power meter connected to the auxiliary arm of a 20 dB directional coupler (10). The reason for the isolation is to provide both the locking signal and the output signal individually as well as for mixing purposes. Both signals must be available without appreciably affecting the main injection-locking circuit. Consequently, the demodulated input FM signal is obtained by monitoring through the auxiliary arm of the 3 dB directional coupler (7) and by demodulating the RF signal by the use of a dual-mode doubly-tuned cavity (14) as a discriminator. The demodulated FM signal is displayed on a low-frequency spectrum analyzer and an oscilloscope. To demodulate the output FM signal, the waveguide switch is moved to its alternate position, so that the output FM signal (coming from the auxiliary arm of the 20 dB directional coupler) is then demodulated by the same discriminator. By means of this circuit arrangement it is possible to compare the input and output

demodulated waveforms with relative ease. In addition, since essentially the same circuit components are used in both measurements many of the errors in the measurements may be assumed to be common to both input and output measurements and may be eliminated by subtraction.

In Fig. 8.2-2, arrow #1 points to the varactor-tuned Gunn diode oscillator, which is used as the locking signal. It has a nominal output power of about 10 milliwatts. Its frequency may be tuned both mechanically (from 8.8 to 10.2 GHz) and electrically (over a 50 to 75 MHz range). Arrow #2 points to a Sylvania avalanche diode oscillator (model SYO-3200, S/N 140). The IMPATT diode is mounted in an end-loaded coaxial cavity and iris-coupled to a X-band waveguide (WR90). The output frequency can be tuned both mechanically and electrically throughout X-band. The oscillator used typically produces about 21 milliwatts of RF power at 9.157 GHz for a reverse bias of about 90 volts and a current of 20 ma. Arrow #3 in Fig. 8.2-2 points to the doubly-tuned cavity which is used as a direct down-conversion FM discriminator. To facilitate using FM signals with a 2MHz deviation it was necessary to increase the 3 dB bandwidth of the cavity and the detector diodes (i.e. lower the Q). In particular, harmonics up to 10 MHz would have to be detected to make this method valid. The cavity bandwidth was increased at the expense of discriminator sensitivity by coating the tuning plunger face with a lossy

material (in this case ECCOSORB powder was used). The bandwidth of the detector diodes was also increased by a) reducing the diode resistance by applying an appropriate forward bias on the diodes, b) reducing the capacitive loading on the diodes, and c) using high input-impedance emitter follower amplifiers.

The set-up described thus far will now be used to verify the nonlinear distortion characteristics of a microwave FM ILO amplifier. The system was characterized and aligned by the procedure outlined and performed by B.C. So and as discussed in the beginning of this chapter. In the specific experiment performed in this study, the maintenance of an initial frequency difference as close to zero as possible assumed major importance since nonlinear distortion is highly dependent upon this factor. Several other factors mentioned during the tuned and detuned theoretical discussions (e.g. frequency drift etc.) necessitated that the alignment procedures for the set-up be repeated between each experimental point. The various power levels were also monitored continuously to ensure that the circuit parameters did not vary appreciably (this was necessary since often this was the only "probe" available to a certain point). Additionally, the combination of a low Q oscillator combined with a higher Q discriminator necessitated the measurements being performed at a fairly high gain to keep the bandwidth small.

The discriminator used in this experiment (after the cavity had its bandwidth extended) had a linear response characteristic over a±1.75 MHz bandwidth about an adjustable center frequency. The maximum detected frequency exceeded 5 MHz when allowance was made for some considerable nonlinear behavior. A typical response curve for the frequency discriminator is illustrated in Fig. 8.2-3. Consequently, a modulating frequency in excess of 1.5 MHz could not have its harmonics detected accurately. As mentioned previously, too high a gain will preclude the accurate frequency alignment of the system for any length of time. As a consequence, a practical compromise was arrived at and the distortion measurements were performed with a gain of 34 dB. The initial frequency difference was maintained to less than fifteen percent of Δ_o in practice. The frequency deviation was set such that the demodulated output showed a frequency deviation of 1.125 MHz, i.e. 75 percent of the maximum frequency difference; namely, 1.5 MHz (this was maintained to better than ten percent by constant monitoring and realignment where necessary). The RF spectrum analyzer and the level of the demodulated output provided the means by which these levels were monitored and maintained.

To obtain accurate experimental measurements the use of the "zero crossing" method will now be explained. The application of this technique will allow the selection of

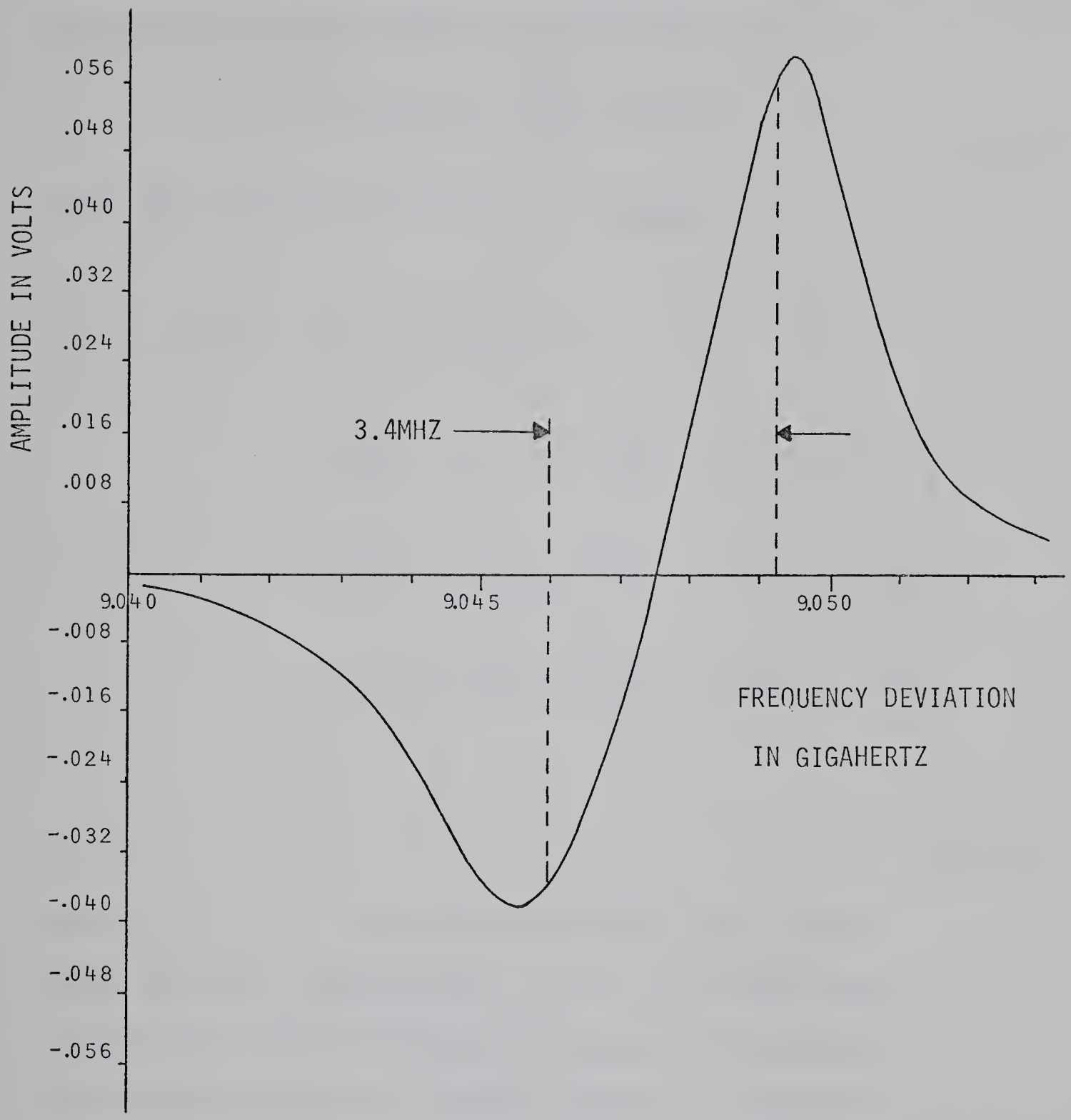

FIG 8.2-3 A PLOT OF THE VOLTAGE AMPLITUDE DEFLECTION OF THE FREQUENCY DISCRIMINATOR VERSUS THE FREQUENCY DEVIATION(SWEPT FROM 9.040 TO 9.060 GHZ) FOR AN INPUT POWER LEVEL OF 0.2 MILLIWATTS.

modulation parameters in the experimental set-up to give several accurate experimental data points on the distortion graphs.

Let the FM modulating signal be expressed as

$$e_{in}(t) = E_{in}\sin(\omega_o t + \left(\frac{A_m}{\omega_m}\right)\sin\omega_m t) \tag{8.2-1}$$

After some manipulation[28], Eq. 8.2-1 becomes

$$\begin{aligned} e_{in}(t) = E_{in}\Bigg\{ & J_o\left(\frac{A_m}{\omega_m}\right)\sin\omega_o t \\ & + J_1\left(\frac{A_m}{\omega_m}\right)\left[\sin(\omega_o + \frac{A_m}{\omega_m})t - \sin(\omega_o - \frac{A_m}{\omega_m}t\right] \\ & + J_2\left(\frac{A_m}{\omega_m}\right)\left[\sin(\omega_o + \frac{2A_m}{\omega_m})t + \sin(\omega_o - \frac{2A_m}{\omega_m})t\right] \\ & + J_3\left(\frac{A_m}{\omega_m}\right)\left[\sin(\omega_o + \frac{3A_m}{\omega_m})t - \sin(\omega_o - \frac{3A_m}{\omega_m})t\right] \\ & + \cdots\cdots \Bigg\} \end{aligned} \tag{8.2-2}$$

where J_o, J_1, J_2,....represent the zeroth, first, second Bessel function, respectively[33]. Now Eq. 8.2-2 has separated the FM signal into its frequency components (or sidebands). Each sideband will have a certain amplitude associated with it and there will be an infinite number of sidebands which are separated from the carrier frequency by integer multiples of the modulating frequency. A very important characteristic for this study is that the carrier amplitude will be reduced

by $J_o\left(\frac{A_m}{\omega_m}\right)$. Additionally, the sideband amplitudes depend upon the value of $J_n\left(\frac{A_m}{\omega_m}\right)$ where n = 1, 2, 3, 4 ... and these will diminish rapidly when $n > \frac{A_m}{m}$. Therefore, the sideband amplitudes diminish rapidly outside the region of the maximum frequency deviation; namely, $A_m/2\pi$ removed from the carrier. Fig. 8.2-4 illustrates these principles for the following set of practical parameters: ω_o = 10.0 GHz, $\Delta_o/2\pi$ = 1.5 MHz, $A_m = .75\Delta_o$, A_m/ω_m = 2.4048, $\omega_m/2\pi$ = 469 KHz. It is interesting to note that the power in each sideband will be proportional to the square of the Bessel coefficient while the total power on the spectra is proportional to the sum of the squares of the carrier and sideband amplitudes. Mathematically this will be expressed as

$$\left[J_o\left(\frac{A_m}{\omega_m}\right)\right]^2 + \sum_{n=1}^{\infty}\left[J_n\left(\frac{A_m}{w_m}\right)\right]^2 = 1 \qquad (8.2\text{-}3)$$

The important result of this study is that for certain values of modulation index A_m/ω_m the zeroth bessel function will go to zero. Consequently, the carrier amplitude will go to zero when $J_o(x)$ equals zero (i.e. for the following values of x = 2.4048, 5.5201, 8.6537, 11.7915, 14.9309, 18.0711, etc.). Therefore, it will be a relatively simple matter to measure these points on the distortion curve accurately. When the maximum frequency deviation is set equal to a constant, then certain modulating frequencies will cause the carrier amplitude in the frequency spectrum to go to zero.

SET OF PARAMETERS

ω_o = 10.0 GHZ

$\Delta_o/2\pi$ = 1.5 MHZ

$A_m = 0.75\Delta_o$

A_m/ω_m = 2.4048

$\omega_m/2\pi$ = 469 KHZ

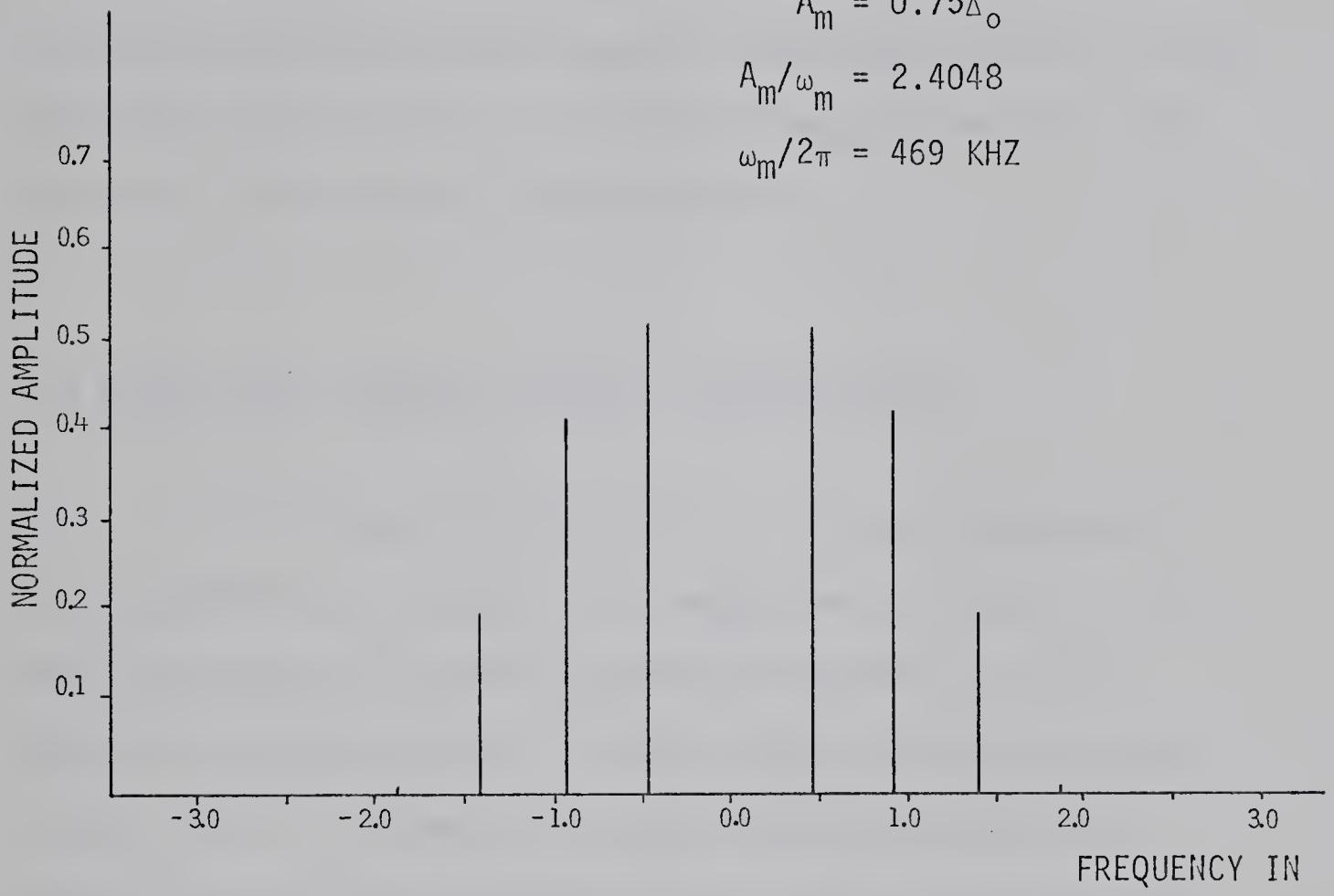

FIG. 8.2-4 FREQUENCY SPECTRUM FOR AN FM SIGNAL WITH CARRIER ZERO.

As a result of the above theory, several experimental runs were performed based upon this technique. The accuracy with which the frequency deviation and the modulating frequency may be maintained limit the accuracy of this experimental technique. For the 34 dB gain case the experimental measurements were performed with relatively good accuracy (discussed in detail in the following section) when the modulating frequency was less than one half of the maximum locking bandwidth.

8.3 Experimental Results and Their Interpretation

In this section, the results of several experiments are presented and discussed. The experiment used was that which has been proposed to verify the model of Chapter IV. This concept was used as the basis of the experimental set-up shown in Fig. 8.2-1. In summary, the experiment was performed to verify the nonlinear distortion curve of Fig. 6.3-1 for an ILO amplifier with a 34 dB gain ratio. The plot shown in Fig. 6.3-1 was found by comparing the demodulated output signal with the input modulating signal and arriving at a percentage distortion by Eq. B-30. Therefore, a similar technique was used in the experiment by the use of a common frequency discriminator on the input and output frequency modulated signals.

The alignment procedures were described in detail in the previous section and in the work of So[3]. To summarize,

the free-running frequency of the oscillator (9) was adjusted such that it coincided with the passband of the frequency discriminator. The modulating signal was then adjusted such that the initial frequency difference as measured by a RF frequency counter was as close to zero as possible. The proper power ratio was then adjusted for a 34 dB gain ratio (based mainly upon the measured frequency deviation allowable for locking and the frequency counter). Then the frequency modulation was applied via an amplitude modulation signal to the voltage that tunes the frequency of the varactor-tuned Gunn diode oscillator. During the entire experimental runs periodic realignment of the initial frequency difference was required to maintain it close to zero. Then the demodulated input FM signal was measured via the frequency discriminator for the parameters necessary to coincide with the zero-crossing method. Then comparable measurements were made of the demodulated output signal and the two waveforms were then compared. For a 34 dB gain ratio the following parameters characterized the system:

$\omega_o/2\pi = 9.57$ GHz

$\Delta_o/2\pi = 1.5$ MHz ($\pm 5\%$)

$A_m = .75\,\Delta_o$

$A_m/2\pi = 1.125$ MHz (to better than 10%)

$\Delta\omega_o/\Delta_o \leq .1$ (i.e. to better than 10%)

The results of a typical experimental run are presented in Table 8.3-1 and Figs. 8.3-1 and 8.3-2. Fig. 8.3-1 displays photos of the demodulated input and demodulated output signals at the third carrier zero; i.e. 130 KHz. The large spike is the "zero" starting pulse of the spectrum analyzer while the second spike is the demodulated fundamental frequency. The remainder of the sidebands are then the distortion products. By use of Eq. B-30 it is a straightforward matter to compute distortion quantities. Fig. 8.3-2 is a display of the experimental points for a typical experimental run versus the theoretically predicted results for the three frequency detuning factors; namely, $\Delta\omega_o$= 0.0, 0.1 and 0.24. As can be seen the experiment data follow the general shape of the predicted curve until about 0.3 of the normalized modulating frequency. As will be recalled, the zero crossing method may only be used to accurately predict the parameters at those points shown in Table 8.3-1. The highest fraction of the normalized modulating frequency to which the zero crossing method is applicable is 0.313 (i.e. the first carrier zero). The experimental points beyond this were measured by the alignment of the ILO with the frequency counter and the spectrum analyzer. However, the amount of distortion measured at these experimental points does not have the same degree of accuracy that the data coinciding with the "zero crossing" points has.

TABLE 8.3-1 EXPERIMENTAL DISTORTION MEASUREMENTS FOR A 34 DB GAIN DETUNED SINGLE-STAGE ILO AMPLIFIER.

ORDER OF CARRIER ZERO	MODULATION INDEX	$\frac{\omega_m}{2\pi}$	$\frac{\omega_m}{\Delta_o}$	VARACTOR AC VOLTAGE	BASEBAND INPUT AMPLITUDE	BASEBAND OUTPUT AMPLITUDE	RATIO	NORMALIZED RATIO IN DB	DISTORTION AS PER EQ.B-30
6	18.0711	62 kHz	0.0413	15mv	0.95mv	1.36mv	1.44	0.0	0.89%
5	14.9309	75 kHz	0.05	15mv	0.95mv	1.37mv	1.44	0.0	1.19%
4	11.7915	95 kHz	0.063	15mv	0.95mv	1.37mv	1.44	0.0	1.33%
3	8.65	130kHz	0.0867	15mv	0.95mv	1.37mv	1.44	0.0	1.74%
2	5.55	203kHz	0.135	15mv	0.95mv	1.37mv	1.44	0.0	2.15%
1	2.40	469kHz	0.313	15mv	1.00mv	1.36mv	1.36	-0.25	3.36%
N/A	-----	1.0MHz	0.667	15mv	0.88mv	1.04mv	1.18	-0.975	2.75%
N/A	-----	1.5MHz	1.0	15mv	0.85mv	0.90mv	1.06	-1.33	1.40%

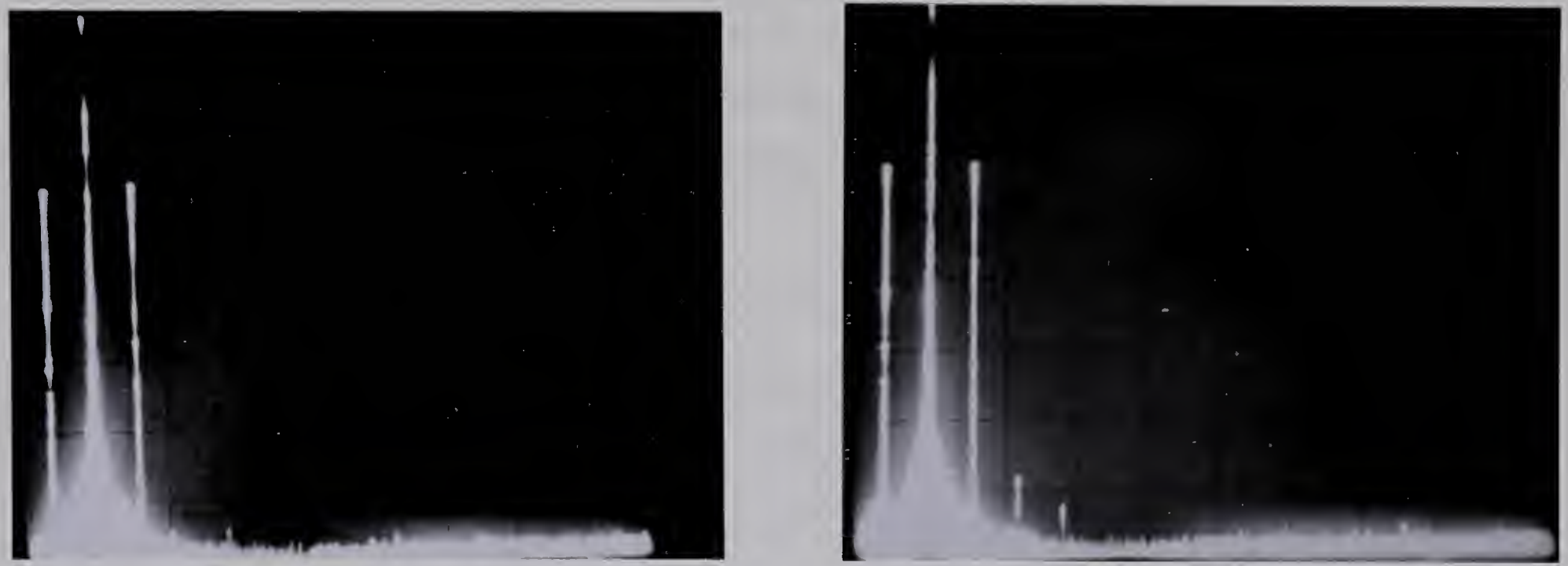

(a)

DEMODULATED INPUT SIGNAL
(LOW FREQUENCY SPECTRUM ANALYZER DISPLAY)

VERTICAL SCALE = 10 DB/CM
HORIZONTAL SCALE = 200 kHZ/CM

(b)

DEMODULATED OUTPUT SIGNAL
(LOW FREQUENCY SPECTRUM ANALYZER DISPLAY)

VERTICAL SCALE = 10 DB/CM
HORIZONTAL SCALE = 200 kHZ/CM

FIG. 8.3-1 AN EXAMPLE OF THE DEMODULATED INPUT AND OUTPUT SIGNALS MEASURED FOR THE 34 DB GAIN CASE

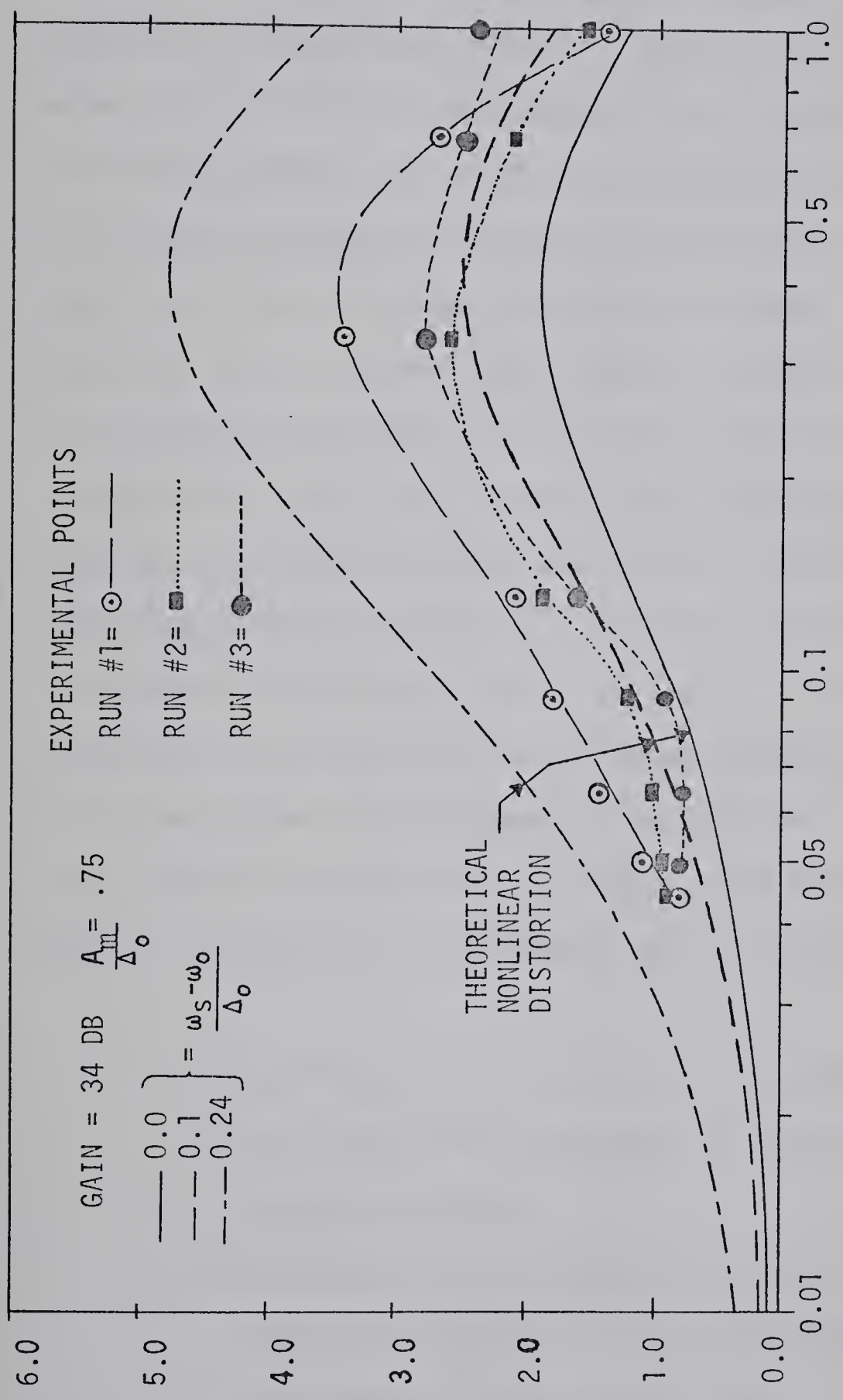

FIG 8.3-2 A PLOT OF THE EXPERIMENTAL VERSUS THE THEORETICAL DISTORTION CHARACTERISTICS FOR THE 34DB GAIN CASE OF THE DETUNED ILO AMPLIFIER.

An examination of Fig. 8.3-2 indicated that the distortion data points between 0.0413 and 0.313 of the normalized modulating frequency follow the slope of the calculated distortion characteristics closely. However, the numerical values of the distortion data points do vary from those which the theory predicts. In practice it was possible to maintain the frequency dependent variables to better than 15 percent (e.g. the initial frequency difference, the peak frequency deviation, etc.). Several other factors that were not considered in this analysis may have an effect (e.g. noise contribution from both the locked oscillator and the locking signal). Therefore, the distortion data points beyond 0.313 of the normalized modulating frequency will not be accurate since the harmonics of the distorted output signal are severely attenuated by the ILO amplifier and these harmonics exceed the linear region of the frequency discriminator. In summary then, the following factors must be considered in any error analysis related to the experimental data of this work; namely,

1) the frequency drift of the "free-running" oscillator
2) the instabilities (expressed as noise) of the locking oscillator
3) the limited linear range of the tuned cavity frequency discriminator versus the larger bandwidth requirement of the ILO amplifier

4) the noise and nonlinear behavior of the detector diodes and amplifiers, and
5) the selection of a high gain case makes the relative error calculations much more sensitive than for a comparable lower gain case.

As a consequence, the experimental results presented in Table 8.3-1 and Figs. 8.3-1 and 8.3-2 may be taken to be a partial verification of the predicted nonlinear distortion characteristics for an FM ILO amplifier. The experimental data appear to fit the theory when the $\frac{\Delta\omega_o}{\Delta_o} = 0.24$ theoretical curve is used as a guide. It is difficult to arrive at a numerical value for the error in these measured data points for the numerous reasons cited above.

CHAPTER IX

SUMMARY AND CONCLUSIONS

A detailed systematic study of the injection-locking properties of microwave IMPATT diode oscillators used as amplifiers of FM signals has been performed. An injection-locked oscillator (ILO) model based upon the generalized Adler's phase-locking equation was used in the mathematical treatment of the locking phenomenon involved. The analysis has treated the ILO as a baseband amplifier whose locking and locked signals are the input and output signals, respectively (see Fig. 4.2-1). This analysis is an important addition to the manner in which an ILO may be characterized--particularly for the dynamic locking condition. It is now possible to theoretically characterize the locked condition when the locking signal is modulated at frequencies approaching the maximum locking bandwidth. The differential equation involved have been solved numerically. The results for the distortion that a single-stage ILO amplifier produces have been presented in the form of design contours (see Chapters V,VI,VII)[25,26].

The equivalent model for the ILO amplifier was based upon the concepts and terminology common to baseband amplifiers and repeaters. The theoretical analysis indicates that an ILO

amplifier behaves as a band-limited amplifier for baseband modulating signals. The ILO amplifier was characterized by the following three parameters; namely, a) the gain variation, b) the phase delay distortion, and c) the nonlinear distortion versus the baseband modulating frequency. This approach indicated that the 3 dB bandwidth of the ILO amplifier model is approximately $\Delta_0/2\pi$ Hz.

Based upon the previous theoretical description of the ILO amplifier characteristics, the following conclusions may be stated:

1. changes in the modulating signal frequency parameters have a more pronounced effect upon the distortion characteristics than variations in the locking signal amplitude.
2. the variation in the demodulated fundamental output amplitude is highly dependent upon the modulating signal frequency; however, it is not sensitive to changes in the peak frequency deviation, the amount of detuning or the gain of the ILO.
3. the phase delay distortion of the demodulated fundamental increases with increasing modulating signal frequency, peak frequency deviation and the amount of detuning.

4. the nonlinear distortion of the demodulated fundamental signal increases with increases in modulating signal frequency, peak frequency deviation, and decreases in the gain of the ILO amplifier.

These theoretically predicted results have been reported in the literature for dynamic locking conditions[25,26]. The nonlinear distortion of the fundamental modulating signal has been experimentally verified (see Chapter VIII) with a microwave IMPATT diode oscillator as the ILO amplifier.

The following items (related to the characterization of ILO's) represent areas for further research:

1. a more precise phase-locking equation may be required to effectively characterize the dynamic phase locking characteristics when the amplitude effect is included in the ILO modelling (i.e. throughout the analysis it has been assumed that the ILO acts as a perfect limiter. This is not correct for certain ratios of locking powers, modulating frequencies or peak frequency deviations on the modulating signal)[23].
2. the manner in which the dynamic phase variation of the locking relationship decays to its steady-

state values throughout each modulation cycle could be treated in more detail (see Chapter III). Further mathematical analysis may uncover a suitable analytic treatment of the distortion added to the modulating signals of an ILO amplifier.

3. further experimental work could be performed with improved experimental techniques to verify the nonlinear distortion characteristics beyond 0.336 of the normalized modulating frequency and to verify the phase delay distortion curves (in particular a much lower Q cavity must be incorporated with a measuring system that will give sufficient voltage deflection for correct measurements).

REFERENCES

1. Adler, R., "A Study of Locking Phenomena in Oscillators," Proc. IEEE, vol. 34, pp. 351-357, June 1946

2. Paciorek, L.J., "Injection Locking of Oscillators," Proc. IEEE, vol. 53, pp. 1717-1723, Nov. 1965

3. So, B.C., Injection Phase-Locking Properties of Microwave IMPATT Diode and GUNN Diode Oscillators With System Applications, Ph. D. Thesis, Department of Electrical Engineering, The University of Alberta, Edmonton, Alberta, 1971

4. Mackey, R.C., "Injection Locking of Klystron Oscillators," IRE Trans. on Microwave Theory and Techniques, pp. 228-235, July 1962

5. Tucker, D.G., "The Synchronization of Oscillators," Electronic Engineering, vol. 15, pp. 412-418, March 1943, pp. 457-461, April 1943, pp. 26-30, June 1943, pp. 114-117, Aug. 1943

6. Stover, H.L., and R.C. Shaw, "Injection Locked Oscillators as Amplifiers For Angle Modulated Signals," Digest of Technical Papers, G-MTT International Symposium, 1966

7. Lee, T.P., and R.D. Standley, "Frequency Modulation of a Millimeter-Wave IMPATT Diode Oscillator and Related Harmonic Generation Effects," Bell Syst. Tech. J., vol. 48, pp. 143-161, Jan. 1969

8. Isobe, T., and M. Tokida, "A New Microwave Amplifier for Multichannel FM Signals Using A Synchronized Oscillator," IEEE Journal on Solid-State Circuits, vol. 4, pp. 400-408, Dec. 1969

9. Isobe, T., and M. Tokida, "Noise Loading Performance of a Phase-Locked IMPATT Oscillator for Multichannel FM Signals," Proc. IEEE, vol. 56, pp. 873-875, May 1968

10. Isobe, T., and M. Tokida, "Effects of Phase Locking on Modulation Characteristics," Proc. IEEE, vol. 56, pp. 453-454, March 1967

11. Isobe, T., and M. Tokida, "Noise Reduction of Oscillators by Phase Locking," J. Inst. Electronics Communications Engineers(Japan), vol. 50, pp. 2093-2100, Nov. 1967

12. Isobe, T., and M. Tokida, "Power Amplification for FM and PM Signals with Synchronized IMPATT Oscillators," IEEE Trans. on Microwave Theory and Techniques, vol. MTT-18, pp. 906-911, Nov. 1970

13. Mastalli, P., et al, "A New Microwave Repeater for FM Radio Links," Alta Frequenza(Italy), vol. 37, pp. 85E-95E, May 1968

14. Hines, M.E., et al, "FM Noise Suppression of an Injection Phase-Locked Oscillator," IEEE Trans. on Microwave Theory and Techniques, vol. MTT-16, pp. 738-742, Sept. 1968

15. Slater, J.C., Microwave Electronics, Princeton, D. Van Nostrand Company, pp. 187-221, 1964

16. Kurokawa, K., "Noise in Synchronized Oscillators," IEEE Trans. on Microwave Theory and Techniques, vol. MTT-16, pp. 234-240, April 1968

17. Kurokawa, K., "Injection Locking of Microwave Solid-State Oscillators," Proc. IEEE, vol. 61, pp. 1386-1410, Oct. 1973

18. Udelson, B.J., and R.E. Hines, "Frequency Modulation of a C.W. Avalanche Oscillator by an Injected R.F. Signal," Microwave Journal, vol. 14, pp. 25-34, Oct. 1971, and pp. 42-46, Dec. 1971

19. Khohlov, R.V., "A Method of Analysis in the Theory of Sinusoidal Self-Oscillations," IRE Trans. on Circuit Theory, vol. 7, pp. 398-410, Dec. 1960

20. Hines, M.E., "Negative Resistance Diode Power Amplification" IEEE Trans. on Electron Devices, vol. 17, pp. 1-9, Jan. 1970

21. Cramer, N.B., "Characterization and Modelling of IMPATT Oscillators," IEEE Trans. on Electron Devices, vol. ED-15, pp. 838-846, Nov. 1968

22. Gray, W., et al, " Applying IMPATT Power Sources to Modern Microwave Systems," IEEE Journal of Solid-State Circuits, vol. 4, pp. 403-413, Dec. 1969

23. Osborne, T.L., "Amplitude Behaviour of Injection Locked Oscillators," IEEE Trans. on Microwave Theory and Techniques, vol. MTT-18, pp. 897-906, Nov. 1970

24. Van der Pol, B., "The Nonlinear Theory of Electric Oscillations," Proc. IRE, vol. 22, pp. 1051-1085, Sept. 1934

25. Nigrin, J., J.F.W. Gurke, and P.A. Goud, "Distortion of FM Modulation in Injection Phase-Locked Oscillator-Amplifiers," Proc. IEEE, vol. 60, pp. 458-459, April 1972

26. Nigrin, J., P.A. Goud, and J.F.W. Gurke, "Distortion of FM Modulation in Detuned Injection Phase-Locked Oscillator-Amplifiers," Proc. IEEE, vol. 60, pp. 731-732, June 1972

27. Marazzi, E., and A. Bellando, "Thin-Film Injection-Locked Oscillators and Negative Resistance Amplifiers for a 2-GHz Radio Repeater," IEEE Journal of Solid-State Circuits, vol. SC-17, pp. 23-32, Feb. 1972

28. Terman, F.E., Electronic and Radio Engineering, New York, Mc Graw-Hill Book Company, 1955, p. 503

29. Altman, J.L., Microwave Circuits, Princeton, D. Van Nostrand Company, 1964, pp. 134-257

30. Van Valkenburg, M.E., Network Analysis, Englewood Cliffs, Prentice-Hall Inc., 1964, pp. 228-374

31. Peirce, B.O., and R. Foster, A Short Table of Integrals, New York, Blaisdell Publishing Co., 1956, pp. 44-46

32. Wozencraft, J., and I. Jacobs, Principles of Communication Engineering, New York, John Wiley & Sons, 1965, pp. 645-665

33. Goldman, S., Frequency Analysis, Modulation and Noise, New York, McGraw-Hill, 1948, pp. 141-204

34. Carson, J., "Notes on the Theory of Modulation," Proc. IRE, vol. 16, pp. 966-975, July 1928

35. Fagot and Magne, Frequency Modulation Theory -- Applications to Microwave Links, New York, Pergamon Press, 1961

36. Members of the Technical Staff, Bell Telephone Laboratories, Transmission Systems for Communications, Western Electric Co., Fourth Edition, 1970, pp. 13-37, pp.97-122, pp. 237-278, pp. 423-432, pp. 450-468

37. Wang, S.C., " Distortion of FM Signals Casued by Channel Phase Nonlinearity and Amplitude Fluctuation," IEEE Trans. on Communication Technology, vol. COM-14, pp. 440-448, Aug. 1966

38. Hammond, S.B., Electrical Engineering, New York McGraw-Hill Book Company, 1961

39. Moreno, T., Microwave Transmission Design Data, New York, Dover Publications, 1948, pp. 210-213

40. Carlson, A.B., Communication Systems: An Introduction to Signals and Noise in Electrical Communication, New York, McGraw-Hill Book Company, 1968

41. Oliver, B.M., and J.M. Cage, Electronic Measurements and Instrumentation, New York, McGraw-Hill Book Company, 1971

42. Dishington, R.H., "Diode Phase-Discrimination," Proc. IRE, vol. 37, pp. 1401-1404, Dec. 1949

43. Korn, G.A., Basic Tables in Electrical Engineering, New York, McGraw-Hill Book Company, 1965, pp. 18-44

44. Struble, R.A., Nonlinear Differential Equations, New York, McGraw-Hill Book Company, 1962

45. Holtzman, J.M., Nonlinear System Theory, Englewood Cliffs, Prentice-Hall Inc., 1970

46. Rall, L.B., Computational Solution of Nonlinear Operator Equations, New York, John Wiley & Sons Inc., 1969

APPENDIX A

SIGNAL DISTORTION IN TRANSMISSION SYSTEMS

The purpose of this appendix is to review the definition of "distortionless transmission" through a communications system and to define the various types of distortion with reference to the ILO amplifier analysis[28-40].

Let a communication system (often referred to as a transmission system) be represented as in Fig. A-1. Then $g(t)$ will represent the linear system transfer characteristics. When an input signal $e_{in}(t)$ is transmitted through a two-port network, the output signal $e_{out}(t)$ will often differ from the input in several ways.

Let $E_{in}(\omega)$ represent the Fourier transform of $e_{in}(t)$ and $E_{out}(\omega)$ represent the Fourier transform of $e_{out}(t)$. Then the linear system characteristics will be

$$G(\omega) = \frac{E_{out}(\omega)}{E_{in}(\omega)} = |G(\omega)| \, e^{j\theta(\omega)} \qquad \text{(A-1)}$$

where $|G(\omega)|$ is the frequency dependent magnitude of $G(\omega)$ and $\theta(\omega)$ is the frequency dependent phase shift of $G(\omega)$. When expressed in the time domain $|G(\omega)|$ will be an amplitude variation and $\theta(\omega)$ will be a phase shift and $\frac{d\theta(\omega)}{d\omega}$ is a time delay.

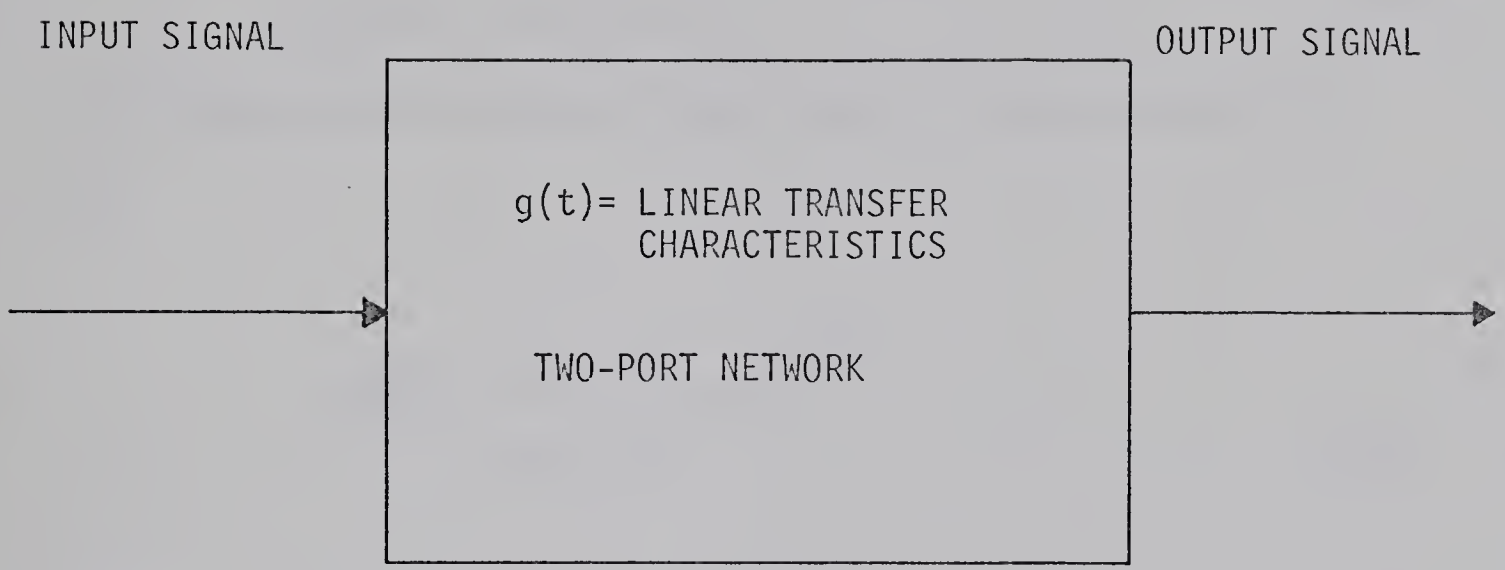

FIG. A-1 ELEMENTARY BLOCK DIAGRAM REPRESENTATION OF A COMMUNICATION SYSTEM.

A transmission system is defined as being distortionless if its output waveform is identical to the input signal with the following two exceptions:

a) the magnitude is scaled by a constant factor, K

b) the output waveform is delayed by a constant time factor which is expressed as t_o seconds.

Mathematically this will be expressed as

$$e_{out}(t) = K\, e_{in}(t-t_o) \tag{A-2}$$

Then the generalized form of the transfer characteristics will be

$$G(\omega) = \frac{E_{out}(\omega)}{E_{in}(\omega)} = Ke^{j\theta(\omega)} \tag{A-3}$$

where

$$\theta(\omega) = -\omega(t-t_o) \tag{A-4}$$

These distortionless transfer characteristics are displayed in Fig. A-2.

In many practical communication systems the representation G (ω) will not be defined explicitly over the entire frequency range of interest. (i.e. $0 \leq \omega \leq \infty$). The concepts presented thus far will still be applicable if $G(\omega)$ is defined over a frequency range greater than the limits of both the input and output signals (i.e. $\omega_1 \leq \omega \leq \omega_2$). Quite often this stipulation is also

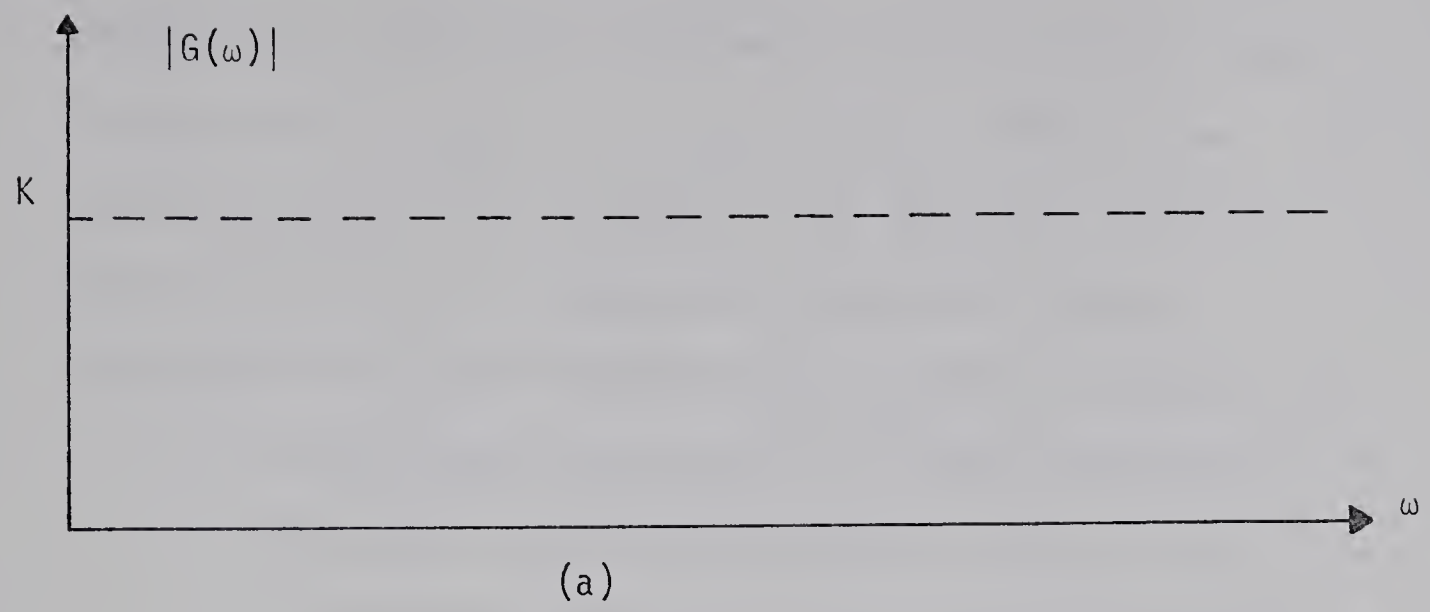

(a)

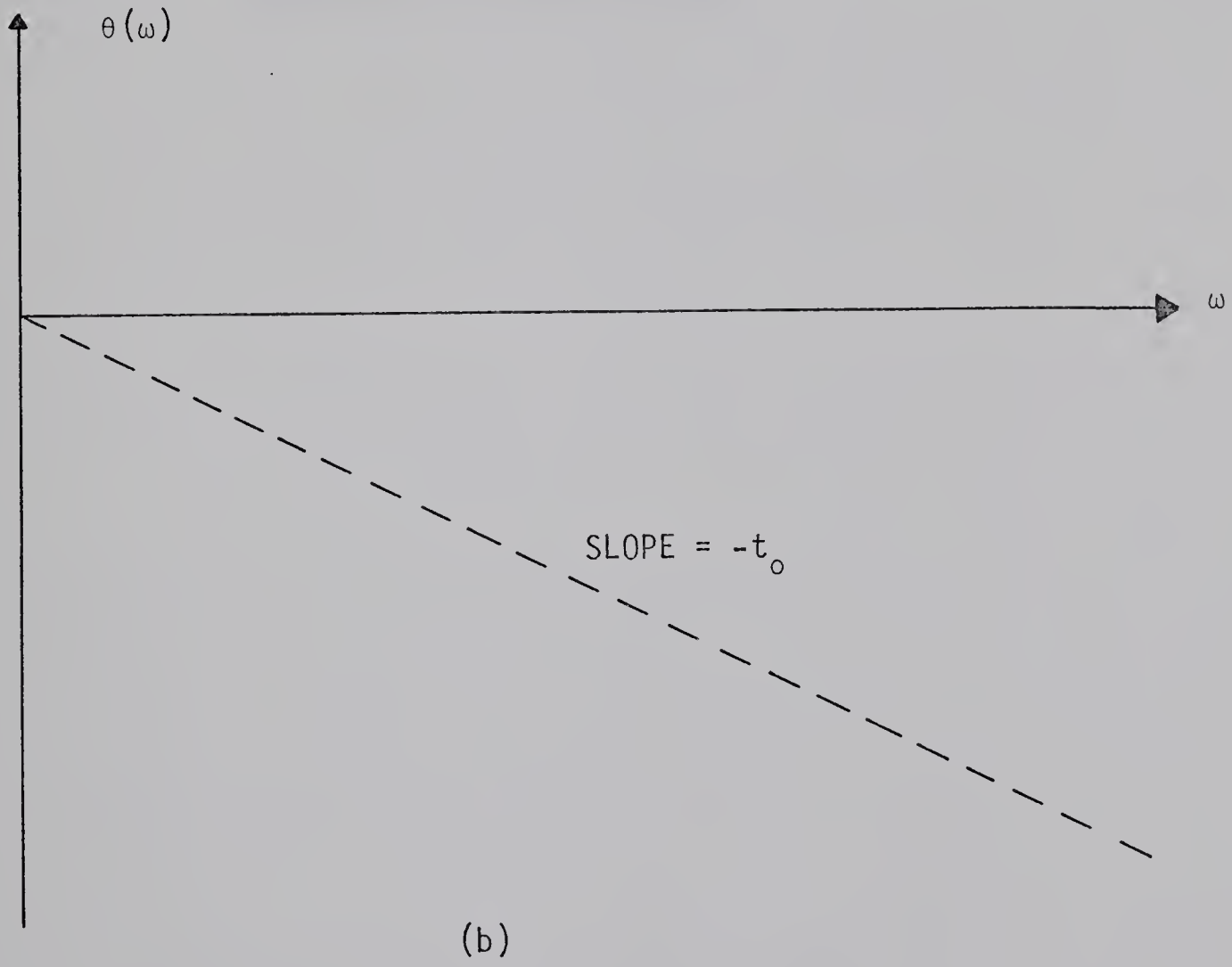

(b)

FIG. A-2 FREQUENCY PLOT OF a) THE MAGNITUDE AND b) THE PHASE VARIATION FOR THE DISTORTIONLESS CASE OF EQ. A-3.

violated and in that case the linear representation for the transfer function g(t) is no longer valid. This will be noted by another form of distortion in the output; namely, nonlinear distortion. Consequently, the main types of distortion that occur in bandlimited transmission systems are

a) amplitude distortion (i.e. $|G(\omega)| \neq$ constant)

b) phase distortion (i.e. $\theta(\omega) \neq -\omega(t-t_0)$), and

c) nonlinear distortion in both the magnitude and phase of the output signal.

APPENDIX B

DETAILED ANALYSIS OF THE TUNED AND DETUNED DISTORTION IN ILO AMPLIFIERS.

This appendix will detail the solution of the generalized Adler's locking equation including nonlinear effects in the time domain. The resulting solution will be used to accurately describe the output demodulated signal from an ILO amplifier in familiar distortion terms. After some rearranging the locking equation of Eqs. 2.2-20 and 5.2-4 becomes

$$(1+R\cos\theta(t))^2 \frac{d\theta(t)}{dt} + (1+R^2+2R\cos\theta(t))\Delta_o \sin\theta(t) =$$

$$=(1+R\cos\theta(t))\cdot(1+R^2+2R\cos\theta(t))\cdot\left(\frac{d\alpha(t)}{dt} + \Delta\omega_o\right) \qquad (B\text{-}1)$$

where the symbols defined in Chapter II apply. Eq. B-1 may further be rearranged to expand the coefficient terms, i.e.

$$[1+2R\cos\theta(t)+R^2\cos^2\theta(t)]\frac{d\theta(t)}{dt} + [1+R^2+2R\cos\theta(t)]\Delta_o\sin\theta(t)$$

$$= \left[\frac{d\alpha(t)}{dt} + \Delta\omega_o\right][1+R^2+(3+R^2)R\cos\theta(t)+2R^2\cos^2\theta(t)] \qquad (B\text{-}2)$$

The baseband modulation term $\frac{d\alpha(t)}{dt}$ will be given by

$$e_{in}(t) = \frac{d\alpha(t)}{dt} = A_m \sin\omega_m t \qquad \text{(B-3)}$$

where A_m is the peak frequency deviation, $\frac{A_m}{\omega_m} \leq 1$, and ω_m is the modulating radian frequency. Now, let all the trigonometric coefficient terms of Eq. B-2 be approximated by their four term power series expansion, i.e.

$$\cos\theta \cong 1 - \frac{\theta^2}{2} + \frac{\theta^4}{24} - \frac{\theta^6}{720} \qquad \text{(B-4)}$$

(here the truncation error is approximately $\theta^8/40{,}320$ or about 0.09% at $\theta = 1.57$ radians), and

$$\cos^2\theta = \frac{1 + \cos 2\theta}{2} = 1 - \theta^2 + \frac{\theta^4}{3} - \frac{\theta^6}{45} \qquad \text{(B-5)}$$

(here the truncation error is about $\theta^8/315$ or 3.6% at $\theta = 1.57$ radians), and

$$\sin\theta \cong \theta - \frac{\theta^3}{6} + \frac{\theta^5}{120} - \frac{\theta^7}{5040} \qquad \text{(B-6)}$$

(the truncation error will be about $\theta^9/362{,}880$ or about

0.015% at $\theta = 1.57$ radians) and,

$$\sin 2\theta \cong 2\theta - \frac{4\theta^3}{3} + \frac{4\theta^5}{15} - \frac{8\theta^7}{315} \qquad \text{(B-7)}$$

(the truncation error is about $4\theta^9/2835$ or about 7.7% at $\theta = 1.57$ radians).

While the approximations of Eq. B-4 through Eq. B-7 may contain relatively large truncation errors near the extremes of their range of applicability, these terms are often multiplied by coefficients much smaller than unity. As a result these approximations will be considered quite accurate when $\theta << 1.57$ radians and less accurate when θ approaches $\pi/2$.

Applying the approximations of Eq. B-4 through Eq. B-7 to the coefficient terms of Eq. B-2, yields

$$1 = 2R\cos\theta + R^2\cos^2\theta = (1 + R)^2 - (1 + R)R\theta^2 + (R(1+4R)/2)\theta^4 - (R(1+16R)\theta^6/360 \qquad \text{(B-8)}$$

and

$$(1+R^2+2R\cos\theta)\sin\theta = (1+R)^2\theta - (1+8R+R^2)\theta^3/6 + (1+32R+R^2)\theta^5/120 - (1+128R+R^2)\theta^7/5040 \qquad \text{(B-9)}$$

and

$$1+R^2 + (3R^2)R\cos\theta + 2R^2\cos^2\theta =$$
$$(1 + R)^3 - (3R+4R^2+R^3)\theta^2/2$$
$$+ R(3+16R+R^2)\theta^4/24 \qquad \text{(B-10)}$$
$$- R(3+64R+R^2)\theta^6/720$$

Then, substituting Eqs. B-8 through B-10 into Eq. B-2 and rearranging the result yields

$$\frac{d\theta(t)}{dt} = \sum_{n=0}^{7} P_n \theta^n \qquad \text{(B-11)}$$

where the coefficients are defined as

$$P_0 = (1+R)(\Delta\omega_0 + A_m \sin\omega_m t)$$

$$P_1 = \Delta_0$$

$$P_2 = \frac{R}{1+R}\frac{d\theta(t)}{dt} - \frac{P_0 R(3+R)}{2(1+R)^2}$$

$$P_3 = \frac{\Delta_0(1+8R+R^2)}{6(1+R)^2}$$

$$P_4 = \frac{-R(1+4R)}{12(1+R)^2}\frac{d\theta}{dt} + \frac{Ru'(R^2+16R+3)}{24(1+R)^2}$$

$$P_5 = \frac{-\Delta_0(1+32R+R^2)}{120(1+R)^2}$$

$$P_6 = \frac{R(1+16R)}{360(1+R)^2}\frac{d\theta}{dt} - \frac{u'(R^3+64R^2+13R)}{720(1+R)^2}$$

$$P_7 = \frac{\Delta_0(1+128R+R^2)}{5040(1+R)^2}$$

$$u' = \Delta\omega_0 + A_m \sin\omega_m t$$

The demodulated output frequency (for both the tuned and detuned cases) will be given by

$$e_{out}(t) = \omega_{out} = [\omega_o + \frac{\Delta_o \sin(t)}{1 + R\cos\theta(t)}] \qquad \text{(B-12)}$$

Applying the approximations Eq. B-4 to Eq. B-10 to Eq. B-12, yields

$$e_{out}(t) = \omega_o + \Delta_o \sum_{n=1}^{4} R_n \theta^{2n-1} \qquad \text{(B-13)}$$

where the 'R' terms are defined as follows:

$$R_1 = 1/(1+R)$$

$$R_2 = (2R-1)/6$$

$$R_3 = (1-13R + 16R^2)/120$$

$$R_4 = (-1 + 60R - 279R^2 + 272R^3)/5040$$

The series approximation Eq. B-11 to the locking equation Eq. B-2 will now be solved by the application of the "successive approximation" technique [35-46]. The nonlinear phase equation Eq. B-2 is only weakly nonlinear for most of the input conditions. Therefore, it is expected that only a few iterations will be required to arrive at an accurate solution. The mechanics of the technique are as follows. First the nonlinear equation Eq. B-11 is linearized by solving

$$\frac{d\theta_o}{dt} - P_1\theta_o = P_o \qquad \text{(B-14)}$$

where the shortened notation is used i.e. $\theta_o = \theta_o(t)$. The solution to Eq. B-14 after the transient has become negligible will be

$$\theta_o = (1+R)\,\Delta\omega_o/\Delta_o + \frac{(1+R)A_m/\Delta_o}{\sqrt{1+\left(\frac{\omega_m}{\Delta_o}\right)^2}} \sin\left[\omega_m t - \tan^{-1}\frac{\omega_m}{\Delta_o}\right] \qquad \text{(B-15)}$$

Eq. B-15 may also be expressed in exponential form. To refine this solution θ_o, the recursive procedure will be to substitute θ_o into Eq. B-11 in the following manner,

$$\frac{d\theta_1}{dt} + P_1\theta_1 = P_o + \sum_{n=2}^{7} P_n\theta_o^n \qquad \text{(B-16)}$$

where $\theta_1 = \theta_1(t)$ and P_o through P_7 have been evaluated at θ_o. The new solution θ_1, will have the general form

$$\theta_1 = G_o + \sum_{k=1}^{7} G_k[\sin k\omega_m t + \phi_k] \qquad \text{(B-17)}$$

where G_o, G_k and ϕ_k are the combined constants that result from the solution of Eq. B-16. More accurate solutions for $\theta(t)$ may be found by repeating this procedure for θ_2. That is, substitute θ_1 in place of θ_o in Eq. B-16, evaluate P_o through P_7 at θ_1, and replace θ_1 by θ_2. This process continues until the "new"

solution has the required degree of accuracy. This outlined procedure will be rapidly converging for the "weakly" nonlinear equations involved here. The resultant solution $\theta(t)$ will then be substituted into either Eq. B-12 or Eq. B-13 for the solution of the demodulated output; namely, ω_{out}.

To mechanize the recursive technique to solve for $\theta(t)$ a few modifications were required to some of the equations. The form of the sinusoidal solution for $\theta_o(t)$ is rewritten in its exponential form, i.e.

$$\theta_o(t) = B_o + B_1 e^{j\omega_m t} + C_1 e^{-j\omega_m t} \qquad \text{(B-18)}$$

where the coefficients are defined as

$$B_o = (1+R)$$

$$B_1 = -jA_m(1+R)/2(\Delta_o + j\omega_m)$$

$$C_1 = jA_m(1+R)/2(\Delta_o - j\omega_m)$$

To compute further solutions of $\theta(t)$ in the exponential form it is only necessary to automate the calculation of the product of the following two series. Let

$$a = A_o + \sum_{r=1}^{M} [A_r e^{jr\omega_m t} + AN_r e^{-jr\omega_m t}] \qquad \text{(B-19)}$$

and

$$b = B_o + \sum_{r=1}^{M} \left[B_r e^{jr\omega_m t} + BN_r e^{-jr\omega_m t} \right] \qquad \text{(B-20)}$$

where A_r refers to the coefficients of $e^{jr\omega_m t}$ and AN_r refers to the coefficients of the conjugate $e^{-jr\omega_m t}$. Let this definition also apply for B_r and BN_r in a similar fashion. The product of these two series may be written (for the case of M = N) as

$$\begin{aligned} axb = {} & A_o B_o + \sum_{r=1}^{M} (A_r BN_r + AN_r B_r) \\ & + \sum_{r=1}^{M} \left[\sum_{s=1}^{r-1} A_{r-s} B_s + \sum_{s=r+1}^{M} (A_s BN_{s-r} + B_s AN_{s-r}) \right. \\ & \qquad \left. + B_o A_r + A_o B_r \right] e^{jr\omega_m t} \\ & + \sum_{r=1}^{M} \left[\sum_{s=1}^{r-1} AN_{r-s} BN_s + \sum_{s=r+1}^{M} (AN_s B_{s-r} + BN_r A_{s-r}) \right. \\ & \qquad \left. + B_o AN_r + A_o BN_r \right] e^{-jr\omega_m t} \end{aligned} \qquad \text{(B-21)}$$

By the use of Eq. B-21, the product of $\theta_i(t)$ may be computed automatically without the cross terms that would be involved when Eq. B-17 is used. Therefore, when the technique

described in Eq. B-16 is generalized, the result is

$$\frac{d\theta_{i+1}}{dt} + P_1\theta_{i+1} = P_o + \sum_{n=2}^{7} P_n\theta_i^n \qquad \text{(B-22)}$$

where P_o through P_7 are calculated at θ_i and θ_i is the i+1 approximation to $\theta(t)$. Then the solution $\theta_i(t)$ may be expressed in general notation as

$$\theta_i(t) = D_o + \sum_{k=1}^{M} [\, D_k e^{jk\omega_m t} + DN_k e^{-jk\omega_m t} \,] \qquad \text{(B-23)}$$

where M is limited to 20.

The following criteria were used to determine when the successive approximation θ_i+1 made for $\theta(t)$ is sufficiently accurate to halt further iterations:

a) comparing the relative change in the fifth harmonic amplitude (i.e. the coefficient of $e^{j5\omega_m t}$) after each iteration and stopping this procedure if the new calculation produced a change of less than o.5%, and,

b) comparing the relative change in the fundamental amplitude (i.e. $\sqrt{D_1^2 + DN_1^2}$) and stopping the calculations when this change is less than 0.02%, and,

c) limiting the highest order of M to 20.

Then the calculated solution θ_i+1 is substituted into Eq. B-12 for a quantitative solution of the output frequency; namely,

$$e_{out}(t) = \omega_o + \frac{\Delta_o \sin \theta_{i+1}(t)}{1 + R\cos\theta_{i+1}(t)} \tag{B-24}$$

In terms of the series solution (which will now be used to define the output frequency in terms of its harmonic components) Eq. B-13 becomes

$$e_{out}(t) = \omega_o + \Delta_o \sum_{n=1}^{4} R_n \theta_{i+1}^{2n-1}(t) \tag{B-25}$$

Both of these solutions for $e_{out}(t)$ may be considered as the steady-state solutions for the output frequency. To compare the output frequency with the input frequency it is convenient to resolve the output into its magnitude and phase representation, i.e.

$$e_{out}(t) = G_0 + \sum_{r=1}^{M} [\, G_r \sin (r\omega_m t + \phi_r)] \tag{B-26}$$

where G_0 represents the dc offset, G_r the amplitudes of the harmonics and ϕ_r the associated phase shifts, and M is limited to 20.

The output demodulated frequency will now be compared to the ideal input frequency by the subtraction of the input Eq. B-3 from the output waveform Eq. B-26. Consequently, the

undesired part of the output will be given by

$$e'_{out}(t) = G_o + (G_1 - A_m)\sin[\omega_m + (\phi_1 - \frac{\omega_m}{\Delta_o})] + \sum_{r=2}^{M\leq 20} [G_r \sin(r\omega_m t + \phi_r)] \qquad \text{(B-27)}$$

The three types of transmission distortion that Eq. B-27 illustrates are:

a) the gain variation as a function of modulating frequency, i.e.

$$|G| = 20\log[G_1/A_m] \qquad \text{(B-28)}$$

b) the phase delay distortion of the fundamental (refer to Chapter IV, and Eq. 4.2-7), i.e.

$$\Delta\theta\,(\text{degree}) = \pi(\phi_1 - \frac{\omega_m}{\Delta_o}) \qquad \text{(B-29)}$$

c) the nonlinear distortion of the fundamental output (expressed in percentages) will be

$$ND(\%) = 100x[\sum_{r=2}^{M\leq 20} G_r^2]^{1/2} / G_1 \qquad \text{(B-30)}$$

where the dc offset is not considered as part of the harmonic content.

Chapters V, VI, VII display the results of the application of the method of successive approximations as outlined here, to the generalized Adler's nonlinear differential equation.